



10TH International Conference on Sustainable Energy and Environmental Protection:

Energy Storage

(June 27TH - 30TH, 2017, Bled, Slovenia)

(Conference Proceedings)

Editors:

Emeritus Prof. dr. Jurij Krope
Prof. dr. Abdul Ghani Olabi
Prof. dr. Darko Goričanec
Prof. dr. Stanislav Božičnik



University of Maribor Press



University of Maribor Press



University of Maribor Press

10TH International Conference on Sustainable Energy and Environmental Protection

Energy Storage

(June 27TH – 30TH, 2017, Bled, Slovenia)

(Conference Proceedings)

Editors:

Emeritus Prof. dr. Jurij Krope

Prof. dr. Abdul Ghani Olabi

Prof. dr. Darko Goričanec

Prof. dr. Stanislav Božičnik

June 2017

- Title:** 10TH International Conference on Sustainable Energy and Environmental Protection (June 27TH – 30TH, 2017, Bled, Slovenia) (Conference Proceedings)
- Subtitle:** Energy Storage
- Editors:** Emeritus Prof. Jurij Kroppe, Ph.D. (University of Maribor, Slovenia), Prof. Abdul Ghani Olabi, Ph.D. (University of the West of Scotland, UK), Asso. Prof. Darko Goričanec, Ph.D. (University of Maribor, Slovenia), Asso. Prof. Stanislav Božičnik (University of Maribor, Slovenia).
- Review:** Prof. Željko Knez, Ph.D. (University of Maribor, Slovenia), Prof. Niko Samec, Ph.D. (University of Maribor, Slovenia).
- Technical editors :** Jan Perša (University of Maribor Press), Armin Turanović (University of Maribor Press).
- Design and layout:** University of Maribor Press
- Conference:** 10TH International Conference on Sustainable Energy and Environmental Protection
- Honorary Committee:** Abdul Ghani Olabi, Ph.D. (Honorary President, University of the West of Scotland, United Kingdom), Igor Tičar, Ph.D (Rector of the University of Maribor, Slovenia), Niko Samec Ph.D. (Pro-rector of University of Maribor, Slovenia), Zdravko Kravanja, Ph-D. (Dean of the Faculty of Chemistry and Chemical Engineering, University of Maribor, Slovenia).
- Organising Committee:** Jurij Kroppe, Ph.D. (University of Maribor, Slovenia), Darko Goričanec, Ph.D. (University of Maribor, Slovenia), Stane Božičnik, Ph.D. (University of Maribor, Slovenia), Peter Trop, Ph.D. (University of Maribor, Slovenia), Danijela Urbanč, Ph.D. (University of Maribor, Slovenia), Sonja Roj (University of Maribor, Slovenia), Željko Knez, Ph.D. (University of Maribor, Slovenia), Bojan Štumberger, Ph.D. (University of Maribor, Slovenia), Franci Čuš, Ph.D. (University of Maribor, Slovenia), Miloš Bogataj, Ph.D. (University of Maribor, Slovenia), Janez Žlak, Ph.D (Mine Trbovlje Hrustnik, Slovenia), LL. M. Tina Žagar (Ministry of Economic Development and Technology), Igor Ivanovski, MSc. (IVD Maribor, Slovenia), Nuša Hojnik, Ph.D. (Health Center Maribor).
- Programme Committee:** Prof. Abdul Ghani Olabi (UK), Emeritus Prof. Jurij Kroppe (Slovenia), Prof. Henrik Lund (Denmark), Prof. Brian Norton (Ireland), Prof. Noam Lior (USA), Prof. Zdravko Kravanja (Slovenia), Prof. Jiri Jaromír Klemesš (Hungary), Prof. Stane Božičnik (Slovenia), Prof. Bojan Štumberger (Slovenia), Prof. Soteris Kalogirou (Cyprus), Prof. Stefano Cordiner (Italy), Prof. Jinyue Yan (Sweden), Prof. Umberto Desideri (Italy), Prof. M.S.J. Hashmi (Ireland), Prof. Michele Dassisti (Italy), Prof. Michele Gambino (Italy), Prof. S. Orhan Akansu (Turkey), Dr. David Timoney (Ireland), Prof. David Kennedy (Ireland), Prof. Bekir Sami Yilbas (Saudi Arabia), Dr. Brid Quilty (Ireland), Prof. B. AbuHijleh (UAE), Prof. Vincenc Butala (Slovenia), Prof. Jim McGovern (Ireland), Prof. Socrates Kaplanis (Greece), Dr. Hussam Jouhara (UK), Prof. Igor Tičar (Slovenia), Prof. Darko Goričanec (Slovenia), Dr. Joseph Stokes (Ireland), Prof. Antonio Valero (Spain), Prof. Aristide F. Massardo (Italy), Prof. Ashwani Gupta (USA), Dr. Aoife Foley (UK), Dr. Athanasios Megartīs (UK), Prof. Francesco Di Maria (Italy), Prof. George Tsatsaronis (Germany), Prof. Luis M. Serra (Spain), Prof. Savvas Tassou (UK), Prof. Luigi Alloca (Italy), Prof. Faek Diko (Germany), Dr. F. Al-Mansour (Slovenia), Dr. Artur Grunwald (Germany), Dr. Peter Trop (Slovenia), Prof. Philippe Knauth (France), Prof. Paul Borza (Romania), Prof. Roy Douglas (UK), Prof. Dieter Meissner (Austria), Dr. Danijela Urbanč (Slovenia), Prof. Daniel Favrat (Switzerland), Prof. Erik Dahlquist (Sweden), Prof. Eric Leonhardt (USA), Prof. GianLuca Rospi (Italy), Prof. Giuseppe Casalino (Italy), Prof. J. Dawson (USA), Dr. José Simoes (Portugal), Prof. Kadir Aydın (Turkey), Dr. Khaled Benyounis (Ireland), Prof. Laszlo Garbai (Hungary), Prof. Mariano Martin (Spain), Prof. Masahiro Ishida (Japan), Prof. Michael Seal (USA), Prof. Marco Spinedi (Italy), Prof. Michio Kitano (Japan), Prof. Milovan Jotanović (BiH), Prof. Nafiz Kahraman (Turkey), Prof. Na Zhang (China), Prof. Naotake Fujita (Japan), Prof. Niko Samec (Slovenia), Prof. Oleksandr Zaporozhets (Ukraine), Prof. Osama Al-Hawaj (Kuwait), Prof. Petar Varbanov (Hungary), Prof. Peter Goethals (Belgium), Prof. Qi Zhang (China), Prof. Rik Baert (The Netherlands), Prof. Rolf Ritz (USA), Dr. Stephen Glover (UK), Prof. Signe Kjelstrup (Norway), Dr. Sumsun Naheer (UK), Prof. Sven Andersson (Sweden), Dr. Salah Ibrahim (UK), Prof. Sebahattin Unalan (Turkey), Prof. Sabah Abdul-Wahab Sulaiman (Oman), Prof. Somrat Kerdsuwan (Thailand), Prof. T. Hikmet Karakoç (Turkey), Prof. Tahir Yavuz (Turkey), Prof. Hon Loong Lam (Thailand), LL.M. Tina Žagar (Slovenia), Prof. A.M.Hamoda (Qatar), Prof. Gu Hongchen (China), Prof. Haşmet Turkoglu (Turkey), Dr. Hussam Achour (Ireland), Dr. James Carton (Ireland), Dr. Eivind Johannes (Norway), Prof. Elvis Ahmetović (BiH), Prof.

D.G.Simeonov (Bulgaria), Prof. Abdelakder Outzourhit (Morocco), Prof. Bilge Albayrak Çeper (Turkey), Prof. Bekir Zühtü Uysal (Turkey), Prof. D. Bradley (UK), Dr. Silvia Tedesco (UK), Dr. Valentin Ivanov (Germany), Dr. Vincent Lawlor (Austria), Prof. Yonghua Cheng (Belgium), Prof. Yasufumi Yoshimoto (Japan), Prof. Yahya Erkan Akansu (Turkey), Prof. Yunus Ali Çengel (Turkey), Prof. Zeljko Knez (Slovenia), Prof. Zoltan Magyar (Hungary), Dr. William Smith (Ireland), Dr. Abed Alaswad (UK).

First published in 2017 by
University of Maribor Press
Slomškov trg 15, 2000 Maribor, Slovenia
tel. +386 2 250 42 42, fax +386 2 252 32 45
<http://press.um.si>, zalozba@um.si

Co-published by
University of Maribor, Faculty of Chemistry and Chemical Engineering
Smetanova ulica 17, 2000 Maribor, Slovenia
tel. +386 (0)2 22 94 400, faks + 386 (0)2 25 27 774
<http://www.fkkt.um.si>, fkkt@um.si

Published: 5. July 2017

© University of Maribor Press

All rights reserved. No part of this book may be reprinted or reproduced or utilized in any form or by any electronic, mechanical, or other means, now known or hereafter invented, including photocopying and recording, or in any information storage or retrieval system, without permission in writing from the publisher.

CIP - Kataložni zapis o publikaciji
Univerzitetna knjižnica Maribor

621.31:502.174.3(082)(0.034.2)

INTERNATIONAL Conference on Sustainable Energy and Environmental Protection (10 ; 2017 ; Bled)

Energy storage [Elektronski vir] : (Conference proceedings) / 10th International Conference on Sustainable Energy and Environmental Protection, (June 27th-30th, 2017, Bled, Slovenia) ; [organised by] University of Maribor [and] University of the West of Scotland ; editors Jurij Krope ... [et al.]. - El. zbornik. - Maribor : University of Maribor Press : Faculty of chemistry and chemical engineering, 2017

Način dostopa (URL): <http://press.um.si/index.php/ump/catalog/book/243>

ISBN 978-961-286-052-3 (pdf)

doi: 10.18690/978-961-286-052-3

1. Gl. stv. nasl. 2. Krope, Jurij 3. Univerza (Maribor)

COBISS.SI-ID [92427777](https://www.cobiss.si/urn:nbn:si:coibis:92427777)

ISBN 978-961-286-052-3

DOI: <https://doi.org/10.18690/978-961-286-052-3>

Price: Free copy

For publisher: Prof. Igor Tičar, Ph.D., rector (University of Maribor)

Preface

The 10th International Conference on Sustainable Energy and environmental Protection – SEEP 2017 was organised on June 27th – 30th 2017 in Bled, Slovenia, by:

- Faculty of Chemistry and Chemical Engineering, University of Maribor, Slovenia,
- University of the West of Scotland, School of Engineering and

The aim of SEEP2017 is to bring together the researches within the field of sustainable energy and environmental protection from all over the world.

The contributed papers are grouped in 18 sessions in order to provide access to readers out of 300 contributions prepared by authors from 52 countries.

We thank the distinguished plenary and keynote speakers and chairs who have kindly consented to participate at this conference. We are also grateful to all the authors for their papers and to all committee members.

We believe that scientific results and professional debates shall not only be an incentive for development, but also for making new friendships and possible future scientific development projects.

General chair
Emeritus Prof. dr. Jurij Krope



Plenary Talk on The Relation between Renewable Energy and Circular Economy

ABDUL GHANI OLABI - BIBLIOGRAPHY



Prof Olabi is director and founding member of the Institute of Engineering and Energy Technologies (www.uws.ac.uk/ieet) at the University of the West of Scotland. He received his M.Eng and Ph.D. from Dublin City University, since 1984 he worked at SSRC, HIAST, CNR, CRF, DCU and UWS. Prof Olabi has supervised postgraduate research students (10 M.Eng and 30PhD) to successful completion. Prof Olabi has edited 12 proceedings, and has published more than 135 papers in peer-reviewed international journals and about 135 papers in international conferences, in addition to 30 book chapters. In the last 12 months Prof Olabi has patented 2 innovative projects. Prof Olabi is the founder of the International Conference on Sustainable Energy and Environmental Protection SEEP, www.seepconference.co.uk

He is the Subject Editor of the Elsevier Energy Journal <https://www.journals.elsevier.com/energy/editorial-board/abdul-ghani-olabi>, also Subject editor of the Reference Module in Materials Science and Materials Engineering <http://scitechconnect.elsevier.com/reference-module-material-science/> and board member of a few other journals. Prof Olabi has coordinated different National, EU and International Projects. He has produced different reports to the Irish Gov. regarding: Hydrogen and Fuel Cells and Solar Energy.

CORRESPONDENCE ADDRESS: Abdul Ghani Olabi, Ph.D., Professor, University of the West of Scotland, School of Engineering and Computing, D163a, McLachlan Building, Paisley, United Kingdom, e-mail: Abdul.Olabi@uws.ac.uk.

<https://doi.org/10.18690/978-961-286-052-3> ISBN 978-961-286-052-3
© 2017 University of Maribor Press
Available at: <http://press.um.si>.

Plenary Talk on Energy Footprints Reduction and Virtual Footprints Interactions

JIRÍ JAROMÍR KLEMEŠ & PETAR SABEV VARBANOV

Increasing efforts and resources have been devoted to research during environmental studies, including the assessment of various harmful impacts from industrial, civic, business, transportation and other economy activities. Environmental impacts are usually quantified through Life Cycle Assessment (LCA). In recent years, footprints have emerged as efficient and useful indicators to use within LCA. The footprint assessment techniques has provided a set of tools enabling the evaluation of Greenhouse Gas (GHG) – including CO₂, emissions and the corresponding effective flows on the world scale. From all such indicators, the energy footprint represents the area of forest that would be required to absorb the GHG emissions resulting from the energy consumption required for a certain activity, excluding the proportion absorbed by the oceans, and the area occupied by hydroelectric dams and reservoirs for hydropower.

An overview of the virtual GHG flow trends in the international trade, associating the GHG and water footprints with the consumption of goods and services is performed. Several important indications have been obtained: (a) There are significant GHG gaps between producer's and consumer's emissions – US and EU have high absolute net imports GHG budget. (b) China is an exporting country and increasingly carries a load of GHG emission and virtual water export associated with consumption in the relevant importing countries. (c) International trade can reduce global environmental pressure by redirecting import to products produced with lower intensity of GHG emissions and lower water footprints, or producing them domestically.

To develop self-sufficient regions based on more efficient processes by combining neighbouring countries can be a promising development. A future direction should be focused on two main areas: (1) To provide the self-sufficient regions based on more efficient processes by combining production of surrounding countries. (2) To develop the shared mechanism and market share of virtual carbon between trading partners regionally and internationally.

CORRESPONDENCE ADDRESS: Jiří Jaromír Klemeš, DSc, Professor, Brno University of Technology - VUT Brno, Faculty of Mechanical Engineering, NETME Centre, Sustainable Process Integration Laboratory – SPIL, Technická 2896/2, 616 69 Brno, Czech Republic, e-mail: klemes@fme.vutbr.cz. Petar Sabeв Varbanov, Ph.D., Associate Professor, Brno University of Technology - VUT Brno, Faculty of Mechanical Engineering, NETME Centre, Sustainable Process Integration Laboratory – SPIL, Technická 2896/2, 616 69 Brno, Czech Republic, e-mail: varbanov@fme.vutbr.cz.

JIRÍ JAROMÍR KLEMEŠ- BIBLIOGRAPHY



Head of “Sustainable Process Integration Laboratory – SPIL”, NETME Centre, Faculty of Mechanical Engineering, Brno University of Technology - VUT Brno, Czech Republic and Emeritus Professor at “Centre for Process Systems Engineering and Sustainability”, Pázmány Péter Catholic University, Budapest, Hungary.

Previously the Project Director, Senior Project Officer and Hon Reader at Department of Process Integration at UMIST, The University of Manchester and University of Edinburgh, UK. Founder and a long term Head of the Centre for Process Integration and Intensification – CPI2, University of Pannonia, Veszprém, Hungary. Awarded by the EC with Marie Curies Chair of Excellence (EXC). Track record of managing and coordinating 91 major EC, NATO and UK Know-How projects. Research funding attracted over 21 M€.

Co-Editor-in-Chief of Journal of Cleaner Production (IF=4.959). The founder and President for 20 y of PRES (Process Integration for Energy Saving and Pollution Reduction) conferences. Chairperson of CAPE Working Party of EFCE, a member of WP on Process Intensification and of the EFCE Sustainability platform.

He authored nearly 400 papers, h-index 40. A number of books published by McGraw-Hill; Woodhead; Elsevier; Ashgate Publishing Cambridge; Springer; WILEY-VCH; Taylor & Francis).

Several times Distinguished Visiting Professor for Universiti Teknologi Malaysia, Xi’an Jiaotong University; South China University of Technology, Guangzhou; Tianjin University in China; University of Maribor, Slovenia; University Technology Petronas, Malaysia; Brno University of Technology and the Russian Mendeleev University of Chemical Technology, Moscow. Doctor Honoris Causa of Kharkiv National University “Kharkiv Polytechnic Institute” in Ukraine, the University of Maribor in Slovenia, University POLITEHNICA Bucharest, Romania. “Honorary Doctor of Engineering Universiti Teknologi Malaysia”, “Honorary Membership of Czech Society of Chemical Engineering”, “European Federation of Chemical Engineering (EFCE) Life-Time Achievements Award” and “Pro Universitaire Pannonica” Gold Medal.

CORRESPONDENCE ADDRESS: Jiří Jaromír Klemeš, DSc, Professor, Brno University of Technology - VUT Brno, Faculty of Mechanical Engineering, NETME Centre, Sustainable Process Integration Laboratory – SPIL, Technická 2896/2, 616 69 Brno, Czech Republic, e-mail: klemes@fme.vutbr.cz.

Plenary Talk on Renewable energy sources for environmental protection

HAKAN SERHAD SOYHAN

Development in energy sector, technological advancements, production and consumption amounts in the countries and environmental awareness give shape to industry of energy. When the dependency is taken into account in terms of natural resources and energy, there are many risks for countries having no fossil energy sources. Renewable and clean sources of energy and optimal use of these resources minimize environmental impacts, produce minimum secondary wastes and are sustainable based on current and future economic and social societal needs. Sun is one of the main energy sources in recent years. Light and heat of sun are used in many ways to renewable energy. Other commonly used are biomass and wind energy. To be able to use these sources efficiently national energy and natural resources policies should be evaluated together with the global developments and they should be compatible with technological improvements. Strategic plans with regard to energy are needed more intensively and they must be in the qualification of a road map, taking into account the developments related to natural resources and energy, its specific needs and defining the sources owned by countries. In this presentation, the role of supply security was evaluated in term of energy policies. In this talk, new technologies in renewable energy production will be shown and the importance of supply security in strategic energy plan will be explained.

CORRESPONDENCE ADDRESS: Hakan Serhad Soyhan, Ph.D., Professor, Sakarya University, Engineering Faculty, Esentepe Campus, M7 Building, 54187 - Esentepe /Sakarya, Turkey, e-mail: hsoyhan@sakarya.edu.tr.

<https://doi.org/10.18690/978-961-286-052-3> ISBN 978-961-286-052-3
© 2017 University of Maribor Press
Available at: <http://press.um.si>.

HAKAN SERHAD SOYHAN- BIBLIOGRAPHY



Professor at Sakarya University, Engineering Faculty. 50 % for teaching and the rest for research activities.

Teaching, courses taught:

Graduate courses:

- Combustion technology;
- Modelling techniques;

Undergraduate courses:

- Combustion techniques;
- Internal combustion engines;
- Fire safety.

Technical skills and competences professional societies:

- 25 journal papers in SCI Index. 23 conference papers;
- Editor at FCE journal. Co-editor at J of Sakarya University;
- Head of Local Energy Research Society (YETA);
- Member of American Society of Mechanical Engineers (ASME);
- Member of Turkish Society of Mechanical Engineers (TSME).

CORRESPONDENCE ADDRESS: Hakan Serhad Soyhan, Ph.D., Professor, Sakarya University, Engineering Faculty, Esentepe Campus, M7 Building, 54187 - Esentepe /Sakarya, Turkey, e-mail: hsoyhan@sakarya.edu.tr.

Table of Contents

CONFERENCE PROCEEDINGS

Energy Analysis of a Complex Heating System with Phase Change Material (PCM) Thermal Storage in Different Climatic Conditions	1
Uroš Stritih & Halime O. Paksoy	
Numerical Modelling of Sorption Systems for Seasonal Solar Energy Storage	11
Uroš Stritih, Vincenc Butala, Rok Stropnik, Rok Koželj & Urška Mlakar	
Towards the Development of Commercially Viable Grid Connected Batteries	23
Jorge Omar Gil Posada, Ismael Rivera, Juan Guillermo Rivera Berrio & Peter J. Hall	
Iron-Copper Based Anode for Large Scale Energy Storage	35
Jorge Omar Gil Posada & Peter J. Hall	
Experimental and Numerical Investigation on a Fixed Bed Regenerator	43
Fabian Mayrhober, Heimo Walter & Michael Hameter	
Transient Numerical Analysis of a Finned Tube Design with Combined Longitudinal and Transversal Fins for Latent Thermal Energy Storage Devices	57
Michael Hameter, Michael Böswarth & Heimo Walter	
Thermal Energy Storage Composites Based on Clay and Phase Change Materials	71
Milena Stojiljković, Staniša Stojiljković, Saša Savić, Sanja Petrović, Mirjana Reljić & Bratislav Todorović	
Materials Selection for Thermal Energy Storage: How to Increase the Thermal Conductivity of Phase Change Materials	83
Florian Hengstberger & Christoph Zauner	

Improving the Functionality of Resorcinol-Formaldehyde Based Carbon Aerogels as Electrode Material for Supercapacitor Applications	93
Qaisar Abbas, Mojtaba Mirzaeian & Abraham A. Ogwu	
Binary Mixtures of Ionic Liquids (ILs) and Aliphatic Nitrile Solvents as Electrolytes for Supercapacitors	105
Flavien Ivol, Johan Jacquemin & Fouad Ghamouss	
Electrochemical Model Development and Overcharging Investigation of the Vanadium Redox Flow Battery	117
Kittima Ngamsai & Amornchai Arpornwichanop	
A Comprehensive Review of Solar Thermal Energy Storage	129
Ioan Sarbu & Calin Sebarchievici	
Greener Synthesis of 1,2-Butylene Carbonate from CO₂ Using Graphene-Inorganic Nanocomposite Catalysis	145
Victor Onyenkeadi, Suela Kellici & Basu Saha	
Sugar Alcohols and Synthetic Derivatives as Phase Change Materials	155
Yago Magan Montoto, Daniel Lager, Christoph Zauner, Ulf Strijowski, Jörg Kowalczyk, Florian Hengstberger & Michael Schnürch	
Methane Production from Atmospheric Carbon Dioxide Utilizing Renewable Energy	165
Janna Veselovskaya, Anton Lysikov, Olga Netskina, Lidiya Kibis & Aleksey Okunev	
Sustainable Solar Energy Storage for Rural Africa	177
R.G. Charles, M.L. Davies, P. Douglas, S.M. Atiemo, Margaret Bates, A. Clews, I. Mabbett, B.S. Martincigh, E.T. Mombeshora, Joanna R. Morgan, V.O. Nyamori & D.A. Worsley	

Energy Analysis of a Complex Heating System with Phase Change Material (PCM) Thermal Storage in Different Climatic Conditions

UROŠ STRITIH & HALIME O. PAKSOY

Abstract An energy analysis of the complex heating system for heating of buildings, consisting of solar collectors (SC), latent heat storage tank (LHS) and heat pump (HP) was performed. The analysis was made for the heating season within the time from October to March for different climatic conditions. These climatic conditions were defined using test reference years (TRL) for cities: Adana, Rome, Ljubljana and Stockholm. The energy analysis was performed using a program which allowed hourly dynamics calculation of losses and gains for a given system. It was found that the system could cover 80% of energy from the sun and the heat pump coefficient of performance (COP) reached 5.7 in Adana, Rome and Ljubljana.

Keywords: • heating system • latent heat storage • heat pump • solar collector • coefficient of performance •

CORRESPONDENCE ADDRESS: Uroš Stritih, Ph.D., Assistant Professor, University of Ljubljana, Faculty of Mechanical Engineering, Aškerčeva 6, 1000 Ljubljana, Slovenia, e-mail: uros.stritih@fs.uni-lj.si. Halime O. Paksoy, Ph.D., Professor, Cukurova University, Faculty of Arts and Science, 01330 Adana, Turkey, e-mail: hopaksoy@cu.edu.tr.

<https://doi.org/10.18690/978-961-286-052-3.1>

ISBN 978-961-286-052-3

© 2017 University of Maribor Press

Available at: <http://press.um.si>.

1 Introduction

Buildings share of total energy consumption is estimated of about 40%. The buildings sector is increasing and this consequently also increases energy consumption. Because of this a reduction of energy consumption and use of energy from renewable sources represent important steps towards reduction of greenhouse gas emissions. Measures to reduce energy consumption could be the increased use of energy from renewable energy sources respecting the Kyoto Protocol and to maintain the global temperature rise below 2 °C. By 2020 total greenhouse gases emissions must be lower at least 20% and meet the requirements of the EPBD 2010/31/EU [1]. Reduced energy consumption and increased use of energy from renewable energy sources play an important role in promoting security of energy supply.

One of the promising alternatives for heating is solar energy. Solar energy as energy source is intermittent so the thermal energy storage unit is important – it ensures more efficient usage of the collected solar energy. In this case heat storage device can have three working modes: charging with heat, heat discharging (while emptying) and contemporary charging and discharging. Energy storage in tanks can be integrated into various systems. One way is the integration in a heating system. A combination of tank and combustion of biomass gives an optimal performance because the heat which is not used for building heating is stored in heat storage and can be used for heating when the heating device does not work [2]. Heat storage device with alcohol as working medium in thermo syphon also gives very good results [3].

The media used for filling heat storages devices are different. One possible medium for heat storing are substances that change the physical state (Phase Change Materials - PCM). It can be used in different systems for both heating and cooling [4] [5]. They are very successful in reducing the energy requirements of buildings [6] so latent heat storage is becoming increasingly important. By using the proper PCM and its proper installation latent heat storage devices can be economically efficient in heating and cooling of buildings. PCM solar tank is able to store the energy in a little space and has bigger heat capacity than the conventional tanks. Energy storage can be carried out according to the melting / solidification characteristics of PCM. Phase change materials can be in the following form: solid–solid, solid–liquid, solid–gas, liquid–gas and vice versa. Solid–liquid transitions have proved to be economically attractive for use in thermal energy storage systems because they have higher latent heat of phase transition than solid-solid transformation and involve smaller change in volume than solid-gas or liquid-gas. The choice of the substances used largely depends upon the temperature level of the application. The right melting point enables that the phase changing comes off during every usage cycle. Thereby the latent heat could be fully utilized. PCMs in solar heating/cooling plants perform better than sensible heat storage during periods when the mean temperature of the storage is around the melting temperature of the selected PCM [7].

Latent heat storage devices can be used in heating systems together with solar collectors and heat pump. Simulation was performed for the system with latent heat storage device with measurements of inlet and outlet temperature of latent heat storage device filled with PCM [8]. In such a system some design factors are important for the performance of the system [9]. Design factor can be for example fins on heat storage device. A comparison was made between a flat heat storage device and a heat storage device with fins. It turned out that in the heat storage with fins PCM melting time was reduced [10].

In this article the energy analysis and CO₂ emissions associated with SAHP operation are compared to conventional heating systems emissions.

2 Description of the system

Solar radiation is a sustainable source of energy. The annual amount of solar energy that falls on Earth is more than eight thousand times larger than the annual global demand for primary energy [11].

Local distribution of the total annual amount of solar energy is determined by climatic and meteorological factors that are highly dependent on their location.

For exploitation of solar energy a system composed of solar energy collector, low-temperature (latent) heat storage device, heat pump and heating system, which is linked to heat storage device, can be used. System is presented in Figure 1.

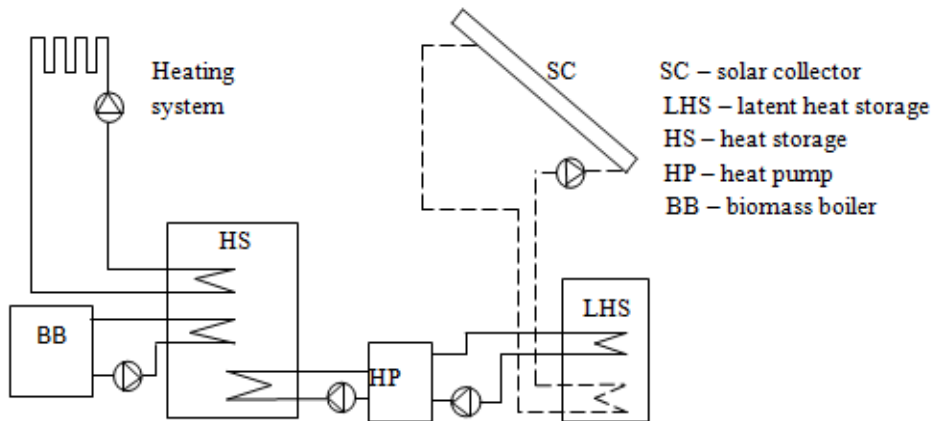


Figure 1. Scheme of the heating system

2.1 System operation

Solar energy collector absorbs solar energy, which is then transmitted by the heat exchanger to the latent heat storage device filled with a phase changing material (PCM)

- paraffin. The phase change material store energy in the process of changing in their physical state from solid to liquid. In our case the melting temperature was 31 °C.

Thermal energy is then used by the heat pump from the latent heat storage device to a higher temperature level. This energy is stored in heat storage device and then sent through a heat exchanger into the heating system which is used for heating of building. In this way a space temperature of 20 °C can be provided. The temperature of the heating system is 40 °C.

3 Mathematical model

In analysis of complex heating system a computer program - application that allowed behavior simulation of the heating system in different climatic conditions was used.

To implement the simulation input data were: hourly solar radiation, the corresponding external temperature, characteristics of the solar energy collector, latent heat storage device filled with paraffin Rubitherm RT31, heat pump characteristic and low-energy house characteristic. For weather data Test Reference Year (TRY) was used.

The calculation scheme is presented in Figure 2.

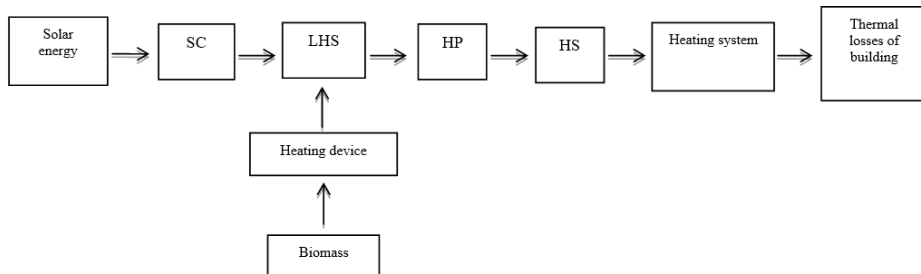


Figure 2. Scheme of the calculation

4 Results and discussion

Analysis of a complex heating system has been conducted for a period of heating season, which we define as the period between October and March. Data on climatic conditions have been obtained for the cities: Adana, Rome, Ljubljana and Stockholm.

Solar gains for all cities are obtained. The analysis showed that the maximum solar gains through the entire heating season are highest in Adana where in March the solar gains reached 10.8 GJ. In Stockholm maximum solar gains were likewise reached in March (3.1 GJ) but the value is unparalleled with solar gains in Adana or Rome. During the months of December and January solar gains in Stockholm are almost zero (only reached 0.03 GJ).

Heat losses in the heating season are the largest in Stockholm (6.2 GJ) and the smallest in Adana (1.8 GJ). For all the considered cities maximal losses are in January (Figure 3). From Figure 3 and Figure 4 the trend can be seen – geographical location of each city determines the solar gains and heat loss of a building. Buildings in southern cities have less heat losses and obtain more solar gains and vice versa.

Figure 4 presents data of heat obtained with a heat pump by month during the heating season. From the diagram we can see that it is possible to get more heat in March. This fact is linked to a sufficient amount of sun energy during this month. On average, the maximum possible gain of heat from heat pump is in Adana and in Rome.

Legend:

- SC – solar collector
- LHS – latent heat storage
- HP – heat pump
- HS – heat storage

(maximum 4.2GJ in January). Maximum heat gain can be achieved in Ljubljana in March, where heat from heat pump reached 4.9 GJ, while the lowest results are in Stockholm in November (0.04 GJ). It can also be seen that in Stockholm during the month of December and January temperatures and solar gains are not appropriate and the heat pump cannot operate.

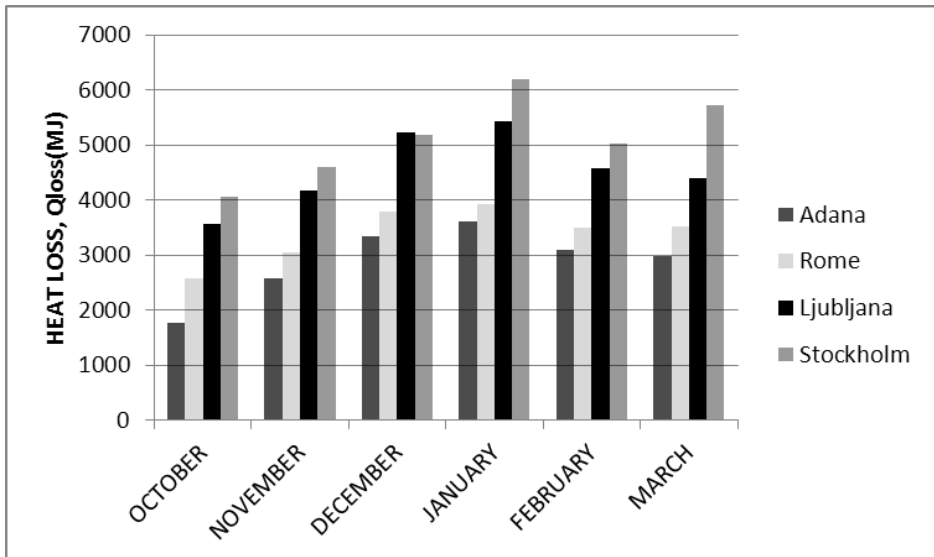


Figure 3. Heat losses during the heating season

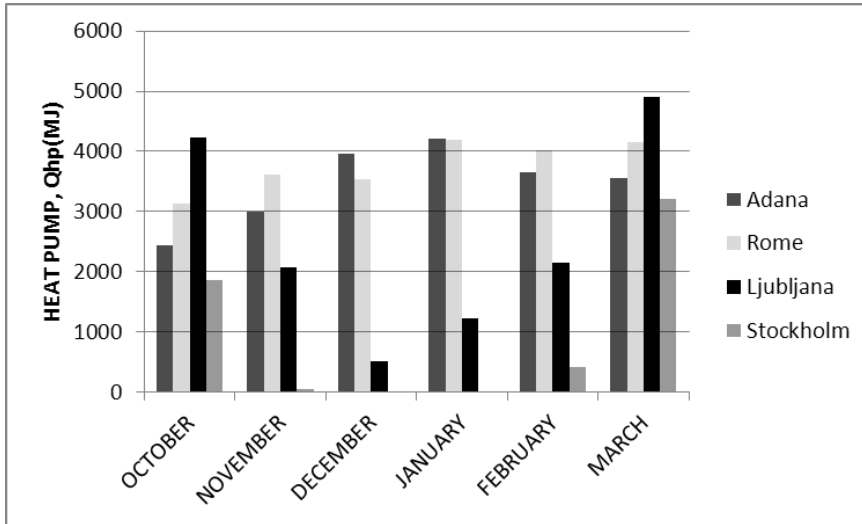


Figure 4. Heating with solar assisted heat pump in the heating season

Efficiency of the heat pump or coefficient of performance (COP) gives us the ratio between produced heat and input energy (electricity). In the presented system COP reached values during the heating season between 1 and 5.69. Value 1 means that there was no (or not enough) solar energy. The value 1 was reached in Stockholm in December and January. The maximum value of COP 5.7 was reached in Adana, Rome and Ljubljana. In Adana COP 5.7 was present during the entire heating season, in Rome this value was attained in the months of October, November, February and March and in Ljubljana during October and March, while in Stockholm the maximum value of COP was 5.12.

There may not be enough solar energy for heating with heat pump through all the heating season in some climates, so as a consequence reheating is needed. As a back-up biomass has been chosen. The greatest need for the biomass is in Stockholm during all heating season and reaches to a maximum in January (nearly 6.2 GJ). In Ljubljana 4.2 GJ of additional heating with biomass is needed in December. Moreover, reheating is necessary through all the heating season in all discussed cities, but it is very small in Adana and Rome, 1% and 7%, respectively. In Ljubljana and Stockholm, the share of reheating by biomass system is 54% and 85%, respectively.

In order to assess the environmental feasibility of SAHP, the CO₂ emissions associated with SAHP operation is compared to conventional heating systems emissions. The overall potential for CO₂ reductions is determined by emissions of each energy source and the efficiency of energy conversion used to meet heating loads. Natural gas produces emissions of 51 kg CO₂ eq./GJ, while heating oil is associated with emissions of 73 kg CO₂ eq./GJ and coal in the range of 93 – 88 kg CO₂ eq./GJ. For carbon dioxide intensities of electricity used by the operation of the heat pump, the values given in Table 1 are used

for the countries where analyzed cities are located. Monthly average heating loads for a 150 m² in the cities analyzed in this study are shown in Table 2. CO₂ emissions savings % S that can be achieved with the proposed SAHP system is calculated from equation 1.

$$\% S = \frac{E_F - E_{SAHP}}{E_F} \times 100 \quad (1)$$

The annual CO₂ emissions based on the heating loads given in Table 2 and % S are compared in Table 3 for total building stock in each city. For the reheating by biomass, CO₂ emissions are taken as zero.

Table 1. CO₂ emissions in kWh from electricity generation for different countries [12]

Country	g CO ₂ /kWh _e
Turkey	489
Italy	423
Slovenia	325
Sweden	22

Table 2. Monthly average heating loads in GJ for 150 m² building in the cities analyzed in this study

Months	Heating Load (GJ)			
	Adana	Rome	Ljubljana	Stockholm
October	1.76	2.58	3.57	4.07
November	2.57	3.06	4.18	4.59
December	3.34	3.80	5.23	5.19
January	3.60	3.93	5.44	6.19
February	3.09	3.49	4.57	5.03
March	2.98	3.52	4.40	5.72
TOTAL	17.34	20.38	27.38	30.78

Table 3. Comparison of CO₂ emissions and % S of SAHP system with reference systems using different fossil fuels for total building stock in each city

		Adana	Rome	Ljubljana	Stockholm
SAHP	CO ₂ (kton/year)	220	285,9	328,1	535,9
Natural gas	CO ₂ (kton/year)	469,9	687,3	97,8	345,8
	%S	53	58	66	98
Oil	CO ₂ (kton/year)	672,7	983,8	139,9	495
	%S	67	71	77	99
Coal	CO ₂ (kton/year)	833,9	1219,6	173,5	613,6
	%S	74	77	81	99

For Adana and Rome, where SAHP could be operated almost all through the heating season the CO₂ emissions saving potential is between 53% and 77%. For Ljubljana the savings are in the order of 66% to 81%. For Stockholm, which uses 85% biomass to meet the heating demand, the savings potential is above 98%. This shows that in climates like Stockholm, where solar energy is scarce in winter, very large savings can be achieved but only with the assumption that the rest of the heat is produced with a biomass system (renewable energy source).

5 Conclusions

The SAHP system proposed here combines solar energy, heat pump and a latent heat storage system. As a backup system when solar energy is not sufficient, wood biomass system reheating is included. Energy performance and environmental benefits of the system are calculated for Adana, Rome, Ljubljana and Stockholm with different climate conditions. The results show that maximum COP values of SAHP system is more than 5 for all cities. This shows that heat pump performance can be increased significantly in a system assisted with solar energy and latent heat storage. SAHP system can be used almost all through the heating season for Adana and Rome, which have abundant solar energy. For Ljubljana and Stockholm a backup system is required to meet the 54% and 85% of the heating demand, respectively. CO₂ emissions savings in Adana and Rome are in the range of 53% to 77%, depending on the fossil fuel used in the reference system. For Ljubljana and Stockholm, the CO₂ savings are also very high reaching to 98% in Stockholm, but the majority of the savings are due to the biomass back-up system. The proposed SAHP system can further be improved by using photovoltaic panels to provide electricity to the heat pump for a zero fossil fuel operation.

References

- [1] Directive 2010/31/EU of the European Parliament and of the Council of 19 May 2010 on the energy performance of buildings, "<http://eur-lex.europa.eu/>".
- [2] U. Stritih, V. Butala, "Optimization of a thermal storage unit combined with a biomass boiler for heating buildings," *Renewable Energy*, vol. 29, pp. 2011-2022, 2004.
- [3] M.C. Lin, L. J. Chun, W. S. Lee, S. L. Chen, "Thermal performance of a two-phase thermo syphon energy storage system," *Solar energy*, vol. 75, pp. 295-306, 2003.
- [4] E. Osterman, V.V. Tyagi, V. Butala, N.A.Rahim, U. Stritih, "Review of PCM based cooling technologies for buildings," *Energy and Buildings*, vol. 49, pp. 37-49, 2012.
- [5] U. Stritih, E. Osterman, H. Evliya, V. Butala, H. Paksoy, "Exploiting solar energy potential through thermal energy storage in Slovenia and Turkey," *Renewable and Sustainable Energy Reviews*, vol. 25, pp. 442-461, 2013.
- [6] V.V.Tyagi, D. Buddhi, "PCM thermal storage in buildings: A state of art," *Renewable and Sustainable Energy*, vol. 11, pp. 1146-1166, 2007.

- [7] A. Sharma, V.V.Tyagi, C.R.Chen, D. Buddhi, “Review on thermal energy storage with phase change materials and applications,” *Renewable and Sustainable Energy Reviews*, vol. 13(2), pp. 318-345, 2009.
- [8] M. Esen, “Thermal performance of solar-aided latent heat store used for space heating by heat pump,” *Solar Energy*, vol. 69, pp. 15-25, 2000.
- [9] O. Comakli, M. Bayramoslu, K.Kajgusuz, “A thermodynamic model of a solar assisted heat pump system with energy storage,” *Solar Energy*, vol. 56, pp. 485-492, 1996.
- [10] U. Stritih, “An experimental study of enhanced heat transfer in rectangular PCM thermal storage,” *International Journal of Heat and Mass Transfer*, vol. 47, pp. 2841-2847, 2004.
- [11] R. Domanski, “Energy Sources and Storage for XXI Century,” in *Futurstock 2003 - 9th International Conference on Thermal Energy Storage*, Warsaw, Poland, xiii-xxxii, 2003.
- [12] “ASHRAE Fundamentals 2013,” in *American Society of Mechanical Engineers*, Atlanta, Georgia, 2013.

Numerical Modelling of Sorption Systems for Seasonal Solar Energy Storage

UROŠ STRITIH, VINCENC BUTALA, ROK STROPNIK, ROK KOŽELJ & URŠKA MLAKAR

Abstract Actual national and international energy strategies generally encourage the use of renewable energy sources. Improving the energy performance of buildings is the key to achieve goals of the European Union (EU) 2030 Energy Strategy, which is to reduce greenhouse gas (GHG) emissions by at least 30 % compared to 1990 levels, because the buildings are responsible for 40 % of energy consumption and 36 % of CO₂ emissions in the EU. One of the possible and easiest solution is to increase the share of renewable energy sources (RES), especially the utilization of solar energy. Due to the intermittent and stochastic nature of solar energy the use of thermal energy storage (TES) technologies is necessary to realize its full potential. Thermochemical heat storage has gained popularity among researches because of higher energy density and lower heat loss compared to sensible and latent heat storage. This paper reviews thermochemical heat storage technologies and systems with emphasis on systems involving solar energy utilization in buildings.

Keywords: • Renewable energy sources (RES) • thermal energy storage (TES) • thermochemical heat storage • solar energy • heating • cooling •

CORRESPONDENCE ADDRESS: Uroš Stritih, Ph.D., Assistant Professor, University of Ljubljana, Faculty of Mechanical Engineering, Aškerčeva 6, SI-1000 Ljubljana, Slovenia, e-mail: uros.stritih@fs.uni-lj.si. Vincenc Butala, Ph.D., Professor, University of Ljubljana, Faculty of Mechanical Engineering, Aškerčeva 6, SI-1000 Ljubljana, Slovenia, Rok Stropnik, Young researcher, University of Ljubljana, Faculty of Mechanical Engineering, Aškerčeva 6, SI-1000 Ljubljana, Slovenia, Rok Koželj, University of Ljubljana, Faculty of Mechanical Engineering, Aškerčeva 6, SI-1000 Ljubljana, Slovenia, Urška Mlakar, University of Ljubljana, Faculty of Mechanical Engineering, Aškerčeva 6, SI-1000 Ljubljana, Slovenia.

1 Introduction

The key targets of the European Union (EU) 2030 Energy Strategy is to reduce greenhouse gas (GHG) emissions by at least 30% compared to 1990 levels, increase the share of renewable energy sources in final energy consumption to at least 27% and achieve an energy efficiency increase of at least 27%. Improving the energy performance of buildings is the key to achieve these goals [1], [2]. The easiest and also the most promising measure is to increase the utilization of solar energy. Due to the stochastic nature of solar energy the use of heat storage technologies is necessary to realize its full potential.

Heat storage can be accomplished through physical or chemical processes. With respect to the form of heat involved we distinguish between sensible and latent physical heat storage methods. Sensible heat storage is achieved through the temperature rise of the storage material. In this case the density of the stored thermal energy (i.e. stored energy per unit volume or mass) depends on the temperature lift and thermal capacity of the storage material. Latent heat storage involves heat interactions associated with a phase change of a material (at constant temperature), commonly from liquid to solid, and vice versa. Latent heat storage generally allows higher heat densities than sensible heat storage, since thermal energy change during phase change is usually significantly higher than the energy change due to temperature rise of a chosen material. Nevertheless sensible heat storage systems are still the prevalent technology for seasonal solar energy storage because of higher thermal stability and significantly lower cost of the involved storage materials compared to phase change materials (PCMs).

On the other side there are thermochemical TES systems which are not yet commercially viable. Thermochemical heat storage involves reversible chemical reactions. During the charging process heat is supplied to the storage material which causes an endothermic reaction. The supplied heat can be stored for an arbitrary time (almost) without heat loss as long as the products of the endothermic reaction are separated. This combined with a several times higher stored thermal energy density compared to sensible and latent storage (Figure 1) makes thermochemical materials (TCM) a promising alternative for mid- and long-term heat storage.

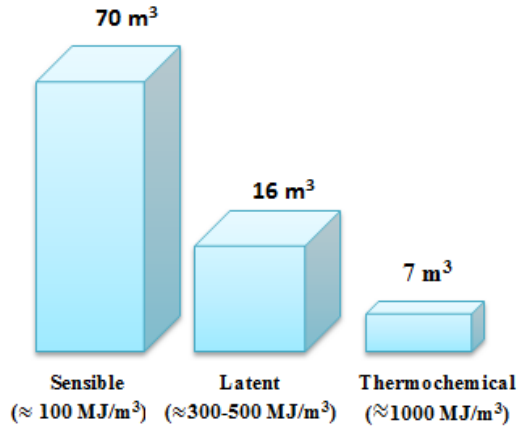


Figure 1: Comparing the necessary buffer volume for energy-efficient passive house (6480 MJ)

The main objective of this paper is to review thermochemical heat storage technologies and systems with emphasis on systems involving solar energy utilization in buildings; hence with focus only on TCMs with a charging temperature below 140 °C [3]. The paper is organized as follows: Section 2 sums up the fundamentals of thermochemical heat storage and contains an overview of TCMs suitable for solar energy storage. Sections 3 presents' possible system configurations for thermochemical heat storage and evaluates applications appropriate for reducing the energy needs of buildings. An overview of models for predicting and optimizing the performance of thermochemical storage systems is included in section 4. Section 5 concludes the paper.

2 Sorption thermal storage

Thermochemical heat storage is generally classified under chemical heat storage processes (Figure 2). Under the term thermochemical heat storage we usually summarize sorption heat storage processes. Some authors [e.g. [4]] also mention thermochemical storage without sorption but with no exact definition of the latter. Sorption can be defined as a phenomenon of fixation of a gas by a substance in solid or liquid phase [5]. We distinguish between adsorption and absorption. The term absorption is used when the molecules of a substance in gas phase enter a liquid (usually) or solid thereby changing the composition of the liquid or solid [6]. Adsorption is defined as binding of a gas on a surface of a solid or porous material [4].

Adsorption is further divided in physical adsorption or physisorption and chemical adsorption or chemisorption. The attraction between the gas and solid in physisorption is caused by Van der Waals forces. Chemisorption on the other hand is based on valence forces which form stronger bonds than Van der Waals forces. Consequently chemisorption processes enable to achieve higher thermal energy densities than

physisorption however may also be irreversible and therefore unsuitable for heat storage applications. In the following sections only reversible sorption processes are considered.

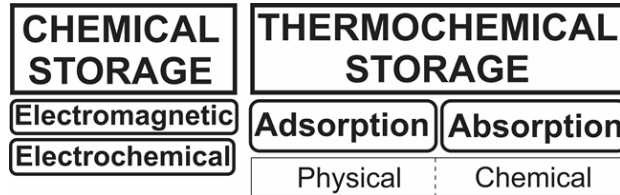


Figure 2: Classification of chemical heat storage

Reversible sorption heat storage processes can be written in the following way:



Where AB is a compound of components A and B, Q designates the heat supplied to dissociate AB into components A and B. Hence the dissociation of compound AB represents an endothermic reaction. When components A and B are put in contact heat is released (exothermic reaction) during the forming of compound AB. The supplied heat Q can be stored with negligible heat loss as long the components A and B are separated. As a result of this the dissociation of compound AB is called charging while the forming of compound AB represents the discharging process of the thermochemical heat storage cycle. The component which is desorbed during charging is named adsorbate. The material capable of adsorbing (absorbing) the other component is called adsorbent (absorbent). The term adsorptive (absorptive) is also used for the adsorbate in the desorbed state, especially when adsorbate and adsorptive differ in chemical structure (not the case in physisorption). In heat storage applications mainly water (vapor) is used as adsorbate because of its availability (i.e. cheap) and nontoxicity [4].

3 Numerical modeling

Sorption storage systems can be designed and simulated with the use of numerical models based on characteristics of the storage material. In this way one can optimize the design of the storage system and analyze its performance on an application scale without having to perform costly experiments. Hence, only the most promising storage systems and materials can be tested in full scale experiments. There are generally three approaches for modelling solid–gas adsorption processes, i.e. steady-state models, lumped-parameter models and spatially resolved models. Steady-state models disregard the heat and mass transfer kinetics inside the adsorbent bed. Since these models assume that the adsorbate and adsorbent are in thermodynamic equilibrium, they are suitable only to predict the upper performance limit of the storage system. Lumped-parameter models on the other hand consider the global heat and mass transfer between the adsorbent bed and the surrounding, but still treat the reactor as a homogenous control volume with an internally uniform state. Because of the higher accuracy compared to steady-state models, lumped-

parameter models can be used to approximately size the reactor or to simulate the global performance of the reactor at different conditions. However, for detailed modelling and optimization of processes occurring inside the reactor spatially resolved models are needed, as they consider both heat and mass transfer during a process inside the reactor, i.e. temporal spatial evolution of state variables (e.g. temperature gradient inside the adsorbent bed). The drawback of using spatially resolved models is that their computation requires solving transient and spatial coupled heat and mass transfer balance equations with complicated boundary conditions, which involves the application of specialized numerical methods. The mostly applied discretization methods are the finite difference method (FDM), the finite element method (FEM) and the finite volume method (FVM).

There are different applications beside seasonal thermal storage where adsorption processes are modeled.

In study [7] the influence of several design parameters on the transient distributions of temperature, pressure and amount adsorbed in the radial direction of a cylindrical adsorbent bed of an adsorption cooling unit using silica gel/water have been investigated numerically. For this purpose, a transient one-dimensional local thermal non-equilibrium model that accounts for both internal and external mass transfer resistances has been developed using the local volume averaging method. A computer simulation program based on the numerical procedure above was written in Matlab.

This study [8] a mathematical model of coupled heat and mass transfer in multi-layers of loose adsorbent grains under realistic conditions of adsorption heat transformation (AHT) cycle is presented. The model allows a simulation of the adsorption dynamics in the adsorbent layer which consists of a low number of loose adsorbent grains. The system of partial differential equations was solved by using the COMSOL Multiphysics simulation environment. The calculated sorption dynamics is in a good accordance with the experimental data obtained.

This study [9] presents a theoretical analysis of heat and mass transfer in a silica gel + water adsorption process using scaling principles. A two-dimensional columnar packed adsorber domain is chosen for the study, with side and bottom walls cooled and vapour inlet from the top. The adsorption process is initiated from the cold walls with a temperature jump of 15 K, whereas the water vapour supply is maintained at a constant inlet pressure of 1 kPa. The study is carried out using ANSYS Fluent employing user defined functions for appropriate source terms in continuity and energy equations.

Researchers in [10] evaluate and compare different models existing in the literature and elucidate those leading to realistic predictions of adsorption enthalpies. This is an important prerequisite for accurate simulations of heat and mass transport ranging from the laboratory scale to the reactor level of the heat store. The implementation was realised in the scientific open-source software package OpenGeoSys.

The combined hot water and sorption store in [11] has been developed using the example of a solar thermal system for domestic hot water preparation. The store consists of a radial stream adsorber integrated in a hot water store. Adsorption and desorption experiments in laboratory have been conducted with a prototype store in full-scale. A numerical model of the combined store has been developed and annual simulations of a solar thermal system including a combined hot water and sorption store have been conducted. A model of the combined hot water and sorption store has been set up in the simulation software TRNSYS.

Table1 presents all mentioned models and the software used.

Table 1: Numerical models of adsorption applications

Ref.	Working pair	Model	Numerical method	Software
[7]	silica gel/H ₂ O	1 D	FDM	MATLAB
[8]	silica gel/H ₂ O	2 D	FEM	COMSOL Multiphysics
[9]	silica gel/H ₂ O	2 D	FVM	Ansys Fluent
[10]	Zeolite/H ₂ O	-	-	OpenGeoSys
[11]	Zeolite/H ₂ O	1 D	-	PDEX, TRNSYS

4 Trnsys

TRNSYS acronym TRaNsient SYStem is one of the most popular simulation system program. It is a complete and extensible simulation environment deals mainly the problems associated with systems having transient behavior such as solar energy applications, buildings thermal analysis, electrical systems, HVAC etc. [12]. We will use the program to simulate the solar energy application with seasonal thermochemical heat storage, below we presented used prototype of heat storage.

4.1 Prototype Modestore

Figure 3 presents a system of the closed solid adsorption process, which we will use in simulation. The system is the working pair of the silica gel and water. The buffer consists of the following components: a spiral heat exchanger in the middle of the reservoir, at the bottom the condenser/evaporator and the lower tube, which connects the evaporator with a second storage tank, where is stored the water to be supplied at a stage of the discharge for the purpose of adsorption. In the spiral heat exchanger is the adsorbent silica gel. Silica gel represent the small balls that are in the spiral heat exchanger arranged in such a way that between them is a space, that the water or water vapor as the working medium is easily adsorbed to the silica gel. The spiral heat exchanger is formed from copper pipes, which are welded to each other. In the stage of filling, is the water vapor from the gel desorbed and travels to the condenser, where it is due to a lower temperature condensed. In stage of discharge, water is supplied to the evaporator through the lower pipe, which

is connected to the storage tank of water and is thereby heated. The water in evaporator is evaporated and passes through a passage into the adsorber, where it is adsorbed in the silica gel, the heat is released [13].

The prototype has very compact structure, and thus certain advantages compared to the previous prototype. The connection between the adsorber and the evaporator/condenser is valve.

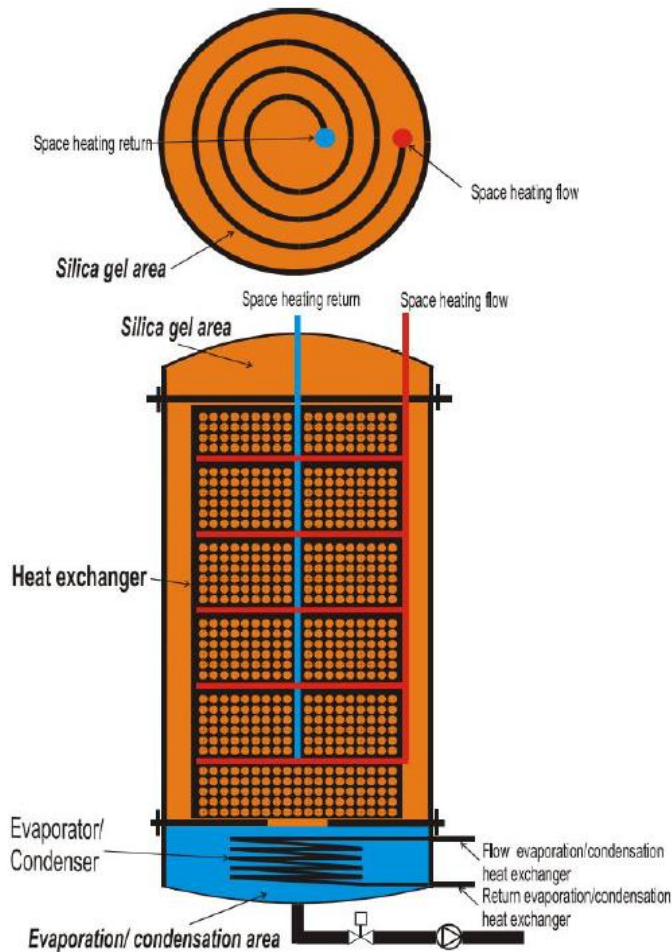


Figure 3: Prototype MODESTORE

4.2 Model

The prototype consists of three models in TRNSYS. The first model is adsorber, the second is evaporator respectively condenser and the third heat exchanger in the adsorber,

which is modeled as an external heat exchanger in TRNSYS presented as type 5. In the model of adsorber we have in TRNSYS made simple energy and mass balance.

The mass flow of the water vapor depends on the water vapor, which is evaporated or condensed in a given time.

Energy balance is shown in Figure 4.

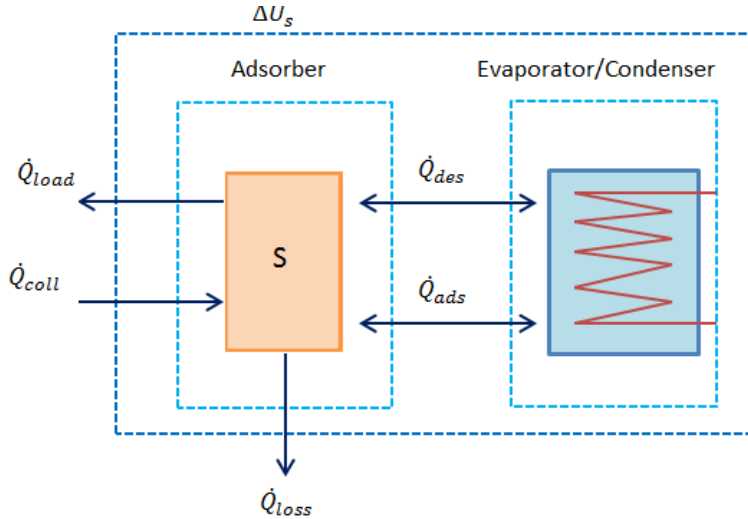


Figure 4: Energy balance of adsorber

The change in internal energy at a time is equal to all incoming and outgoing heat flows in and out of the adsorber:

$$\frac{dU_A}{dt} = -\dot{Q}_{load} + \dot{Q}_{coll} - \dot{Q}_{des} + \dot{Q}_{ads} - \dot{Q}_{loss} - W_{sorp} \quad (2)$$

From the internal energy we can calculate the temperature of the adsorber according to the equation:

$$T_A = \frac{U_A}{m_A \cdot c_{p,A} + x \cdot m_A \cdot c_{p,water}} \quad (3)$$

Model of the heat exchanger of the evaporator / condenser is modeled by the model of the logarithmic temperature difference. On the primary side of the heat exchanger we have a temperature difference in the entrance and exit. On the secondary side, evaporation/condensation temperature of this side remains constant (T_{vap}).

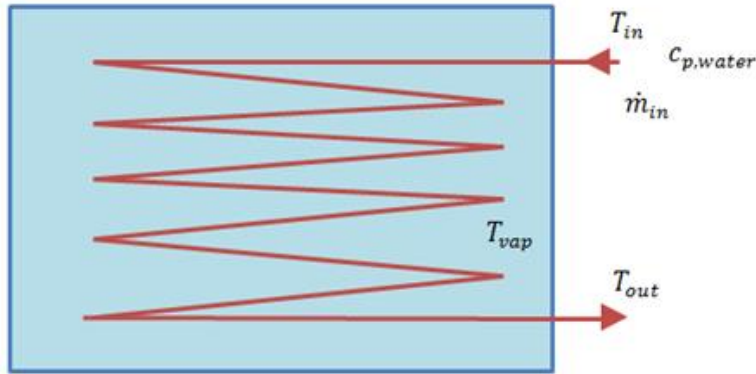


Figure 5: The heat exchanger of evaporator/condenser

The temperature at the outlet of the primary side of the heat exchanger is calculated:

$$T_{out} = \frac{T_{in} - T_{vap}}{e \frac{U \cdot A}{c_{p,water} \cdot \dot{m}_{in}}} \quad (4)$$

Heat flow of the exchanger is calculated according to the following equation:

$$\dot{Q}_{ads} = (T_{out} - T_{in}) \cdot c_{p,water} \cdot \dot{m}_{in} \quad (5)$$

With TRNSYS simulations of the energy use for building, which will have a heating system without heat storage and once with thermochemical heat storage presented above. The comparison can give us energy savings.

5 Conclusions

The main drawback of renewable energy sources is the variability and intermittence in their availability; causing significant mismatches between the time of energy demand and energy production. To make these future energy sources and conversion technologies a viable solution, it is necessary to use significant levels of energy storage technologies that enable matching of supply and demand. Energy storage technologies especially seasonal will play a crucial role in designing and operating high performance sustainable buildings and are definitely needed for the efficient use of renewable energy resources by dealing with the intermittency of energy supply and demand.

To simulate the performance of seasonal thermal storages different softwares are used. On macro scale TRNSYS is one of the options were we can calculate energy saving for the building.

For simulation of the behaviour in adsorption thermal storage on micro scale another softwares are use (ANSYS fluent for example). An important challenge is how to combine tolls on macro and micro scale together.

Acknowledgements

This study was financially supported by the Slovenian Research Agency through research project L1-7665 and research program P2-0223.

References

- [1] “European Commission, Directive 2002/91/EC of the European Parliament and of the 8 Council of 16 December 2002 on the energy performance of buildings, Off. J. Eur. Union. 9 (2002) 65–71. doi:10.1039/ap9842100196,.” [Online].
- [2] “EU, Directive 2010/31/EU of the European Parliament and of the Council of 19 May 2010 11 on the energy performance of buildings (recast), Off. J. Eur. Union. (2010) 13–35. 12 doi:doi:10.3000/17252555.L_2010.153.eng,.” [Online].
- [3] A. Ristić, N.Z. Logar, S.K. Henninger, V. Kaučič, “The performance of small-pore 14 microporous aluminophosphates in low-temperature solar energy storage: The structure-15 property relationship,” *Advanced functional materials*, vol. 22, p. 1952–1957, 2012.
- [4] Gorazd Krese, Vincenc Butala, Uroš Stritih, “Thermochemical seasonal solar energy storage for heating and cooling of buildings,” *Energy and Buildings*, 2017 (In the process of approving).
- [5] A. Hauer, “Sorption theory for thermal energy storage,” *Thermal Energy Storage for Sustainable Energy Consumption*, p. 393–408, 2007.
- [6] M.L. McGlashan, “Manual of symbols and terminology for physicochemical quantities and,” *Pure Applied Chemistry*, 1970.
- [7] Ismail Solmus, D. Andrew S. Rees, Cemil Yamalı, Derek Baker, Bilgin Kaftanoglu, “Numerical investigation of coupled heat and mass transfer,” *International journal of refrigeration*, vol. 35, pp. 652 - 662, 2012.
- [8] A. Freni, G. Maggio, F. Cipiti, Yu. I. Aristov, “Simulation of water sorption dynamics in adsorption chillers: One, two and four,” *Applied Thermal Engineering*, vol. 44, pp. 69-77, 2012.
- [9] Sourav Mitra, N. Aswin, Pradip Dutta, “Scaling analysis and numerical studies on water vapour adsorption,” *International Journal of Heat and Mass Transfer*, vol. 95, pp. 853-864, 2016.
- [10] C. Lehmann, S. Beckert, R.Glaeser, O. Kolditz, T. Nagel “Assessment of adsorbate density models for numerical simulations,” *Applied Energy*, vol. 185, p. 1965–1970, 2017.
- [11] Rebecca Weber, Henner Kerskes, Harald Drück, “Development of a combined hot water and sorption store for solar,” *Energy procedia*, vol. 48, pp. 464-473, 2014.

- [12] R.L. Shrivastava, Vinod Kumar, S.P.Untawale, “Modeling and simulation of solar water heater: A TRNSYS perspective,” *Renewable and Sustainable Energy Reviews*, vol. 67, pp. 126-143, 2017.
- [13] Uroš Stritih, Vincenc Butala, Gorazd Krese, Urška Mlakar, “Sezonski shranjevalniki toplote,” *EGES*, vol. 4, pp. 12-14, 2016.

Towards the Development of Commercially Viable Grid Connected Batteries

JORGE OMAR GIL POSADA, ISMAEL RIVERA, JUAN GUILLERMO RIVERA BERRIO & PETER J. HALL

Abstract This manuscript lists some of the most promising batteries with the potential to balance the electric grid and highlights their weaknesses and strengths; it also illustrates a systematic approach to evaluate the performance of any grid connected battery system. A detailed algorithm that considers the running costs, depreciation, and capital investment of energy storage components under a time of use electric tariff was used.

Keywords: • energy storage • grid connected • electric tariff • renewable sources • battery •

CORRESPONDENCE ADDRESS: Jorge Omar Gil Posada, Ph.D., Research Associate, University of Sheffield, Department of Chemical and Biological Engineering, Faculty of Engineering, Kroto Research Institute, North Campus, Broad Lane, S3 7HQ, South Yorkshire, UK, email: j.o.gil-posada@sheffield.ac.uk. Ismael Rivera, Ph.D., Lecturer, Facultad de Ingenieria, Institución Universitaria Pascual Bravo, Calle 73 No 73A- 226, Medellín, Colombia, e-mail: ismael.rivera@pascualbravo.edu.co. Juan Guillermo Rivera Berrio, Ph.D., Vicerrector, Institución Universitaria Pascual Bravo, Calle 73 No 73A- 226, Medellín- Colombia, e-mail: vicerrec@pascualbravo.edu.co. Peter J. Hall, Ph.D., Chair in Chemical Engineering, University of Sheffield, Department of Chemical and Biological Engineering, Faculty of Engineering, Kroto Research Institute, North Campus, Broad Lane, S3 7HQ, South Yorkshire, UK, email: peter.hall@sheffield.ac.uk.

1 Introduction

During the last few years there has been a continuous increasing demand of energy from renewable sources [1-3]. Unfortunately, renewable sources are intermittent in nature and there is a natural generation-demand mismatch, for example, availability of sun light, wind profiles, etc.). Different approaches have been taken to tackle this problem (i.e. energy storage, distribution, transmission and/or full backup capacity).

A crucial aspect of energy distribution is the ability of satisfying the peaks of the load demand (high generation costs during peak-demand periods), and energy storage is undoubtedly, one of the most effective ways to compensate for load variations without changing the energy generation matrix.

It is important to understand that renewable sources would allow for the generation of energy but mainly in the form of electricity. This situation raises an additional concern, and is the difficulty in storing electricity.

There is basically one practical way of storing electricity, which is transforming it into another form of energy that is more suitable for storage, for example in the form of potential energy by pumping water from a low level reservoir to a second reservoir placed at a higher location. Once the energy is required, then water would be allowed to flow from the upper reservoir through a series of hydroelectric turbines, thus generating electricity. The processes that are currently used for storing electricity are inefficient, unpractical or expensive.

Table 1 lists selected energy storage options (other than batteries) currently available on the market and lists some of their advantages and disadvantages.

Table 1. Selected Energy Storage (ES) Technologies

Technology	Advantages	Challenges
Chemical storage	-Mature technology	-Relatively low efficiency
Compressed Air	-Ramp fast -Large capacity -Mature technology	-Low efficiency -Environmental impact -Plant size
Electrochemical Capacitors	-Long life -Fast discharge	-Energy density -Cost
Flow Battery	-Long life	-Developing technology -Energy density
Flywheel	-Long cycle life -Rapid response -Maintenance	-Rotating parts -Low efficiency -Self-discharge
Pumped Hydro	-Ramp fast -Mature technology	-Low efficiency -Plant size
Superconductive Magnetic.	-Cycle life -High efficiency	-Cost -Energy density
Thermochemical	-High efficiency	-Current cost

This manuscript focuses on electricity storage by using commercially viable grid-connected batteries.

2 Batteries

Relying on the principle that electrical energy can be transformed into chemical energy and vice versa, batteries would provide an efficient way of storing electricity. There is a plethora of rechargeable batteries with the potential to balance the electric grid; however, this manuscript focuses on some of the most promising low-cost secondary batteries suitable for the home market.

2.1 Lead Acid Batteries

Dominating the global market for small-medium scale rechargeable electrochemical energy storage, lead acid batteries are aqueous batteries widely used for engine starting, lightning and ignition [4, 5].

Implementing positive and negative plates based upon lead-dioxide and metallic lead respectively, lead acid batteries utilize an aqueous solution of concentrated sulphuric acid [6].

Lead acid batteries are well known for low rate of self-discharge, low cost of raw materials, recyclability, and good performance over a wide range of operating temperatures; in addition, the production of lead acid batteries has evolved and is currently a very mature technology. Unfortunately, these batteries exhibit low energy density values (in the order of 30 Wh kg⁻¹), limited cycle life (usually not exceeding 500 cycles of charge and discharge), relatively low round trip efficiency (typically up to 80%), and toxicity [5, 7-9].

Selected companies that are currently commercialising lead-acid battery technology for domestic scale energy storage applications include Powervault, Ecoult and Rolls.

2.2 Lithium Ion Batteries

Exhibiting high specific capacities, long cycle life, high round trip efficiency and environmentally friendliness, lithium ion batteries are regarded as our today's best batteries. On these batteries, lithium ions would flow through a non-aqueous electrolyte from cathode to anode during the charging of the battery, and conversely from anode to cathode during the discharge of the battery.

Although, the prices for these batteries have started to come down, prices are still high.

Selected companies that are currently commercialising lithium-ion battery technology for domestic scale energy storage applications include Tesla, Bosch, Balquon, CODA Energy, JLM Energy, Samsung SDI, LG, and Panasonic.

2.3 NiFe Batteries

These rechargeable aqueous batteries were successfully back in the early 20th century but fell out of favour against cheaper lead acid batteries. However, there has been a resurgence of interest on these batteries for several reasons, including: abundance and low cost of raw materials, eco-friendliness, long cycle life, tolerance to electrical abuse, and compatibility with intermittent power sources [24-26].

Unfortunately, NiFe batteries are well known for their low charge/discharge efficiencies (in the order of 50-60%) [10-12], low specific energy (30-50 Wh kg⁻¹) and toxicity of nickel.

Selected companies that are currently commercialising NiFe battery technology include Seawill, Iron Edison Industrial Batteries, and Ironcore Batteries.

2.4 Figure of Merit of Selected Batteries

Representative figures of merit of selected battery types can be found in Table 2 [13-18].

Table 2. Figures of merit of selected batteries

Battery	Cost (£ kWh ⁻¹)	Life Cycle	%η	Self-discharge (% month ⁻¹)
Pb Acid	30	500	70	30
NiFe	40	2000	65	20
Li ion	200	1200	90	10-

The values reported on Table 2 consider charge and discharge at nearly C/5 and the state of charge was comprised in the range from between 20 and 100%.

3 Grid connected batteries

Figure 1 sketches an example of an energy generation and storage system. The basic design would consist of a bank of batteries that can be charged either by using renewable energy or from the AC grid.

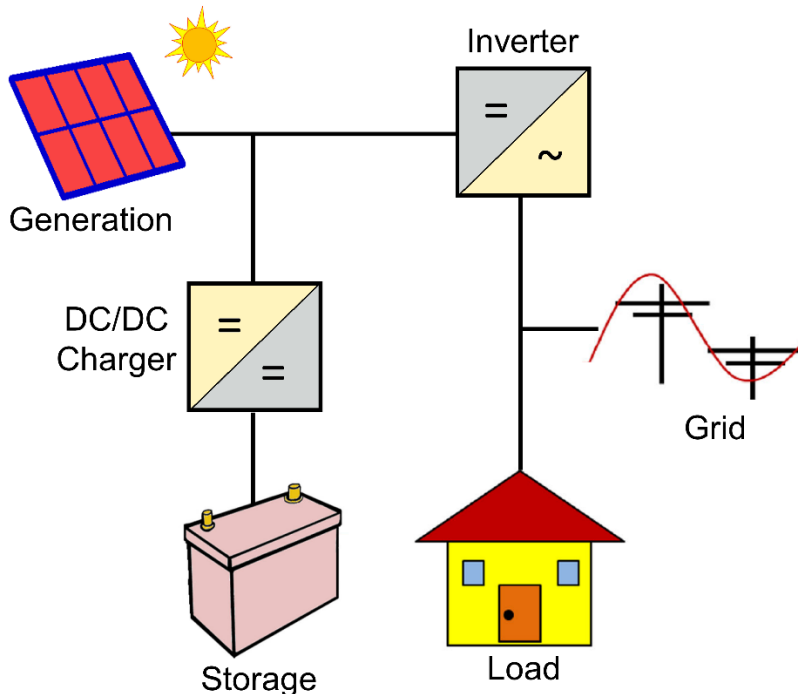


Figure 1. Schematic diagram of grid connected battery with renewable energy generation

The DC/DC charger allows the charging of the battery pack. The inverter takes the DC load from the battery pack and transforms it into an AC load.

3.1 Renewable Generation

Solar energy has become one of the most rapidly growing renewable sources of electricity. Selected companies that are currently commercialising solar panels for domestic scale applications include Sharp, Sanyo, Panasonic, Schuco and Kyocera.

3.2 Energy Storage Considerations

It is well known that the way and conditions at which batteries are used will affect their performance and lifetime.

Depth of Discharge

The depth of discharge (DoD) will affect the overall operational life of the battery. Basically, the greater the depth of discharge, the shorter is the operational life of the battery.

Temperature

The temperature conditions at which the batteries are operated will also influence their performance and lifecycle. High ambient temperatures might increase the rate of corrosion, evolution of gases and even reduce capacity faster than in colder climates. Low temperatures would render sluggish reactions with the battery and at sufficiently cold temperatures the electrolyte might even freeze.

Self-Discharge

The rate of self-discharge can be understood as the process in which internal reactions would reduce the stored charge of the battery even without any connection between its terminals.

4 Grid energy storage

4.1 Arbitrage

Electric energy time-shift (arbitrage) allows purchasing electric energy during periods when prices are low, to charge the storage system; in this way, energy can be used or sold at a later time when the energy prices are high.

4.2 Frequency Regulation

Electrochemical energy storage can be used to balance a local grid with high frequency instabilities. Frequency regulation typically operates on short time periods, usually in the order of minutes to seconds.

4.3 Integration of Renewable Sources

Electrochemical energy storage can help to mitigate fluctuations of renewable peak generation in times of high production and low demand.

5 Methods

In this section, the model used to evaluate long-run performance of grid connected batteries is provided. Essentially, a time per use electric tariff where seasonal energy prices would hold across the entire simulation were used to build the model.

5.1 Modelling of Grid-Connected Battery

By considering a discrete time domain, the instantaneous energy demand can be estimated with high precision.

Off-Peak Time

During off peak time, the charging current should be kept as large as possible without exceeding the maximum charging current recommended by the manufacturer. In addition, the maximum power load available from the grid is determined by the supplier.

Mid-Peak Time

During mid-peak time, stored energy is retained in the battery. Self-discharge of the battery bank is the only process that might take place.

On-Peak Time

During on-peak time, the discharging current to the battery should not exceed the maximum value recommended by the manufacturer.

Charging/Discharging Considerations

Note that the battery bank should be neither overcharged nor over-discharged at any time. Likewise, the rated power of the bidirectional converter should never be exceeded, nor the maximum required discrete power load should ever be exceeded.

Costs

For simulation purposes, an average life time of 20 years for each component included in Figure 1 was assumed.

6 Results

The implementation of the model was achieved by using the ASP.NET framework, and the algorithm was developed by using the C# programming language.

Figure 2 illustrate the energy requirements and energy prices considered for the simulation.

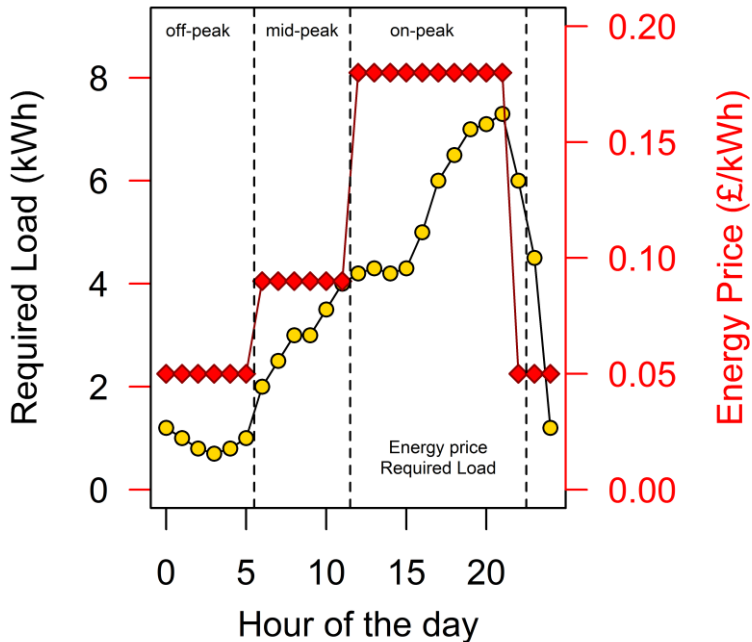


Figure 1. Required load (gold disks) and energy cost (red diamonds).

The results of the simulation were obtained by considering batteries operating under similar conditions. The simulation parameters are listed in Table 3.

Table 3. Simulation parameters

Parameter	Values
Capacity (kWh day ⁻¹)	10
Charging Efficiency (%)	65-95
Discharging Efficiency (%)	65-95
Rectifier (AC/DC converter) efficiency (%)	90
Inverter (DC/AC converter) efficiency (%)	90
DC bus voltage (V)	440
Self-discharge (% month ⁻¹)	5 - 30
Battery operating DC voltage (V)	45
Battery maximum charging current (A)	42
Battery maximum discharging current (A)	42
Maximum allowed state of charge of battery (%)	100
Minimum allowed state of charge of battery (%)	25
Nominal charge/discharge current (A)	42
Parameter	Values

Table 4 shows the results of the simulation.

Table 4. Payback Period

Battery	Price (£)	Payback (years)	No cycles
Lead-Acid	1,200	6.3	2,268
NiFe	1,400	7.3	2,628
Li-Ion	2,600	10.3	3,708

Lead acid batteries would never exceed 500 cycles of charge and discharge, so several replacements are needed to reach the 3166 cycles, each costing £300 and rendering another 500 cycles, so the total investment would not be recoverable.

NiFe batteries would exceed 2,000 cycles of charge and discharge, so a replacement might not be needed to reach 2,628 cycles, but even with replacement an additional investment of £400 would render another 2,000 cycles, so the total investment would be recoverable with the second battery.

As lithium ion batteries would reach something like 1200 cycles of charge and discharge, so a replacement is needed to reach the 3720 cycles, but this would require at least another £2000, so the total investment would not be recoverable.

7 Conclusions

The results of the simulation indicate that NiFe batteries have the potential to provide a cost effective way to balance the electric grid.

In spite of their low cost, from a practical point of view, it is difficult to recover the capital investment when utilizing lead acid batteries. This is mainly due to their very low cycle life.

For lithium ion batteries to achieve large scale utilization for the home market, then a reduction in price is required.

Acknowledgements

The authors would like to acknowledge the U.K. Engineering and Physical Sciences Research Council for supporting this work (EP/K002252/1: Grid Connected Energy Storage).

Finally, the authors would like to acknowledge funding from the STFC (ST/N002385/1)

References

- [1] K. Hedegaard and P. Meibom, "Wind power impacts and electricity storage – A time scale perspective," *Renewable Energy*, vol. 37, pp. 318-324, 1// 2012.
- [2] H. Chen, T. N. Cong, W. Yang, C. Tan, Y. Li, and Y. Ding, "Progress in electrical energy storage system: A critical review," *Progress in Natural Science*, vol. 19, pp. 291-312, 3/10/ 2009.
- [3] A. Jacob, "Wind energy — the fuel of the future," *Reinforced Plastics*, vol. 45, Supplement 1, pp. 10-13, // 2001.
- [4] M. Fernández, J. Valenciano, F. Trinidad, and N. Muñoz, "The use of activated carbon and graphite for the development of lead-acid batteries for hybrid vehicle applications," *Journal of Power Sources*, vol. 195, pp. 4458-4469, 7/15/ 2010.
- [5] M. Saravanan, M. Ganesan, and S. Ambalavanan, "An in situ generated carbon as integrated conductive additive for hierarchical negative plate of lead-acid battery," *Journal of Power Sources*, vol. 251, pp. 20-29, 4/1/ 2014.
- [6] J. O. G. Posada, A. J. R. Rennie, S. P. Villar, V. L. Martins, J. Marinaccio, A. Barnes, *et al.*, "Aqueous batteries as grid scale energy storage solutions," *Renewable and Sustainable Energy Reviews*, vol. 68, Part 2, pp. 1174-1182, 2// 2017.
- [7] D. R. Battlebury, "A high performance lead–acid battery for EV applications," *Journal of Power Sources*, vol. 80, pp. 7-11, 7// 1999.
- [8] L. Chen, Z. Xu, M. Liu, Y. Huang, R. Fan, Y. Su, *et al.*, "Lead exposure assessment from study near a lead-acid battery factory in China," *Science of The Total Environment*, vol. 429, pp. 191-198, 7/1/ 2012.
- [9] B. Hong, L. Jiang, K. Hao, F. Liu, X. Yu, H. Xue, *et al.*, "Al/Pb lightweight grids prepared by molten salt electroless plating for application in lead-acid batteries," *Journal of Power Sources*, vol. 256, pp. 294-300, 6/15/ 2014.
- [10] A. K. Shukla, S. Venugopalan, and B. Hariprakash, "Nickel-based rechargeable batteries," *Journal of Power Sources*, vol. 100, pp. 125-148, 11/30/ 2001.

- [11] J. O. Gil Posada and P. J. Hall, "Multivariate Investigation of Parameters in the Development and Improvement of NiFe Cells," *Journal of Power Sources*, vol. 262, pp. 263-269, 2014.
- [12] J. O. G. Posada and P. J. Hall, "The Effect of Electrolyte Additives on the Performance of Iron Based Anodes for NiFe Cells," *Journal of The Electrochemical Society*, vol. 162, pp. A2036-A2043, January 1, 2015 2015.
- [13] J. Peters, D. Buchholz, S. Passerini, and M. Weil, "Life cycle assessment of sodium-ion batteries," *Energy & Environmental Science*, vol. 9, pp. 1744-1751, 2016.
- [14] T. Ibn-Mohammed, S. Koh, I. Reaney, A. Acquaye, D. Wang, S. Taylor, *et al.*, "Integrated hybrid life cycle assessment and supply chain environmental profile evaluations of lead-based (lead zirconate titanate) versus lead-free (potassium sodium niobate) piezoelectric ceramics," *Energy & Environmental Science*, vol. 9, pp. 3495-3520, 2016.
- [15] J. O. G. Posada, A. J. R. Rennie, S. P. Villar, V. L. Martins, J. Marinaccio, A. Barnes, *et al.*, "Aqueous batteries as grid scale energy storage solutions," *Renewable and Sustainable Energy Reviews*, 2016.
- [16] H. Wang, Y. Liang, M. Gong, Y. Li, W. Chang, T. Mefford, *et al.*, "An ultrafast nickel-iron battery from strongly coupled inorganic nanoparticle/nanocarbon hybrid materials," *Nature Communications*, vol. 3, Jun 2012.
- [17] J. O. G. Posada and P. J. Hall, "Towards the development of safe and commercially viable nickel–iron batteries: improvements to Coulombic efficiency at high iron sulphide electrode formulations," *Journal of Applied Electrochemistry*, vol. 46, pp. 451-458, 2016.
- [18] J. O. G. Posada and P. J. Hall, "Controlling hydrogen evolution on iron electrodes," *International Journal of Hydrogen Energy*, vol. 41, pp. 20807-20817, 12/7/ 2016.

Iron-Copper Based Anode for Large Scale Energy Storage

JORGE OMAR GIL POSADA & PETER J. HALL

Abstract Aqueous NiFe cells are secondary batteries that have been identified as a means to store large amounts of energy coming from intermittent power sources such as wind or solar. Unfortunately, there are still several performance limitations preventing these batteries from becoming the dominant solution for large scale applications. This manuscript demonstrates the potential of the iron-copper system as the basis for the production of cost effective anodes for large scale energy storage.

Keywords: • NiFe • aqueous battery • hydrogen evolution • electrolyte decomposition • battery •

CORRESPONDENCE ADDRESS: Jorge Omar Gil Posada, Ph.D., Research Associate, University of Sheffield, Department of Chemical and Biological Engineering, Faculty of Engineering, Kroto Research Institute, North Campus, Broad Lane, S3 7HQ, South Yorkshire, UK, email: j.o.gil-posada@sheffield.ac.uk. Peter J. Hall, Ph.D., Chair in Chemical Engineering, University of Sheffield, Department of Chemical and Biological Engineering, Faculty of Engineering, Kroto Research Institute, North Campus, Broad Lane, S3 7HQ, South Yorkshire, UK, email: peter.hall@sheffield.ac.uk.

1 Introduction

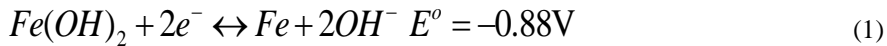
It is well known that during the last few years there has been a growing demand of energy from renewable sources. Unfortunately, due to the intermittency of these sources (such as temporary energy profile, availability of sun light, seasonal availability of water, etc.) it is not currently possible to fully back up all our energy needs just with them. Energy storage, the most natural solution to the aforementioned problem, emerges as the most practical and cost-effective solution.

Successfully commercialised since the beginning of the 20th century, nickel-iron batteries are secondary batteries that fell out of favour against lead acid batteries. Due to the toxicity and reduced cycle life of lead acid batteries, there has been a resurgence of interest on NiFe batteries.

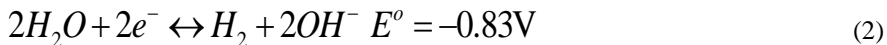
In fact, NiFe batteries are well known for their very long cycle life, tolerance of electrical abuse (over-charge, over-discharge, short circuiting conditions, electrolyte starvation), compatibility with intermittent power sources such as wind and solar, environmental friendliness and abundance of raw materials (i.e. low cost). Moreover, it is believed this technology could provide a cost effective solution for grid scale energy storage, particularly in applications where relatively low specific energy would be required (in the order of 30 to 50 Wh kg⁻¹) [1].

There are still many challenges preventing these batteries from achieving large scale utilization including: low cell efficiency, electrolyte decomposition, hydrogen evolution, low energy and power densities [2, 3].

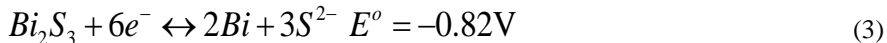
The main process that takes place during the charging of an iron electrode is the reduction of ferrous ions (Fe²⁺) to elemental iron (Fe⁰) as illustrated by Equation 1.



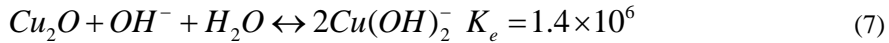
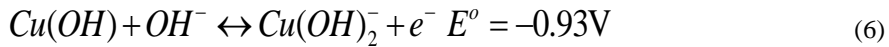
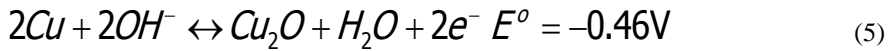
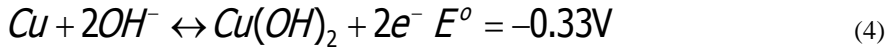
Unfortunately, during the charging of the iron electrode, water is decomposed into hydrogen and hydroxyl ions as illustrated by Equation 2.



It has been reported that bismuth sulphide would prevent water decomposition on iron by increasing the overpotential for hydrogen evolution [4, 5], this competing effect of bismuth is described by Equation 3.

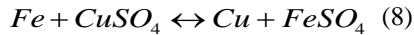


The absorption of copper on the iron surface would create a passive layer thus reducing the over-potential for hydrogen evolution [6]. It has been reported that the electrochemical behaviour of the Cu²⁺/Cu⁺ pair closely resembles the Fe³⁺/Fe²⁺ pair, as shown by Equations (4-7) [7-9].



In addition, it has been shown that the composition of the electrolyte system used to produce any NiFe cell will drastically impact on its performance [10, 11].

Finally, it is well known that when placing elemental iron with a solution of copper sulphate a single replacement reaction would occur as indicated on Equation 8.



The anodes thus produced are expected to exhibit an increased resistance towards electrolyte decomposition under strong alkaline conditions.

2 Experimental

In order to improve the performance of iron electrodes, small iron particles (purity 99.5%, <10 μm, from Alfa Aesar) were treated with a saturated aqueous solution of copper sulphate (CuSO₄·5H₂O, 98% ≤ 10 μm, Alfa Aesar), so iron particles were treated with copper sulphate solutions and mixed with differing amounts of metallic copper and bismuth sulphide (Bi₂S₃, purity 99.5%, < 5μm, from Sigma Aldrich).

By using the same procedure described in our previous publications [12, 13], an iron rich paste was produced by using varying amounts of the previously prepared iron rich paste with varying amounts of PTFE (Teflon 30-N, 59.95% solids, from Alfa Aesar). Essentially, nickel foam (purity 99.0%, density 350 g/m², Sigma Aldrich) was cut into strips of 10 mm × 40 mm × 1.8 mm; a portion of approximately 1.0 cm² of each strip was then coated with the iron rich paste in such a way that approximately 0.2 – 0.25 g of iron powder were loaded on each electrode.

The electrolyte used for the cells was a concentrated solution of 5.1M KOH that was prepared by dissolving differing amounts of KOH (purity $\geq 85.0\%$, pellets, from Sigma Aldrich) with deionized water (produced by using an Elix 10-Milli-Q Plus water purification system, Millipore, Eschborn, Germany).

Electrode formulations were tested in the conventional way by using a three electrode cell. Commercially available nickel electrodes were used as cathodes; in-house made iron electrodes were used as anodes and a concentrated solution of 5.1 M KOH was used as the electrolyte. All potentials were measured against a mercury/mercury oxide (Hg/HgO) reference electrode ($E^0_{\text{Hg/HgO}} = + 0.098 \text{ V vs. NHE}$). Figure 1 illustrates the cell configuration used for testing the batteries.

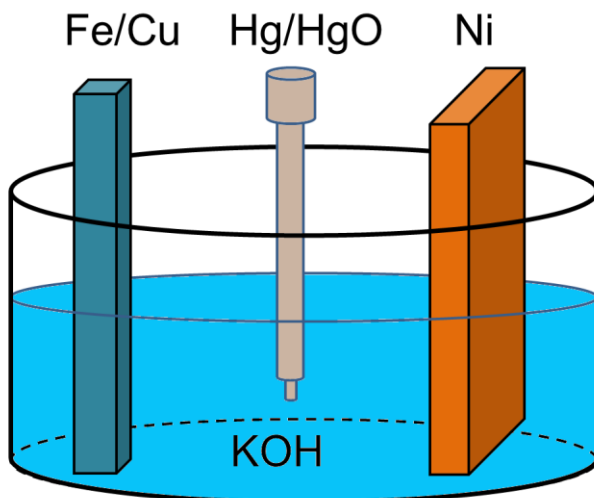


Figure 1. Test cell configuration

Experiments of galvanostatic charge and discharge were conducted on a 64 channel Arbin SCTS battery cycler at room temperature. Cells were cycled from between 0.6 and 1.4 V vs. Hg/HgO at a C/5 rate. It has been reported that iron electrodes require a conditioning period before they reach their full potential [10, 13, 14]. Our experimental results reveal that formation and stabilization of the electrodes were found to be complete after thirty cycles of charge and discharge.

3 Results and discussion

3.1 Electrode Formation

It has been reported that iron electrodes require a conditioning period before they would develop their full potential [6, 15, 16]. Once that conditioning period was completed, cells reach the steady state and meaningful among formulations can be made. Figure 2

confirms our in-house made iron electrode require approximately 28 cycles to reach the steady state.

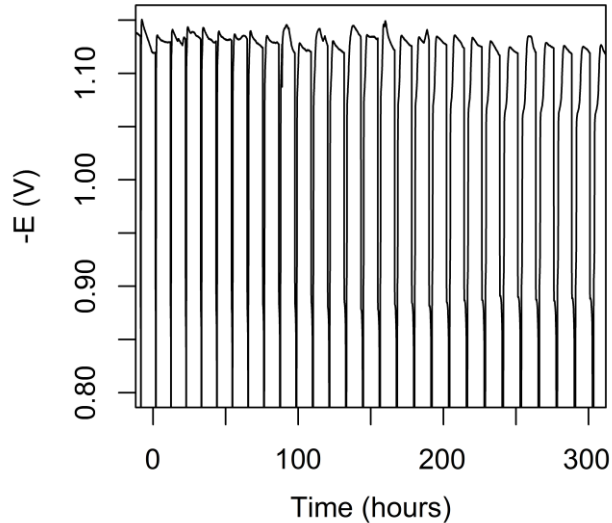


Figure 2. Galvanostatic charge and discharge profile (Fe + 5%Bi₂S₃ + 8% PTFE) iron electrode coated with copper for 1.2 hours

3.2 Time Series Analysis

Time series analysis was used to determine the effect of coating time on the performance of electrode formulation. Basically, iron particles were treated with a saturated solution of copper sulphate for different periods of time. Once this was done, electrodes were assembled and submitted to galvanostatic charge-discharge until cells reached the steady state.

Intuitively, for iron electrodes to be able to cycle, then sufficient electroactive material should be available for the cycling of the battery; however, the surface of the iron electrode provides the correct conditions for water to decompose, so the idea is to modify the surface of the electrode in such a way that electrolyte decomposition was minimised without adversely affecting the charge and discharge process of the electrode. Figure 3 confirms the addition of copper (usually less than 2%) on the surface of the iron electrode would improve its cycling properties.

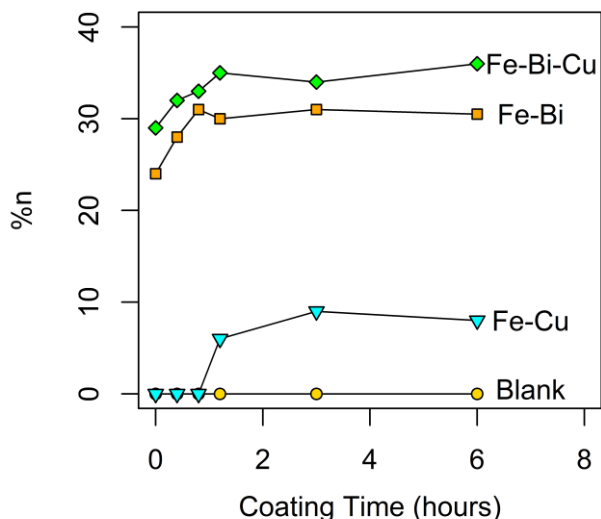


Figure 3. Time series analysis of selected anode formulations (5%Bi₂S₃ and 8% PTFE)

As can be seen from Figure 3, low coating times (up to two hours) would render cells that are virtually indistinguishable from the non-treated samples; electrodes that were prepared by utilising larger coating times out perform their non-treated counterparts. The increase in cell performance can be ascribed to the minimization of electrolyte decomposition and hydrogen evolution as shown in Equation 2. It is not clear whether larger coating times would render better electrodes and more research is still needed. It is also interesting to note that copper addition tends to improve the performance of iron electrodes; however, the overall improvement of the cell seems to be dominated by the presence of bismuth.

In our previous publications we have seen that the production of iron electrodes would benefit from utilising sulphur containing additives such as bismuth sulphide and iron sulphide; unfortunately, sometimes there is price to pay for getting a more efficient battery, which is either getting a shorter cycle life or a reduced capacity or energy density [10, 13, 15-19].

The authors believe there are merits in further investigating the effect of copper in the development of iron electrodes for large scale energy storage, but this additive by itself would not be sufficient to solve the problem of developing a highly efficient anode for stationary applications.

It is proposed to look at the combined effect of such additives in conjunction with copper coating.

4 Conclusions

This manuscript demonstrates the usefulness of copper as a means to reduce electrolyte decomposition and so hydrogen evolution.

The methodology described within this manuscript would suggest that copper coating could be used in conjunction with other strategies for reducing hydrogen evolution (such as utilizing sulphur containing compounds) to further improve the performance of iron electrodes.

Copper alone might not be sufficient for producing a cost effective anode for large scale energy storage, but this element certainly has the potential to improve the performance of iron electrodes and it therefore merits further investigation.

Copper and bismuth sulphide can be used to control electrolyte decomposition and hydrogen evolution during the charging of an iron electrode.

Acknowledgements

The authors would like to acknowledge the U.K. Engineering and Physical Sciences Research Council for supporting this work (EP/K002252/1: Grid Connected Energy Storage).

References

- [1] P. Gao, Y. Liu, W. Lv, R. Zhang, W. Liu, X. Bu, *et al.*, "Methanothermal reduction of mixtures of PbSO₄ and PbO₂ to synthesize ultrafine α -PbO powders for lead acid batteries," *Journal of Power Sources*, vol. 265, pp. 192-200, 11/1/ 2014.
- [2] A. Chaurey and S. Deambi, "Battery storage for PV power systems: An overview," *Renewable Energy*, vol. 2, pp. 227-235, 6// 1992.
- [3] G. Halpert, "Past developments and the future of nickel electrode cell technology," *Journal of Power Sources*, vol. 12, pp. 177-192, 7// 1984.
- [4] A. K. Manohar, C. Yang, S. Malkhandi, B. Yang, G. K. S. Prakash, and S. R. Narayanan, "Understanding the Factors Affecting the Formation of Carbonyl Iron Electrodes in Rechargeable Alkaline Iron Batteries," *Journal of the Electrochemical Society*, vol. 159, pp. A2148-A2155, 2012 2012.
- [5] T. S. Balasubramanian and A. K. Shukla, "Effect of metal-sulfide additives on charge/discharge reactions of the alkaline iron electrode," *Journal of Power Sources*, vol. 41, pp. 99-105, 1/5/ 1993.
- [6] A. Abdalla, C. Oseghale, J. Gil-Posada, and P. Hall, "Rechargeable Nickel-Iron Batteries for large-scale Energy storage," *IET Renewable Power Generation*, 2016.
- [7] S. D. Giri and A. Sarkar, "Electrochemical study of bulk and monolayer copper in alkaline solution," *Journal of The Electrochemical Society*, vol. 163, pp. H252-H259, 2016.
- [8] T. R. Paixão, E. A. Ponzio, R. M. Torresi, and M. Bertotti, "EQCM behavior of copper anodes in alkaline medium and characterization of the electrocatalysis of ethanol oxidation by Cu (III)," *Journal of the Brazilian Chemical Society*, vol. 17, pp. 374-381, 2006.

- 42 | 10TH INTERNATIONAL CONFERENCE ON SUSTAINABLE ENERGY AND ENVIRONMENTAL PROTECTION (JUNE 27TH– 30TH, 2017, BLEED, SLOVENIA), ENERGY STORAGE
J. Omar Gil Posada & P. J. Hall: Iron-Copper Based Anode for Large Scale Energy Storage
- [9] M. Jayalakshmi and K. Balasubramanian, "Cyclic voltammetric behavior of copper powder immobilized on paraffin impregnated graphite electrode in dilute alkali solution," *Int. J. Electrochem. Sci.*, vol. 3, pp. 1277-1287, 2008.
- [10] J. O. G. Posada and P. J. Hall, "The Effect of Electrolyte Additives on the Performance of Iron Based Anodes for NiFe Cells," *Journal of The Electrochemical Society*, vol. 162, pp. A2036-A2043, January 1, 2015 2015.
- [11] J. O. G. Posada, A. J. R. Rennie, S. P. Villar, V. L. Martins, J. Marinaccio, A. Barnes, *et al.*, "Aqueous batteries as grid scale energy storage solutions," *Renewable and Sustainable Energy Reviews*, 2016.
- [12] J. O. G. Posada and P. J. Hall, "Surface response investigation of parameters in the development of FeS based iron electrodes," *Sustainable Energy Technologies and Assessments*.
- [13] J. O. Gil Posada and P. J. Hall, "Multivariate Investigation of Parameters in the Development and Improvement of NiFe Cells," *Journal of Power Sources*, vol. 262, pp. 263-269, 2014.
- [14] J. O. Gil Posada and P. J. Hall, "Post-hoc comparisons among iron electrode formulations based on bismuth, bismuth sulphide, iron sulphide, and potassium sulphide under strong alkaline conditions," *Journal of Power Sources*, vol. 268, pp. 810-815, 12/5/ 2014.
- [15] J. O. Gil Posada, A. H. Abdalla, C. I. Oseghale, and P. J. Hall, "Multiple regression analysis in the development of NiFe cells as energy storage solutions for intermittent power sources such as wind or solar," *International Journal of Hydrogen Energy*, 2016.
- [16] J. O. G. Posada and P. J. Hall, "Controlling hydrogen evolution on iron electrodes," *International Journal of Hydrogen Energy*, vol. 41, pp. 20807-20817, 12/7/ 2016.
- [17] J. O. G. Posada and P. J. Hall, "Towards the development of safe and commercially viable nickel–iron batteries: improvements to Coulombic efficiency at high iron sulphide electrode formulations," *Journal of Applied Electrochemistry*, vol. 46, pp. 451-458, 2016.
- [18] B. Yang, S. Malkhandi, A. K. Manohar, G. K. Surya Prakash, and S. R. Narayanan, "Organo-sulfur molecules enable iron-based battery electrodes to meet the challenges of large-scale electrical energy storage," *Energy & Environmental Science*, vol. 7, pp. 2753-2763, 2014.
- [19] A. K. Manohar, S. Malkhandi, B. Yang, C. Yang, G. K. S. Prakash, and S. R. Narayanan, "A High-Performance Rechargeable Iron Electrode for Large-Scale Battery-Based Energy Storage," *Journal of the Electrochemical Society*, vol. 159, pp. A1209-A1214, 2012 2012.

Experimental and Numerical Investigation on a Fixed Bed Regenerator

FABIAN MAYRHUBER, HEIMO WALTER & MICHAEL HAMETER

Abstract The present contribution deals with the experimental and numerical analysis of the storage behaviour of a fixed bed regenerator (FBR). During the charging and discharging process the temperature and the mass flow of the heat transfer fluid (HTF) and also the temperature distribution within the storage device was measured. For the numerical simulation the local thermal non-equilibrium model is used to solve the transient heat and mass transfer problem of the FBR based on porous media approach. The transport and thermophysical characteristics which are not included in software ANSYS Fluent are programmed by user defined functions (UDFs). The measured HTF mass flow and entrance temperature into the FBR are used as boundary condition for the three dimensional transient numerical simulation. The simulation result is compared with the experimental data and shows a good agreement.

Keywords: • sensible storage device • fixed bed regenerator • experimental analysis • heat transfer fluid • numerical analysis •

CORRESPONDENCE ADDRESS: Fabian Mayrhuber, Bac., TU Wien, Institute for Energy Systems and Thermodynamics, Department Thermodynamics and Thermal Engineering, Getreidemarkt 9/302; 1060 Vienna, Austria; email: fabian.mayrhuber@gmx.at. Heimo Walter, Ao.Univ.Prof.Dr., TU Wien, Institute for Energy Systems and Thermodynamics, Department Thermodynamics and Thermal Engineering, Getreidemarkt 9/302; 1060 Vienna, Austria, email: heimo.walter@tuwien.ac.at. Michael Hameter, Dipl.-Ing., TU Wien, Institute for Energy Systems and Thermodynamics, Department Thermodynamics and Thermal Engineering, TU Wien, Getreidemarkt 9/302; 1060 Vienna, Austria; email: michael.hameter@tuwien.ac.at.

1 Introduction

With the Renewable Energy Directive (2009/28/EG) of the European Union a European framework for funding energy supply from renewable energy sources in context with binding national objectives was established. This should result in an increase of the renewable energy share with 20% in the final energy consumption and of 10% in the transport sector. Simultaneously these targets are core objectives of the strategy Europe 2020 for economic growth, because they should lead to innovative solutions for the industry and contribute to the technological leadership of Europe. A further result should be the reduction of both the carbon dioxide emissions and the dependency of the different member countries of the European Union from the energy import [1].

The increase of the renewable energy share on the energy production has on the one hand the consequence that conventional power plants must operate more flexible and often under low load conditions and on the other hand the energy supply in form of electricity is becoming more volatile. This high volatility of the electrical power grid is a great challenge because the renewable energy sources require a high flexibility, rapidness, and adaptability. Separate technological solutions like energy storage, smart grids, load management, flexible power plants and so on serve as so called flexible elements for the power grid [2].

This, however, will result in a transformation of the energy market. Thermal energy storage devices can help to improve the flexibility of the power grid as well as the load management of power plants (see e.g. [3]) and industrial processes (see e.g. [4]) by storing energy for a later use. Therefore thermal energy storage devices will play amongst others a significant role in the future power grid.

The results of a comparison between an experimental and numerical analysis of a sensible storage device - a so called fixed bed regenerator - will be presented in this article. The impacts of variation in heat transfer models are also investigated numerically.

2 Experimental analysis

To analyse the dynamic behaviour of a sensible storage device a fixed bed regenerator (FBR) filled with crushed rocks of a grain size of 30 to 72 mm (see Figure 1) was erected at the laboratory of the Institute for Energy Systems and Thermodynamics (IET) at TU-Wien.



Figure 1. Photo of the crushed rock

2.1 Test rig

A sketch of the test rig used for measuring the temperature distribution over the storage height and the pressure drop of the heat transfer fluid (HTF) air is shown in Figure 2. The FBR is admitted with a hot HTF stream of up to 330°C which is generated by an 15 kW electrical heating register. During the charging process the HTF is sucked by an Aerzen roots-blower (maximum pressure height of approx. 0,4 bar) from the ambient and flows through the thermal mass flow measuring system Proline t-mass A 150 from Endress+Hauser in direction to the heating register. Within the heating register the HTF is heated up to the inlet temperature of the FBR. After leaving the heating register the hot HTF mass flow enters the FBR at the top and leaves the FBR at the bottom in direction to the chimney. During the flow through the FBR heat is released to the storage material.

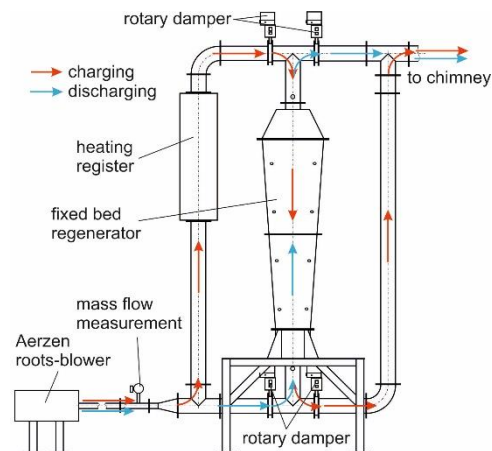


Figure 2. Sketch of the FBR test rig

The discharging process is compared to the charging process characterized by a different HTF flow direction. The sucked air mass flow enters the FBR unheated at the bottom and leaves the FBR at the top in direction to the chimney (see blue arrows in Figure 2). During this process the storage thermal energy is discharged to the HTF. The different flow directions through the FBR are controlled via rotary damper.

Figure 3 left presents the overall dimensions of the FBR storage device as well as the locations of the calibrated NiCr-Ni thermocouples (type K, 4 piece per layer) and the right side of Figure 3 shows the computational model of the FBR. The storage vessel itself consist of three cone-shaped and one cylindrical steel rings whereby the later is arranged at the bottom of the storage device. The storage vessel as well as the piping is insulated with mineral wool of a thickness of 200 mm. A more detailed description of the test rig, the measurement instrumentation and the measurement uncertainties is provided in [5].

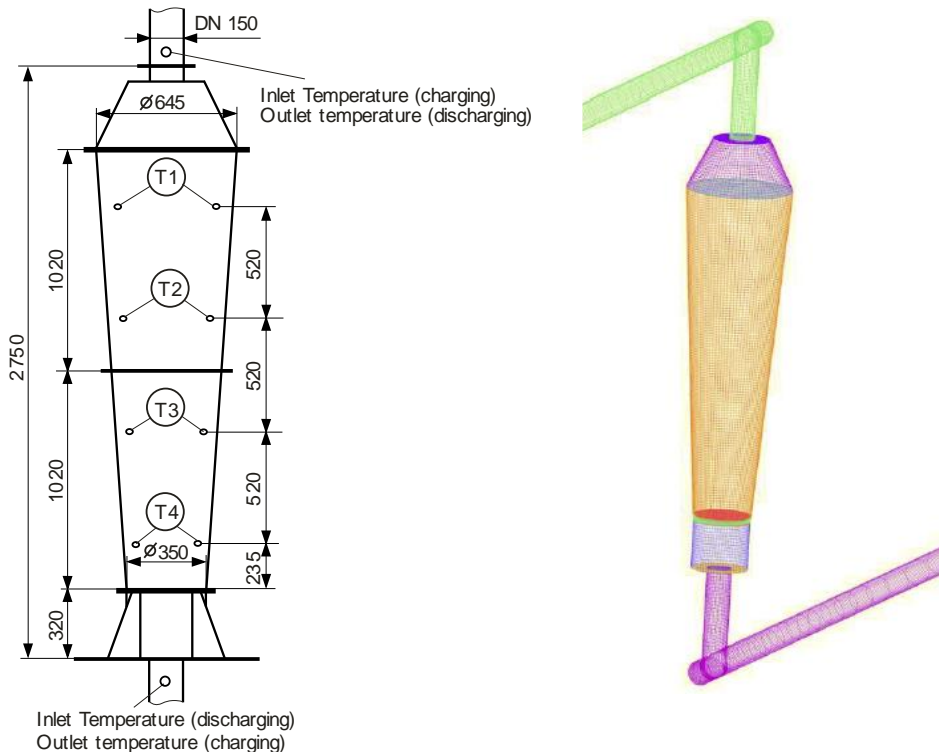


Figure 3. left: Overall dimensions of the FBR and location of temperature measurement; right: computational model of the FBR

2.2 Measurement results

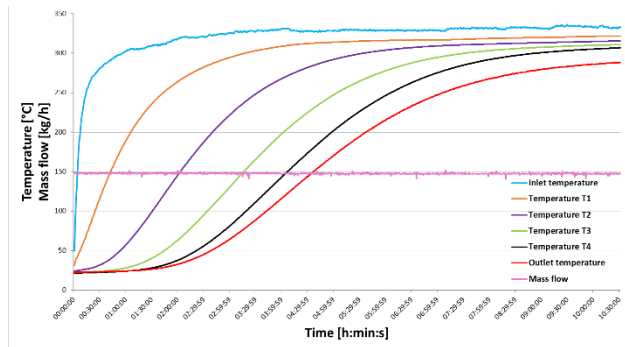


Figure 4. Mass flow and temperature distribution during charging process

Figure 4 shows the measured chronological temperature distribution over the storage height (Temperature T1 to T4) as well as the HTF inlet and outlet temperature, and mass flow for the charging process. As it can be seen in Figure 4 the storage device shows a strong development of temperature layers. With increasing charging time the difference between the single temperature layer decreases. During the charging process the mass flow of the HTF was constant at a averaged value of approx. 147,6 kg/h while the HTF inlet temperature increases rapidly from approx. 50°C to the maximum temperature of approx. 330°C. The total charging time was approx. 10h.

The chronological temperature distribution within the FBR as well as the mass flow and the temperature at the inlet and the outlet of the HTF during the discharging process is depicted in Figure 5. Compared to the charging process a similar behaviour by the development of the thermoclines during the discharging process is given within the FBR. A comparison of the charging and discharging time shows that the discharging process is faster by approx. 180 minutes.

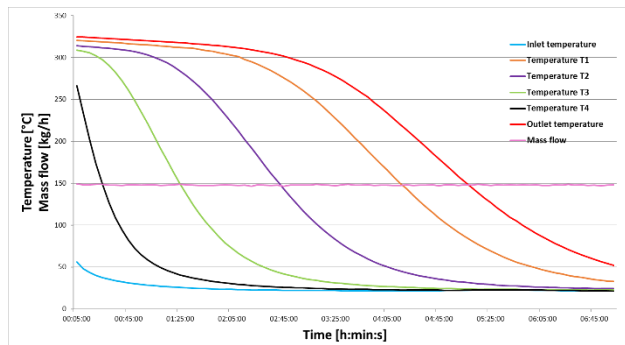


Figure 5. Mass flow and temperature distribution during discharging process
 Numerical investigation

In the following the mathematical model, the physical properties as well as the boundary conditions used for the numerical simulation of a 3D model of the FBR will be presented. Mathematical model

In the present work the commercial CFD-Code ANSYS Fluent was used to obtain the numerical solution. In ANSYS Fluent [6] the porous media approach was used for the numerical simulation of the rock-filing. The porous media model in ANSYS Fluent for single phase flow uses the superficial velocity porous formulation which calculates the superficial phase velocities based on the volumetric flow rate in a porous region. The momentum equation can be expressed as

$$\frac{\partial \rho_f \vec{u}}{\partial t} + \nabla \cdot (\rho_f \vec{u} \vec{u}) = -\nabla p + \nabla \cdot \tau + \rho_f \vec{g} + S_m \quad (1)$$

where ρ_f is the fluid density, \vec{u} the fluid superficial velocity, p the fluid pressure, τ the stress tensor, t the time, \vec{g} the gravity, and S_m the momentum source term to calculate e.g. the fluid pressure drop resulting from porous media. In this study the Darcy-Forchheimer equation [7]

$$S_m = \frac{\mu}{K} \vec{u} + \beta \rho_f |\vec{u}| \vec{u} \quad (2)$$

was used for calculating the pressure drop. In Equation (2) μ is the dynamic viscosity, K the permeability of porous media, and β is the Forchheimer coefficient. For calculating the permeability of the porous media K and the Forchheimer coefficient β the model of Ergun [8] was used which is based on measurements of the pressure drop of a fluid flow through different fillings. The porosity ϕ and the particle diameter d_p are determined as decisive parameters within the model of Ergun. For the particle diameter d_p of the filling an averaged diameter of 60 mm was used. The permeability of the porous media K and the Forchheimer coefficient β can be expressed as:

$$K = \frac{\phi^3}{(1 - \phi)^2} \frac{d_p^2}{150} \quad (3)$$

and

$$\beta = \frac{1 - \phi}{\phi^3} \frac{1,75}{d_p} \quad (4)$$

Within the model it was assumed that the porosity ϕ along the radial direction of the cross section area of the storage device is not constant. For calculating the porosity ϕ for irregular particles along the radial direction of the cross section area the correlation from Giese [9]

$$\phi = \phi_{\infty} \left[1 + 1,36 \exp \left(-5 \frac{R-r}{d_p} \right) \right] \quad (5)$$

which is based on experimental investigations, was used with R the local outer radius of the FBR and r the distance from the storage axis.

For the energy balance of the porous media the non-equilibrium thermal model was selected for the numerical investigation. This model corresponds to a two-phase-model which do not require a local thermal equilibrium.

For the fluid phase:

$$\begin{aligned} \frac{\partial \phi \rho_f E_f}{\partial t} + \nabla \cdot [\vec{u} (\rho_f E_f + p)] = \\ \nabla \cdot (\phi \lambda_{eff,f} \nabla T_f + \tau \cdot \vec{u}) + \alpha_{sf} A_{sf} (T_s - T_f) + S_f \end{aligned} \quad (6)$$

with the total energy of the fluid phase

$$E_f = h_f - \frac{p}{\rho_f} + \frac{u^2}{2} \quad (7)$$

For the solid phase:

$$\begin{aligned} \frac{\partial (1 - \phi) \rho_s h_s}{\partial t} = \nabla \cdot [(1 - \phi) \lambda_{eff,s} \nabla T_s] + \\ \alpha_{sf} A_{sf} (T_f - T_s) + S_s \end{aligned} \quad (8)$$

where, the spec. enthalpie of the solid h_s , the solid temperature T_s , the fluid temperature T_f , the heat transfer coefficient α_{sf} , the spec. surface area per volume A_{sf} , and the effective thermal conductivity of the fluid and solid phase $\lambda_{eff,f}$ and $\lambda_{eff,s}$ respectively. The symbols S_f and S_s delegate the heat source term of the fluid phase and solid phase respectively. The energy balance for the solid and fluid phase are connected through the heat exchange and they are solved simultaneous. The volumetric convection heat transfer coefficient is calculated from Equation (9).

$$\alpha_v = \alpha_{sf} A_{sf} \quad (9)$$

For calculating the heat transfer coefficient, three models put forward by Wakao et al. [10], Coutier et al. [11], and Singh et al. [12] are selected for comparison in this study.

The standard $k-\varepsilon$ model was used for calculating the turbulence within the fluid flow where, k is the turbulent kinetic energy and ε is the turbulent dissipation. For the model constants of the turbulence model the default settings of ANSYS Fluent was used.

The storage vessel (dimensions see Figure 3) as well as the isolation of the storage vessel was modelled in ANSYS Fluent with the help of the so called “Shell Conduction-Modell”. For simplification reasons the steel casing of the storage unit was modelled in such a way that a constant wall thickness of 7,39 mm over the storage height was assumed. The mass of the stell casing and the flanges was summed and an averaged wall thickness was calculated. With this assumption the heat capacity of the real storage vessel is equivalent to the model. The isolation itself was subdivided into four equal sublayers.

The grid size used for the discretization of the computational grid was determined after a careful examination of the results of a grid refinement process, see Ref. [14]. A further decrease of the control volume size did not show noticeable changes in the results. A short description of the heat transfer correlations used for comparison in this study will be presented.

3.1.1 Wakao model

In the Wakao et al. [10] model the volumetric convection heat transfer coefficient is calculated from Equation (9) and the heat transfer coefficient α_{sf} between the fluid and solid phase is given be equation (10).

$$\alpha_{sf} = \frac{(2 + 1,1 Pr^{1/3} Re_p^{0,6}) \lambda_f}{d_p} \quad (10)$$

For the specific surface area per volume A_{sf} , the correlation according to Vafai [13]

$$A_{sf} = \frac{6(1 - \phi)}{d_p} \quad (11)$$

was applied. In Equation (10) Re_p denotes the particle Reynolds number and Pr the Prandtl number. The definition region for the correlation is given by $Re_p = 15$ to 8500.

3.1.2 Coutier model

Coutier et al. [11] have proposed a volumetric heat transfer coefficient model based on experimental data.

$$\alpha_v = 700 \left(\frac{u \rho_f}{d_p} \right)^{0,76} \quad (12)$$

The size of the bulk material in [11] was 18 to 30 mm.

3.1.3 Singh model

The model of Singh et al. [12] is based on measurements in the region of $Re_p = 503$ to 866. For calculating the heat transfer coefficient Singh et al. propose the following Nusselt number:

$$Nu = \frac{0,0614 Re_p^{1,1186} \psi^{2,5098} e^{(5,2979(\ln \psi)^2)}}{\phi^{1,0203}} \quad (13)$$

with the sphericity ψ . The Nusselt number has to be calculated with

$$Nu = \frac{\alpha_v d_p^2}{\lambda_f} \quad (14)$$

For non-spherical particles the particle diameter to use must be calculated as volume equivalent.

3.2 Thermophysical properties

The thermophysical properties for the HTF air are obtained from the data included in ANSYS Fluent. As state equation for the HTF the Soave-Redlich-Kwong equation with the ANSYS Fluent default settings was used. The dynamic viscosity μ_a and the heat conduction λ_a of the HTF was calculated using the correlations presented in [15]. In the region of the porous media the heat conduction for the HTF was converted into following form:

$$\lambda_{eff,f} = \phi \lambda_a + 0,1 Pr Re_p \lambda_a \quad (15)$$

The thermophysical properties for the steel of the storage vessel was calculated by using the data implemented in ANSYS Fluent. The thermophysical properties for the density and the heat conduction of the mineral wool was taken from the data sheet of the producer [16] while for the spec. heat capacity the correlation according to [17] was used.

The definition of the thermophysical properties of the storage material is clouded with uncertainty because the bulk material is commercial available crushed rock. For this bulk material no detailed material analysis is available and therefore the material composition is unknown. However, for the numerical simulation correlations from the literature are applied as user defined function. For the spec. heat capacity the correlation proposed by [18] was used in which the parameters are selected as mean values of different rock types [19]. The heat conduction of the rock stones was calculated by using the correlation presented in [20].

3.3 Boundary and initial conditions

The inlet and the outlet piping for the HTF from and to the FBR are modelled as adiabatic tubes while for the FBR a heat exchange between the storage insulation and the surrounding was taken into account. For calculating the heat exchange with the surrounding the correlation according to [21] was applied to compute the natural convection heat transfer coefficient.

At the inlet and the outlet of the computational grid boundary conditions must be set for the transient numerical simulation as a function of time. At the entrance into the computational grid the mass flow and the temperature of the HTF and at the outlet the pressure of the HTF was defined. For the mass flow and the temperature of the HTF at the entrance into the computational grid the values taken from the experimental analysis are used which are presented in Figure 3 and 4. The ambient pressure was defined as pressure boundary condition at the outlet flow of the HTF for both the charging and the discharging process.

The initial conditions for the charging process was set in such a way that the temperature in the computational grid (HTF and storage material) was set to 20°C and the fluid mass flow was set to zero while for the discharging process the temperature in the computational grid was set to the temperature distribution at the end of the charging process and the fluid mass flow was set to zero too.

4 Results and discussion

In the Figures 6 to 8 the simulated temperature data for the mass flow and the storage material are evaluated at the same layers as the corresponding thermocouples installed in the test rig. The curves in the Figures 6 to 8 referred to as inlet temperature and outlet temperature comply with the HTF temperature at the inlet (in case of the charging process located at the top and in case of a discharging process located at the bottom of the FBR)

and the outlet (at the bottom during charging and at the top during the discharging process) of the storage vessel.

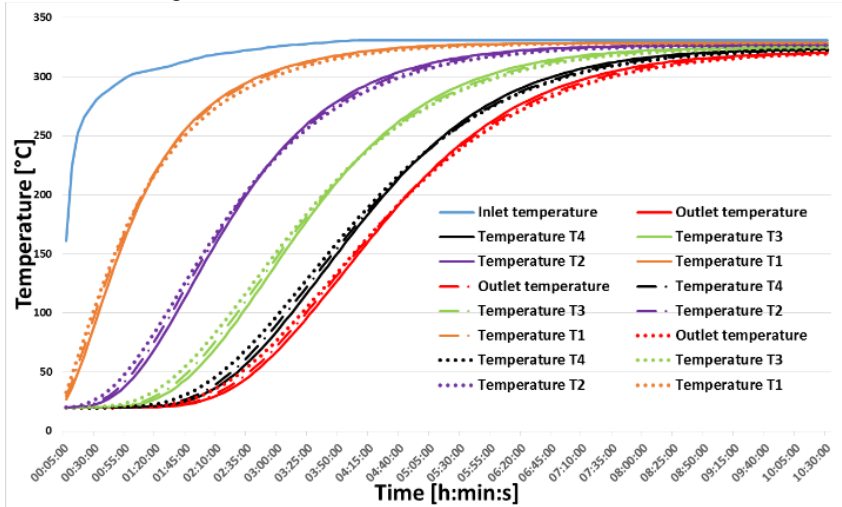


Figure 6. Temperature distribution in FBR and HTF during charging process calculated with different heat transfer correlations

The temperature development of the crushed rock and HTF over the time is presented in Figure 6. The curves pictured as full lines are calculated with the help of [10], the dotted lined curves with [11], and the dotdashed lines with [12]. As illustrated in Figure 6 that no significant difference between the single temperature curves (at the same layer of the FBR or the inlet and outlet temperature of the HTF) is given. This suggests that it makes no difference which of the correlations will be used for further investigations. In the further simulations the correlation according to Wakao et al. [10] was selected.

In the following Figures 7 and 8 the dashed lines represent the measured and the full lines the simulated data.

In Figure 7 the simulation result for the charging and in Figure 8 the result for the discharging process is compared with experimental data. The numerical simulation was done for a porosity of $\phi = 0,6$. As it can be seen in Figure 7 the deviation between the experimental and numerical data increases with progressing charging time. The deviation is larger at layers close to the HTF outlet at the bottom of the FBR while at the HTF inlet (located at the top of the FBR) the deviation is small. However, the simulated temperature growth slightly too fast compared to the experimental data. This has the consequence that the charging process is completed faster compared to the real application.

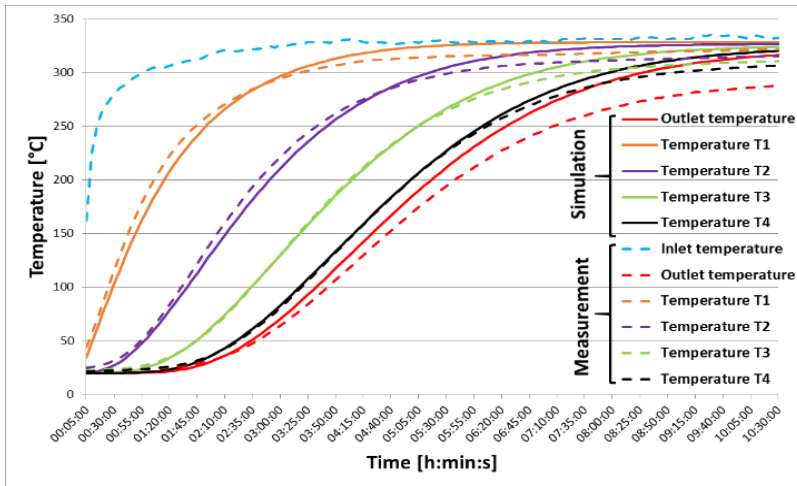


Figure 7. Temperature comparison between measurement and simulation during charging process

A comparison of the simulation result with experimental data for the discharging process which is presented in Figure 8 shows a similar behaviour as the charging process.

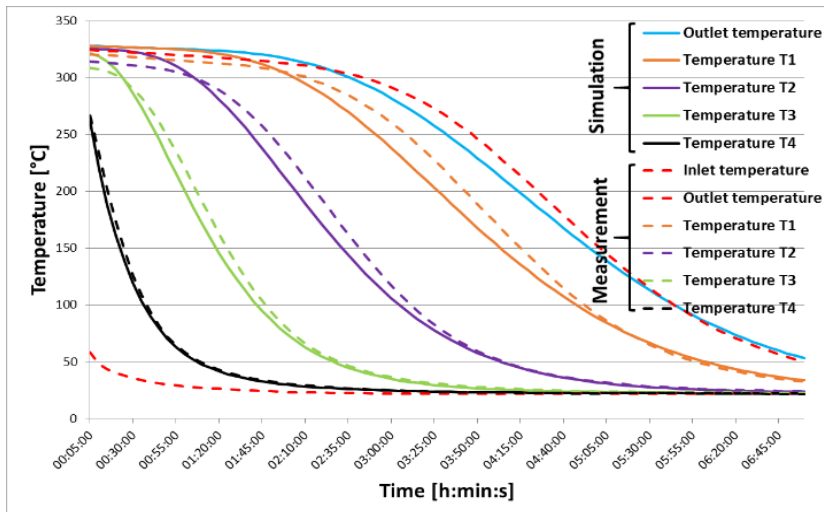


Figure 8. Temperature comparison between measurement and simulation during discharging process

The deviation of measured data and simulation is larger especially in the region where the temperature of the HTF and the storage material is high and the simulation time is advanced (between approx. 1,5 h and 5 h). With decreasing temperature (HTF outlet temperature as well as crushed rock temperature) the deviation decreases.

This behaviour of the storage vessel maybe can be a result of an slightly underestimation of the porosity or with other words the bulk material within the storage vessel was somewhat overrated compared to the laboratory test rig.

However, the overall behaviour of the numerical simulation shows a good agreement with the experimental data.

5 Conclusion

The energy market changes in direction to a high volatile power grid based on the increasing proportion on renewables (e.g., biomass, wind, photovoltaics, water, ...) within the electrical grid. This must be result in new strategies for the energy supply (renewable or thermal), distribution, and storage.

This article deals with the experimental and numerical analysis of a thermal energy storage behaviour of a fixed bed regenerator. In a first step measurements of the temperature and mass flow of the HTF as well as of the temperature distribution within the storage material was done. After that a three dimensional numerical model of the FBR was created. The numerical simulation of the FBR was done under the same conditions as the experimental investigation. The comparison of the experimental data with the numerical result shows a good agreement. Only a slightly underestimation of the porosity used for the numerical investigation was found.

Additional a comparison of three heat transfer correlations for the heat transfer between the crushed rock and the HTF was presented. The comparison has shown no significant difference between the numerical results calculated with the different correlations.

Acknowledgements

The K-Project GSG—GreenStorageGrid (grand number 836636) is funded in the framework of COMET—Competence Centers for Excellent Technologies by the Federal Ministry of Transport, Innovation and Technology, the Federal Ministry of Science, Research and Economy, the Vienna Business Agency, the Federal Province of Lower Austria and by the Federal Province of Upper Austria. The program line COMET is administrated by the Austrian Research Promotion Agency (FFG (Österreichische Forschungsförderungsges.)). The authors would also like to thank the project partners Valmet GesmbH., EVN AG, ENRAG GmbH. and Primetals Technologies GmbH.

References

- [1] European Commission, “Report of the Commission to the European Parliament, Council, the European Economic- and Social Committee and the Committee of the Regions” - progress report "Renewable energy", 2013.
- [2] Austria Energy Agency, “Actual developments of the global power supply and their influence to the national and international energy market”, Federal Ministry of Science, Research and Economics, 2014.

- [3] P. Steiner, K. Schwaiger, M. Haider, H. Walter, M. Hämmerle, “Increasing load flexibility and plant dynamics of caloric power plants via the implementation of thermal energy storage”, presented at the ASME 2016 Power Conference, Charlotte, North Carolina, Paper-No. POWER2016-59181, 2016, p. 10.
- [4] R. Hofmann, M. Haider, S. Dusek, M. Koller, H. Walter, “Integration von thermischen Speichertechnologien als Flexibilisierungsmaßnahme für industrielle Energieanlagen”, *VGB Power Tech*, vol. 96, No. 8; pp. 27 - 35, 2016
- [5] P. Drochter, “*Design, construction and erection of a fixed bed regenerator*”, MS-thesis, TU-Wien, 2016 (in German).
- [6] ANSYS, „ANSYS Fluent User's Guide, Release 15.0, 2014.
- [7] M. Kaviany, “*Principles of heat transfer in porous media*”, Springer-Verlag, 1995.
- [8] S.. Ergun, “Fluid flow through packed columns”, *Chemical Engineering Science*, vol. 48, No. 2, pp. 89-94, 1952.
- [9] M. Giese, “Strömung in porösen Medien unter Berücksichtigung effektiver Viskositäten”, PhD. TU-Munich, 1998.
- [10] N. Wakao, S. Kagueli, T. Fuazkri, “Effect of fluid dispersion coefficients on particle-to-fluid heat transfer coefficients in packed beds”, *Chemical Engineering Science*, vol. 34, pp. 325-336, 1979
- [11] J. Coutier, E. Farber, “Two applications of a numerical approach of heat-transfer process within rock beds”, *Solar Energy*, vol. 29, No. 6, pp. 451-462, 1982.
- [12] S. R. P. H. Singh, J. Saini, “Performance of a packed bed solar energy storage system having large sized elements with low void fraction”, *Solar Energy*, vol. 87, pp. 22-34, 2013.
- [13] K. Vafai, M. Sözen, “Analysis of energy and momentum transport for fluid flow through a porous bed”, *Journal of Heat Transfer*, vol. 112, pp. 690-699, 1990.
- [14] F. Mayrhuber, “*Transient numerical simulation of the storage behaviour of a fixed bed regenerator*”, MS-thesis, TU-Wien, 2017 (in German; in completion stage).
- [15] K. Kadoya, N. Matsunaga, A. Nagashima, “Viscosity and Thermal Conductivity of Dry Air in the Gaseous Phase”, *Journal of Physical and Chemical Reference Data*, vol. 14, no. 4, pp. 947-970, 1985
- [16] Knauf isolation GmbH, “Data sheet for Wired Mat WM 640”, May 2014.
- [17] S. Al-Ajlan, “Measurements of thermal properties of insulation materials by using transient plane source technique”, *Applied Thermal Engineering*, vol. 26, no.17-18, pp. 2184-2191, 2006
- [18] K. Kelley, “Contribution to the data on theoretical metallurgy: XIII. high-temperature heat-content, heat-capacity, and entropy data for the elements and inorganic compounds”, U.S. Government Printing Office, Washington, 1960.
- [19] G. Zanganeh, A. Pedretti, S. Zavattoni, M. Barbato, A. Steinfeld, “Packed-bed thermal storage for concentrated solar power – Pilot-scale demonstration and industrial-scale design”, *Solar Energy*, vol. 86, pp. 3084-3098, 2012.
- [20] W. H. Somerton, “*Thermal properties and temperature-related behavior of rock/fluid systems*”, series in Developments in Petroleum Science, Elsevier, vol. 37, 1st. edition 1992.
- [21] W. Churchill, H. H. S. Chu, “Correlating equations for laminar and turbulent free convection from a horizontal cylinder”, *Int. Journal Heat Mass Transfer*, vol. 18, pp. 1049–1053, 1975.

Transient Numerical Analysis of a Finned Tube Design with Combined Longitudinal and Transversal Fins for Latent Thermal Energy Storage Devices

MICHAEL HAMETER, MICHAEL BÖSWARTH & HEIMO WALTER

Abstract The present paper deals with the numerical modeling and simulation of latent heat thermal energy storage (LHTES) systems. The results of a comparison of a numerical investigation on the melting process of sodium nitrate, by using longitudinal finned tubes with and without additional transversal fins will be presented. In a former numerical study it was found that tubes with longitudinal fins shows an unfavorable melting behavior at the top of the tube with respect to the heat fed to the sodium nitrate while for tubes with transversal fins a high number of fins (small fin spacing) must be used to get the same charged power into the storage material.

The numerical analysis shows that the overall time for charging and discharging of the LHTES can be significantly reduced by the use of transversal fins in combination with the longitudinal fins.

Keywords: • latent energy storage • sodium nitrate • phase change material • heat exchanger tube design • numerical simulation •

CORRESPONDENCE ADDRESS: Michael Hameter, Dipl.-Ing., Department Thermodynamics and Thermal Engineering, TU Wien, Institute for Energy Systems and Thermodynamics, Getreidemarkt 9/302; 1060 Vienna, Austria, email: michael.hameter@tuwien.ac.at. Michael Böswarth, Bac., Department Thermodynamics and Thermal Engineering, TU Wien, Institute for Energy Systems and Thermodynamics, Getreidemarkt 9/302; 1060 Vienna, Austria, email: michael.boeswarth@htlstp.at. Heimo Walter, Ao.Univ.Prof.Dr., Department Thermodynamics and Thermal Engineering, TU Wien, Institute for Energy Systems and Thermodynamics, Getreidemarkt 9/302; 1060 Vienna, Austria, email: heimo.walter@tuwien.ac.at.

1 Introduction

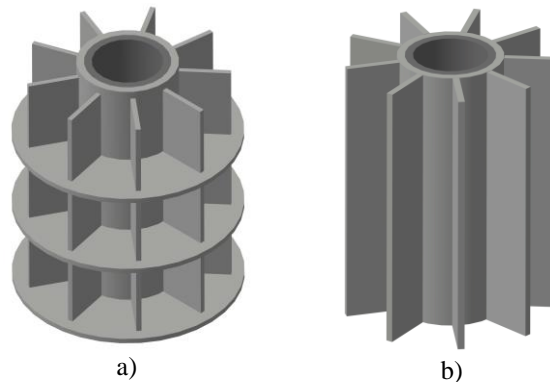
The electricity production from renewable energy sources like wind, photovoltaic, and thermal solar energy is less predictable than the primary energy resources oil, gas, or coal. At the present the only way to decouple the renewable energy sources from consumption and integrate them efficiently in the power grids are energy storage systems. Storage systems could also significantly reduce the needed backup capacities in the power grids [1], which are nowadays provided by fossil fuelled power plants. In 2014, the share of renewable energy sources reached 16% of gross final energy consumption in the European Union [2]. To achieve the ambitious goals to higher the share of renewable energy sources to 20% till 2020 further expansion of renewable energies has to be implemented. Therefore energy storage and energy distribution will be growing markets and key topics for research and development for the next decades. One possibility to store electricity as well as heat (this can be waste heat or electrical energy transformed to heat by for example electrode boilers or heat pumps, see e.g. [3]) are thermal energy storage (TES) devices. TES devices can be subdivided into sensible, latent and thermo-chemical systems. At the moment increased efforts are being made in research and development of all three systems see e.g. [4], [5], [6] and [7]. The energy density of a so called phase change material (PCM) which is used in a latent heat thermal energy storage systems (LHTES) can be 5-14 times higher than a sensible storage material such as water, sand, or rocks [8], due to the fact that the enthalpy of fusion of the PCM can be utilized in LHTES systems. A further advantage of a LHTES system is that the charging and discharging take place at a small temperature difference around the melting point. Therefore they are well suited to store heat from condensation or for evaporation processes in an exergetically optimal way. A very common problem for the most PCMs is however the fact, that they suffer from a poor thermal conductivity in the solid as well as liquid phase. To overcome this problem, various enhancement techniques are under investigation, see e.g. [9].

In this article vertical arranged finned heat exchanger tubes are used to enhance the heat transfer into the PCM. Two different finned heat exchanger tube designs for LHTES systems will be compared in this numerical study. In [10] it was stated that longitudinal fins should be the preferred design. Additionally in the former thesis [11] it was found that the division of a simulation model over its height in several unconnected chambers leads to faster melting and solidification of the storage material, e.g. NaNO_3 . Therefore in a new design longitudinal fins were complemented by transversal fins, which should help to prevent that the molten salt instantly rises up to the highest point of the heat exchanger (HEX). Thereby the molten salt doesn't form a large molten area at the upper part of the HEX where the temperature is approx. identical to the melting temperature, which will reduce the effective heat transfer area and thus the heat transport into the system.

2 Numerical Model of the Analysed Heat Exchanger Tube

2.1 Physical model

In Figure 1 the models of the two heat exchanger tubes used in the present study for the heat transfer from the working fluid, which flows inside the tube, to the surrounding sodium nitrate (NaNO_3), which is used as PCM is pictured. The finned tubes consist of a plain steel tube while the fin material is aluminum. To take the heat transfer by natural convection into consideration a three dimensional numerical simulation of the melting behaviour of the PCM must be done, see [12]. Design a) consists of a combined design out of longitudinal fins with transversal fins, while in design b) just longitudinal fins are used.



a) with b) without transversal fins
Figure 1. Heat exchanger tube design

2.2 Mathematical model

The numerical simulations presented in this paper have been carried out in the commercial CFD code ANSYS FLUENT 15.0. For the modelling of the solidification and melting processes in ANSYS FLUENT the predefined enthalpy-porosity model according to [13] has been used. For the pressure velocity coupling the COUPLED scheme was applied. For the mushy zone constant C which effects the pressure drop in a porous media (mushy zone, see [13]) $C=10^6 \text{ kg/m}^3\text{s}$ was used. All the other parameters have been chosen accordingly to the simulations described in [14] and [15]. The thermo physical properties of aluminium and steel are taken from the ANSYS FLUENT property data base. For the important values of the PCM for the numerical simulation, melting temperature $T_m=579.15 \text{ K}$, heat of fusion $L=176.256 \text{ kJ/kg}$, specific heat capacity, thermal conductivity, dynamic viscosity, and density an user defined function was programmed, which is also described in detail in Ref. [15].

2.3 Numerical model

To reduce the needed computation time the simulation domain is reduced to a 100 mm high wedge of the finned tube, by use of the 18-fold rotational symmetry. In Figure 2 the dimensions of the two finned heat exchanger tubes are depicted.

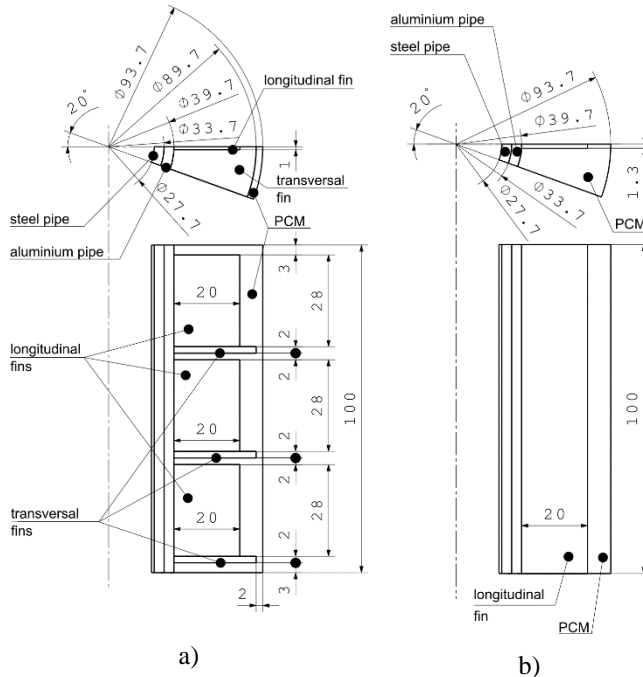


Figure 2. Computational domain and geometry data of the analyzed heat exchanger tube a) with b) without transversal fins

For better comparability the geometrical dimensions of the different designs have been selected in such a way, that the fin thickness, the fin height as well as the tube dimensions are nearly identical in both design configurations as well as in the former work [12]. The analysis was done for a vertical arrangement of the heat exchanger tubes. In the present study the fin height of the longitudinal fin was 20 mm, the fin thickness 2 mm for the design with transversal fin and the plain tube dimension was $\text{Ø}33.7 \times 3$ mm for all analyzed designs. To compensate the additional HEX volume due to the transversal fins the fin thickness of the design b) without transversal fin had to be enlarged to 2,5 mm. The three transversal fins divide the PCM volume in three big and one small vertical arranged chamber. These chambers are connected by a 2 mm gap between the tip of the transversal fin and the outer shell so that the PCM can expand and a pressure between the fins due to expansion of the PCM is reduced

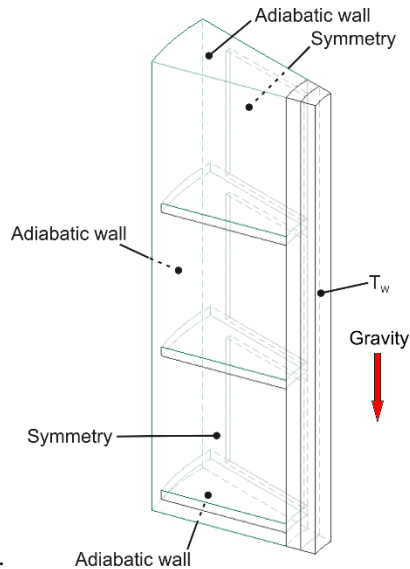


Figure 3. Boundary conditions used for the analyzed heat exchanger configurations

The boundary conditions used in the simulations are presented in Figure 3. For both lateral surfaces symmetry boundary conditions are used, while at the top and the bottom as well as at the outer shell an adiabatic wall is defined. For the numerical simulations, the initial temperature of the whole system (steel tube, aluminium profiles and NaNO_3) was 569.15 K for the melting simulation. The wall surface temperature T_w , which represents the boundary conditions at the inner steel tube diameter surface to the heat transfer fluid, was 599.15 K. For the whole charging process T_w was kept constant.

For a better comparison of the two design cases the volume ratio \square and the reciprocal length \square (definition see [15]) should be approximately the same. Table 1 shows these parameters for both design cases. They are in the same range as the models described in [10], [12], [14] or [15].

Table 1. Parameters of the design cases

Parameter	Unit	Case a)	Case b)
Volume ratio \square	-	0.799	0.828
Reciprocal length \square	1/m	0.7828	0.609
Control volumes	-	120425	101530

3 Numerical Results and Discussions

3.1 Melting process

In Figure 4 and 5 the evolution of liquid fraction of the NaNO_3 for the two different analyzed heat exchanger tube designs at the specific points of time of 115s, 400s, 600s after simulation start are presented.

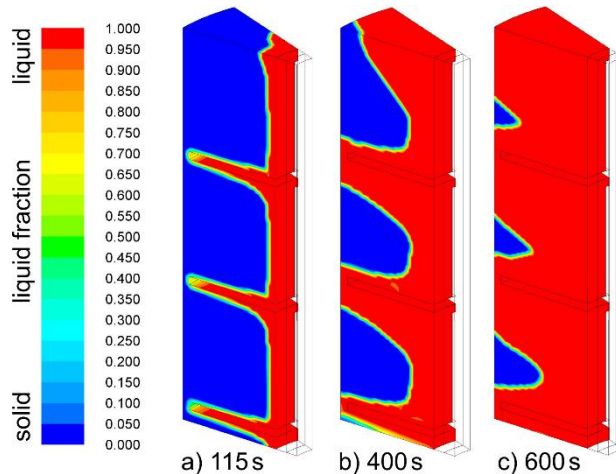


Figure 4. Contours of the liquid fraction evolution of the PCM during melting a) 115 s, b) 400 s, c) 600 s after simulation start, design with transversal fins

At the beginning of the charging process the thermal energy coming from the tube is first distributed over the steel tube to the aluminium tube and furthermore to the fins because of the higher thermal conductivity of the HEX compared to the PCM. At this time the melted zone is very small, and heat conduction is the dominant heat transfer mechanism. In radial direction melting starts at the tubular inner parts of the HEX where the longitudinal fin is connected with the tube. Over the height of the computational domain the melting front first starts in case of the design b) without transversal fin at the upper surface and then the melting front grows downwards and synchronous in direction to the outer shell of the computational domain (see Figure 5). With the transversal fin design a) the melting starts synchronous under each transversal fin and shortly after also over each transversal fin. Due to the density difference the molten NaNO_3 rises up along the surface of the aluminium tube and fins and the cooler liquid sodium nitrate moves downward along the solid NaNO_3 . This vortex flow enhances the heat transfer in the molten region to the porous mushy zone. The originating asymmetric melt front of the PCM indicates that the influence of natural convection (buoyancy-driven currents) during the charging process plays a key role. This was also observed experientially in [5]. Whereas without the transversal fins the molten salt instantly rises up to the highest point of the HEX,

where the molten PCM sensibly heats up, the transversal fins prevents that the salt rises through the small gap between the top of the transversal fin and the outer shell to the next chamber during the first period.

Based on the horizontal orientation of the transversal fins (see Figure 1a), the buoyancy-driven flow is restricted over a long period of the melting time to the volume between two opposite fins. However the space between the fins is as high that further enlarging of the distance between two transversal fins would just slightly increase the velocity of natural circulation. Furthermore the heat transfer is increased by the longitudinal fins in each free space. Not till the PCM in the 2 mm wide gap between outer shell and horizontal fin is molten, approx. 220 s after simulation start and a free path originate, the molten PCM can flow upwards from one chamber to the next one. Simultaneously the still solidified PCM is separated in three portions.

It can be seen in Figure 5 that without the transversal fins, the molten salt forms a large area of liquid PCM approx. 400 s after simulation start. This molten area further enlarges downward and heats up approx. the same of the HEX.

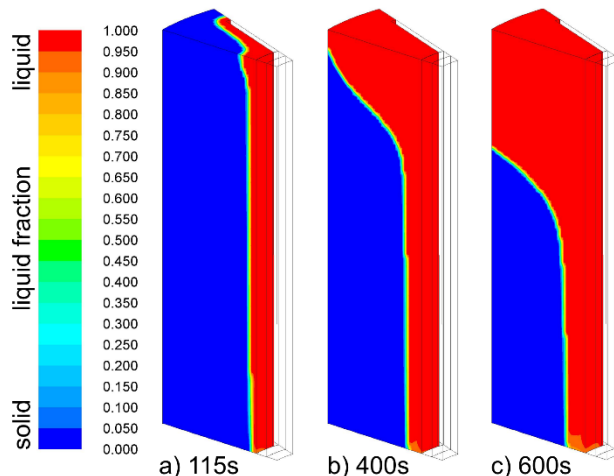


Figure 5. Contours of the liquid fraction evolution of the PCM during melting a) 115 s, b) 400 s, c) 600 s after simulation start, design without transversal fins

Due to the small temperature difference between HEX and PCM the buoyancy driven currents and hence the velocity in the molten PCM reduces to zero (see Figure 6). Thereby this area of resting molten PCM reduces the effective heat transfer area and thus the heat transport into the storage system. Figure 6 shows the vector plot of the liquid velocity of the molten PCM.

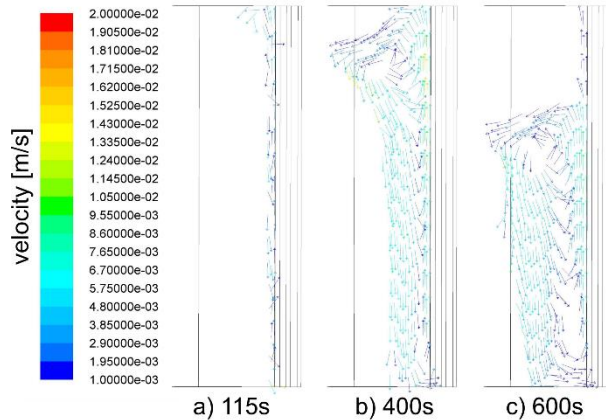


Figure 6. Vector plot of the liquid velocity of the PCM during melting in the vertical centre plane a) 115 s, b) 400 s, c) 600 s after simulation start, design with transversal fin

The temperature distribution for both design cases is depicted in Figure 7 and Figure 8. It can be identified in Figure 7 that the transversal fins yield a better radial temperature distribution as a result of the higher heat conductivity in the aluminium fins compared to the NaNO_3 .

Moreover it can be observed that the molten PCM at the top of the design without transversal fins is already heated to the temperature of the HEX so that this area doesn't support the heat transfer anymore, it is ineffective at this time. In contrast to that, a design with transversal fins leads to a more uniform temperature distribution over the height of the HEX and even the molten salt at the top of each chamber is not fully heated to the HEX temperature.

Although a possible sinking of the solidified PCM isn't considered in these simulations, it can be said that another advantage of the transversal fin is that they would prevent the sinking of solid PCM. Without sinking of the solid PCM it can be assured that there will be a solidified PCM over the whole HEX-height for a longer time, therefore a faster and more uniform heat transfer is assured.

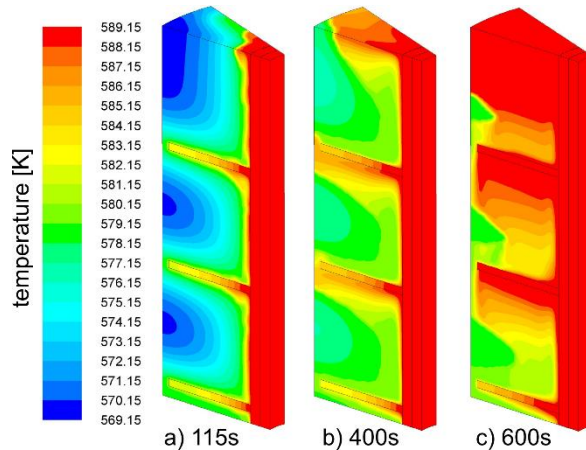


Figure 7. Contours of the temperature of the design with transversal fin a) 115 s, b) 400 s, c) 600 s after simulation start

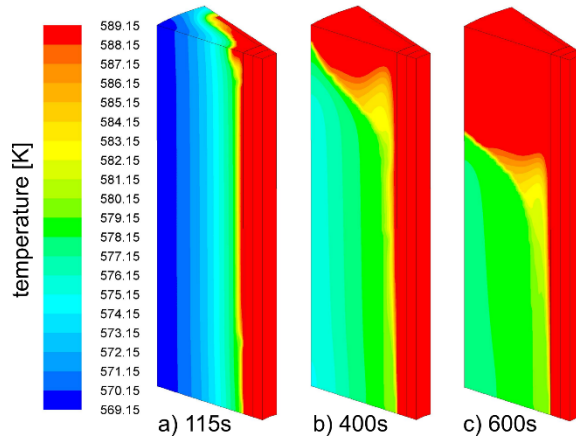


Figure 8. Contours of the temperature of the design without transversal fin a) 115 s, b) 400 s, c) 600 s after simulation start

Figure 9 shows a comparison of the time sequences of the volume averaged temperature and of the liquid fraction of the NaNO_3 for the two analyzed design cases. In Figure 9 also the point in time where the melting process of the sodium nitrate is completed can be observed. The overall melting time for a complete melting show the higher performance of the fin design with transversal fins. The use of transversal fins shortens the time for complete melting by 40% from 1200 s to 700 s compared to the design without this additional fin arrangement. During the first 40 s there is no difference between both designs in the time sequences of volume averaged temperature and liquid fraction observable because of the heat distribution in the finned tube. After approx. 115s

both designs show a linear increase of liquid fraction with constant melting speed of approx. 0,183 %/s for the design with transversal fins and 0,108 %/s without these fins up to 90% liquid fraction. During the first 500 s there is hardly any difference in the time sequence of volume average temperature between the two fin designs and just slight increase of temperature observable after the first sensible heating-up. After 500 s approx. 90% of sodium nitrate is molten with the transversal fin design and the three last solid PCM areas begin to melt which leads to a fast increase in volume average temperature. At the time of complete melting after approx. 700 s the curve flattens and the volume average temperature increases to the steady state. At this point of time further transferred heat is stored just in sensible way and the temperature difference between the HTF and the PCM becomes very small.

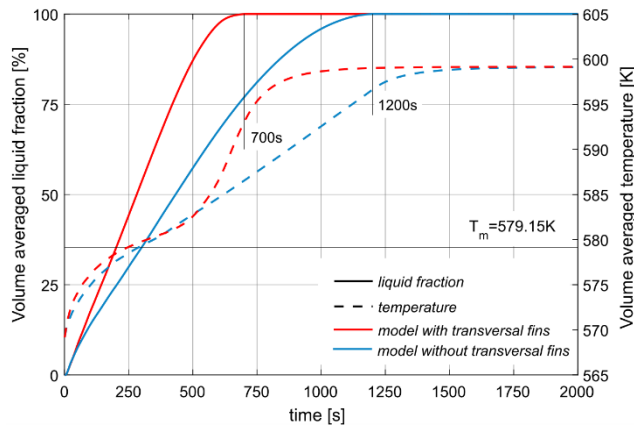


Figure 9. Chronological sequence of the volume averaged temperature and liquid fraction of the NaNO_3

A comparison of the development of the volume average charged power density of the NaNO_3 over the time is presented in Figure 10. Starting with values higher than 100 kW/kg for both designs during heating of the HEX the power density drops after approx. 115 s to approx. 19.5 kW/kg and stays constant at this value for the design with transversal fins, whereas without the transversal fins the power density drops to approx. 14.5 kW/kg and stays constant at approx. 12.5 kW/kg. 400 s after simulation start the molten salt reaches the outer shell. This reduces the overall heat flow because the solid PCM isn't anymore available as heat sink over the full height of the HEX.

It can be observed that as a result of the better heat transfer of the design with additional transversal fins the transferred power into the NaNO_3 is higher during the first charging period compared to the second design case.

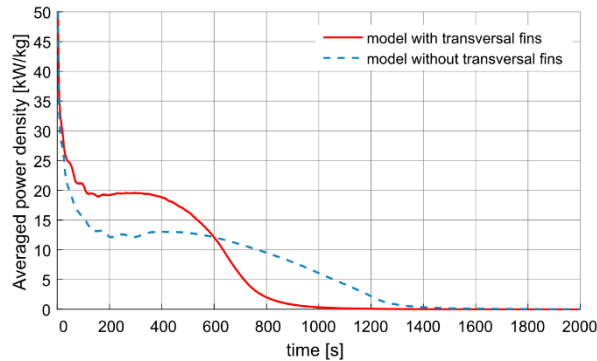


Figure 10. Chronological sequence of the volume averaged charged power density of the NaNO₃

In Figure 11 and 12 the heat flux over height and time for both designs is presented. As mentioned above the heat flux for the design without transversal fins (Figure 12) quickly drops too zero for the upper part of the HEX (height = 0.1 m) while the lower part (height = 0.0 m) is transferring most of the energy. Therefore the heat flux even rises again after 500 s and a local maximum can be observed for the lower area of the HEX.

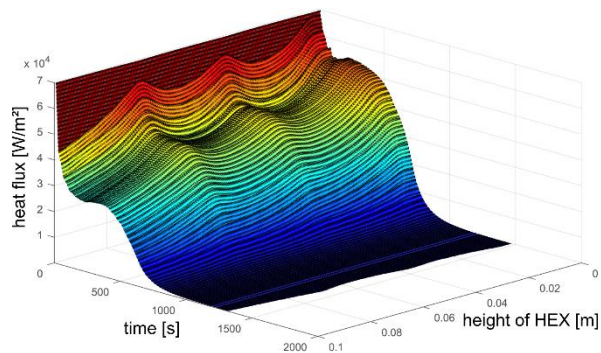


Figure 11. Heat flux as function of time and height for the design with transversal fins

Whereas the design with transversal fins (Figure 11) shows higher heat fluxes as well as a more uniform heat flux distribution over the height in which also the higher parts of the HEX are efficiently transferring heat. Nevertheless also with the transversal fins the bottom of the HEX has a higher heat flux than at the top. The vertical position of the transversal fins can be clearly identified in the chart by local maximums of heat flux over the height.

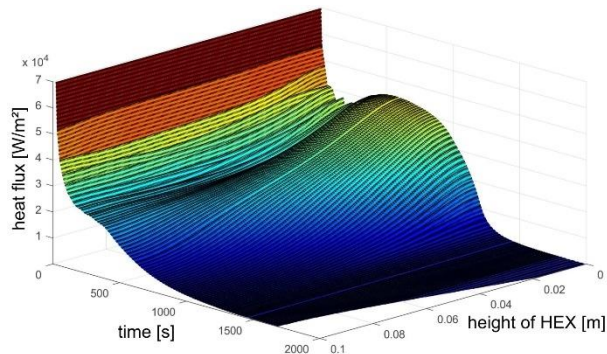


Figure 12. Heat flux as function of time and height for the design without transversal fins

4 Conclusions

In the present work numerical simulations have been conducted to compare two different finned tube designs for the use in a LHTEs system. The results have shown that the use of transversal fins together with longitudinal fins shortens the time for complete melting by 40% from approx. 1200 s to approx. 700 s compared to the design without this transversal fins. Simultaneously the charging power is increased. The reason for the higher performance is that the transversal fins prevent that the molten salt instantly rises up to the highest point of the HEX. Thereby the molten salt doesn't form a large molten area at the upper part of the HEX where the temperature is approx. identical to the melting temperature, which will reduce the effective heat transfer area and thus the heat transport into the system. That leads to a more uniform temperature distribution over the height of the HEX and even the molten salt at the top of each chamber is not fully heated to HEX temperature. Therefore the combined heat exchanger tube design of longitudinal fins with transversal fins should be the preferred design. In the future experiments should be conducted to validate the positive effect of the combined longitudinal fin design with transversal fins.

Acknowledgements

The K-Project GSG—GreenStorageGrid (grand number 836636) is funded in the framework of COMET—Competence Centers for Excellent Technologies by the Federal Ministry of Transport, Innovation and Technology, the Federal Ministry of Science, Research and Economy, the Vienna Business Agency, the Federal Province of Lower Austria and by the Federal Province of Upper Austria. The program line COMET is administrated by the Austrian Research Promotion Agency (FFG (Österreichische Forschungsförderungsges.)).

The authors would also like to thank the project partners Valmet GesmbH., EVN AG, ENRAG GmbH. and Primetals Technologies GmbH. for the pleasant and constructive working relationship.

References

- [1] F. Steinke, P. Wolfrum and C. Hoffmann, "Grid vs. storage in a 100% renewable Europe", *Renewable Energy*, vol. 50, pp. 826-832, Feb. 2013.
- [2] European Commission, "Report from the Commission to the European Parliament, the Council, the European Economic- and Social Committee and the Committee of the Regions" - progress report "Renewable energy", 2017.
- [3] C. Pieper et al., "Die wirtschaftliche Nutzung von Power-to-Heat Anlagen im Regelenergiemarkt", *Chemie Ingenieur Technik* (4), vol. 87, pp. 390-402, Apr. 2015
- [4] P. Steiner et al., "Fluidized bed particle heat exchanger for supercritical carbon dioxide power cycles", presented at 10th International Conference on Energy Sustainability, Charlotte, North Carolina, 26.06.2016 - 30.06.2016, Paper-Nr. ES2016-59053.
- [5] G. Urschitz, H. Walter, M. Hameter, "Laboratory Test Rig of a LHTES (Latent Heat Thermal Energy Storage): Construction and First Experimental Results", *Journal of Energy and Power Engineering*, vol. 8, no.11, pp. 1838-1847, Nov. 2014.
- [6] S. Almsater et al., "Development and experimental validation of a CFD model for PCM in a vertical triplex tube heat exchanger", *Applied Thermal Engineering*, vol. 116, pp. 344-354, Apr. 2017.
- [7] J. Widhalm et al., "Thermochemical Energy Storage as A Way to Increase The Sustainability of Energy Generation", presented at the Asian Conference on Sustainability, *Energy and the Environment*, Kobe, Jun 2015.
- [8] A. Sharma et al., "Review on thermal energy storage with phase change materials and applications", *Renewable and Sustainable Energy Reviews*, vol. 13 (2), pp. 318-345, Feb. 2009.
- [9] Agyenim F. et al., "A review of materials, heat transfer and phase change problem formulation for latent heat thermal energy storage systems (LHTESS)", *Renewable and Sustainable Energy Reviews*, vol. 14, pp. 615–628, 2010.
- [10] A. Beck et al., "Transient numerical analysis of different finned tube designs for use in latent heat thermal energy storage devices", presented at the 2015 ASME Power and Energy Conference, San Diego, CA, USA, 28.06.2015 - 02.07.2015, Paper-Nr. PowerEnergy2015-49144
- [11] C. Lohninger, "Investigation of the influence of the model size on the result of the numerical simulation of melting and solidification processes", Bachelor's Thesis, Vienna University of Technology, Vienna, Austria, 2015 (in German).
- [12] H. Walter, A. Beck, M. Hameter, "Influence of the Fin Design on the Melting and Solidification Process of NaNO₃ in a Thermal Energy Storage System", *Journal of Energy and Power Engineering*, vol. 9, pp. 913-928, Nov. 2015.
- [13] M. Hameter, H. Walter, "Influence of the Mushy Zone Constant on the Numerical Simulation of the Melting and Solidification Process of Phase Change Materials", presented at the 26th European Symposium on Computer Aided Process Engineering, Portoroz, Slovenia, 12.06.2016 - 15.06.2016, pp. 439-444.
- [14] M. Koller et al., "Comparison of Different Heat Exchanger Tube Designs used in Latent Heat Thermal Energy Storage Systems - a Numerical Study", presented at the 26th European Symposium on Computer Aided Process Engineering, Portoroz, Slovenia, 12.06.2016 - 15.06.2016, pp. 277-282.
- [15] M. Koller, H. Walter, M. Hameter, "Transient Numerical Simulation of the Melting and Solidification Behavior of NaNO₃ Using a Wire Matrix for Enhancing the Heat Transfer", *Energies*, vol. 9 (3), Mar. 2016, Paper-Nr. 205.

Thermal Energy Storage Composites Based on Clay and Phase Change Materials

MILENA STOJILJKOVIĆ, STANIŠA STOJILJKOVIĆ, SAŠA SAVIĆ, SANJA PETROVIĆ,
MIRJANA RELJIĆ & BRATISLAV TODOROVIĆ

Abstract To optimize the heat conversion, the key is to integrate it with the system thermal energy storage. Among the many materials for storage of thermal energy materials include phase change due to the latent heat of melting-fusion. In general all materials which change phase having low thermal conductivity. Nanoadditive are necessary to enable the power of continuous linear exchanged. Nanomaterials are used as additives in order to change the characteristics of the basic materials. Added into the fluid it creates the mixture which is referred to as nanofluids. Adding nanomaterials to phase change materials obtained the nanocomposites. In our work we integrated nanocomposites in nanofluids. The modified bentonite clay is a nanomaterial, which builds with water a gel, which is well blended with the phase change materials, hydrated salts, activated carbon, etc. The resulting composite is nanofluids gel, with very pronounced thixotropy. The clay-water nanofluid gel shows a high thermal conductivity and specific heat. Hydrate salt (Glauber's salt), paraffin and stearic acid have a relatively high melting latent heat. Clay nanoparticles containing aluminum oxide and silicon, provide better dispersion and homogeneous distribution of the composite material. The purpose of our work is to find the ratio of clay nanocomposites by phase change material in order to achieve a good heat capacity and a good thermal regeneration. The aim is to determine the composite mixture that has the best storage capacity of heat to 100°C.

Keywords: • Thermal storage • bentonite clay • Glauber's salt • paraffin • stearic acid • activated carbon •

CORRESPONDENCE ADDRESS: Milena Stojiljković, University of Nis, Faculty of Technology, Bulevar Oslobođenja 124, Leskovac, Serbia, e-mail: milena0919@yahoo.com. Staniša Stojiljković, University of Nis, Faculty of Technology, Bulevar Oslobođenja 124, Leskovac, Serbia, e-mail: Saša Savić, University of Nis, Faculty of Technology, Bulevar Oslobođenja 124, Leskovac, Serbia, e-mail: Sanja Petrović, University of Nis, Faculty of Technology, Bulevar Oslobođenja 124, Leskovac, Serbia, e-mail: Mirjana Reljić, 2Cis Institute, Vojislava Ilića 88, Belgrade, Serbia, e-mail: Bratislav Todorović, University of Nis, Faculty of Technology, Bulevar Oslobođenja 124, Leskovac, Serbia, e-mail:

1 Introduction

To optimize the heat conversion, the key is to integrate it with the thermal energy storage system. Among the many materials for storage of thermal energy, we highlight the phase change materials due to the latent heat of melting-fusion [1].

Generally, all materials that change the phase having low thermal conductivity. Nano-additives are necessary to enable continuous - linear energy exchange. Nanomaterials are used as additives to change the characteristics of the basic materials. Added to the fluid, produce mixture called nanofluids. Adding nanomaterials to phase change materials provide nanocomposites.

In this work we have integrated nanocomposites in nanofluids. The modified bentonite clay is the nano-material which form gel with water, and it is well miscible with a phase change materials, hydrated salts, activated carbon and others. The resulting composite is nanofluid gel, with very pronounced thixotropy. Nanofluid gel made of clay and water has a high thermal conductivity and specific heat. Hydrate salt, paraffin wax and stearic acid have a relatively high latent heat of melting [2].

The hygroscopic property of bentonite coupled with rapid, intense exothermic reaction when taken from dehydrated to hydrated form (heat of adsorption), makes bentonite effective in the storage of solar and waste heat energy [3].

Clay had a big role in ancient civilizations both as a protective agent and as a diagnostic tool and finally as a thermoregulation appliance. The gel based on clay and the corresponding salts provide multiple heating which can be used for thermal treatment of sensitive or cold parts of the body, neck or low back [4].

Montmorillonite is a typical natural mineral with nano-stratiform structure, which can be exfoliated into nanosheet or nanotube structure in water or some other solutions. The unit layer structure of MMT is 2:1 type (TOT): one octahedral clayte layer is sandwiched between two tetrahedral silica layers, together linked to slices in a two-dimensional space and then accumulates towards c-direction. Because of the isomorphous replacement (for example, the Al³⁺ in octahedron is replaced by Mg²⁺ or Fe²⁺, the Si⁴⁺ in tetrahedron is replaced by Al³⁺, there are some excess negative charges among the layers [5].

In this work was used a bentonite clay, Glauber's salt, paraffin wax, stearic acid and activated carbon powder. The aim is to determine the composite mixture that has the largest heat storage capacity to 100°C.

1.1 Thermal energy storage in buildings

In buildings where solar energy is used for heating, daily can be managed through the absorption of solar energy during the day, storing the accumulated heat and release heat at night, to prevent the fall of temperature. Also in the summer stored heat can be used as

a drive absorption cooling systems. In this way, the stored heat can be used for both heating and cooling [6].

Thermal energy storage nanocomposites gel based on clay, is made to eliminate the existing shortcomings of heat storage. Water has a linear heat and get rapidly heated and rapidly cooled, so it can not meet the needs of heat storage. Water has a higher coefficient of convection and high specific heat, which is one of the conditions is that the mixture need to comprise a high heat capacities and high thermal conductivities. On the other hand injecting material with melting latent heat at lower temperatures allows us greater thermal energy storage per unit mass of the working medium [7].

As phase-change material are used inorganic hydrate salts and organic materials such as paraffin. Exponential current changes of accumulated heat increases entropy of the system. In order to mitigate abrupt changes due to the latent heat whether using organic or inorganic additives bentonite clay must be added. Thus the amount of accumulated heat is not reduced, but possible loss of entropy is reduced due to latent phase change.

The application of the thermal energy storage phase change is of particular interest for buildings and for human clothing. These two fields allow interesting about the quality of life.

Base clay is made alkaline by modification of clay, which allows homogenization of the materials which are capable of melting heat, whether an organic or inorganic nature. Alkaline clay modification creates a gel that has a strong thixotropic. Minimal mixing it becomes a fluid and easily maneuverable. After a while it becomes firmer consistency. This combination allows the presence of water, hence high specific heat primarily. The aim is to achieve a stable thermal cycles without loss of mass media work. Increasing the thermal conductivity allow the clay particles.

By combining the mass ratio of the gel with the hydrated clay salts and paraffin wax obtained composites are obtained which can have a larger storage capacity, the thermal energy and the desired degree of cooling, or for heat recovery [8, 9].

Previous studies showed essentially the mixture of materials with a latent heat of fusion, without the participation of water and clay. The density of the heterogeneous mixture of clay based materials with the possibility of phase change is greater than organic materials. Changing the volume of heterogeneous mixtures based on clay is negligible. The advantage of this system is that the storage temperature may be higher than 100°C, but the pressure is very close to atmospheric pressure. Thermal energy storage is expanding in the last few decades, especially the global trend towards renewable energy technologies. The principle of heat storage based on the transfer of heat from the storage medium during the charging period, and then the reverse procedure takes the disclosure of heat. As reviewed, there are three main options thermal storage; conventional or linear heat storage, latent heat storage and chemical heat storage [10, 11].

1.2 Thermal energy storage with the clothing and footwear

The technology of thermal energy storage in clothes and shoes in the textile industry include the impregnation of the material with changes in fase textile structure. This improves thermal performance textiles. It would be most ideal if the excess heat produced when a person can be saved directly somewhere in the system of clothing and then, in accordance with requirements, will activate it again when there is a need for heat [12, 13].

Textile-based materials of materials with phase change react immediately upon change of the ambient temperature or the change of temperature in the different parts of the body. PCM microcapsules react by absorbing excess heat and storage phase change material. When the temperature falls again, the microcapsules released chamber that is the stored heat by phase change material to solidify. This reversibility of heat is very important to maintain a constant body temperature as in some patients, both with the profession of special purpose.

Temperature of the skin has an important role as a sensor member, which is independent of thermal comfort [14, 15]. Thus, changes in skin temperature and activate the autonomic nervous system, which triggers a series of metabolic processes. The different regions of the skin have different temperature [16, 17]. The face, chest, neck, and lower back are more sensitive to temperature changes than for example, the thigh and the leg.

1.3 Principles of thermal energy storage phase change

Thermal energy storage may be linear, then the phase change of the working fluid and a phase change storage nanoparticles [18, 19, 20]. The change in enthalpy or heat by the linear dependence is a function primarily of the specific heat. Thermal energy storage phase change depends on the latent heat of melting and is dependent on the type of material and it is jumpy and takes place at a constant temperature. While the storage of thermal energy and nanoparticles uniformly phase-change part, we can say homogeneous process, wherein the temperature profile is gentle and resembles a Gaussian distribution.

In Figure 1 is shown the temperature dependence of the enthalpy for all three methods of heat storage. Any sudden increase in enthalpy increases the entropy of the system. Nanomaterials as phase change materials with the working medium have a lower loss in entropy on the phase-shifting.

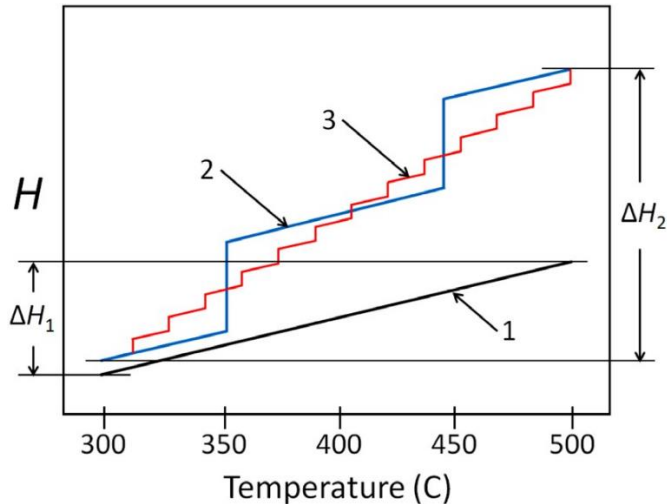


Figure 1. Dependence of enthalpy from temperature. 1-Heat stored as sensible heat, H , in a macroscale system 2-Sensible and latent heat stored in a macroscale system with two phase changes 3-Sensible and latent heat stored in a nanoscale system with many phase changes.

2 Materials and Methods

2.1 Reagents

Bentonites clay with locations Prisjan (Serbia) dried at 110°C has the following chemical composition: 51.82% SiO₂, 0.34% TiO₂, 26.86% Al₂O₃, 2.30% Fe₂O₃, 0.10 % MnO, 1.27% MgO, 1.44% CaO, 0.75% Na₂O and 2.07% K₂O, stearic acid (ARIHEM Nis), powdered charcoal (Miloje Zakic Krusevac), bentonite clay (Quartz Mladnovac), paraffin, Glauber's salt (ARIHEM Nis), clay (SHENEMIL Nis), borax (ARIHEM Nis).

2.2 Materials

We used a modified base gel of bentonite clay with additives (stearic acid, paraffin, Glauber's salt and activated charcoal). The basis of the heterogeneous system, 100 ml of water, the addition of the bentonite clay, 60 g. Intensive mixing of the resulting liquid was concentrated, which was activated with 5 g of NaOH. By further stirring the resulting gel is easily flowable mass in which are added to stearic acid, Glauber's salt, activated charcoal, and paraffin. In order to provide better nucleation Glauber's salt mixture was added 5 g borax.

2.3 Methods

The mixture was heated to a temperature of 95°C, then is placed in an isolating vessel made of polystyrene of 10 cm, which is shown in figure 2. A drop in temperature was measured every hour for 8 hours.

Prepared bases determined by the viscosity and electrical conductivity. Viscosity was tested on a rotary viscometer FUNGILAB-Visco Basic Plus using the radius R3 of the spindle 600 with the rotation speed with-1. The conductivity of the system is determined by the conductivity meter HANNA Instruments HI 8820N

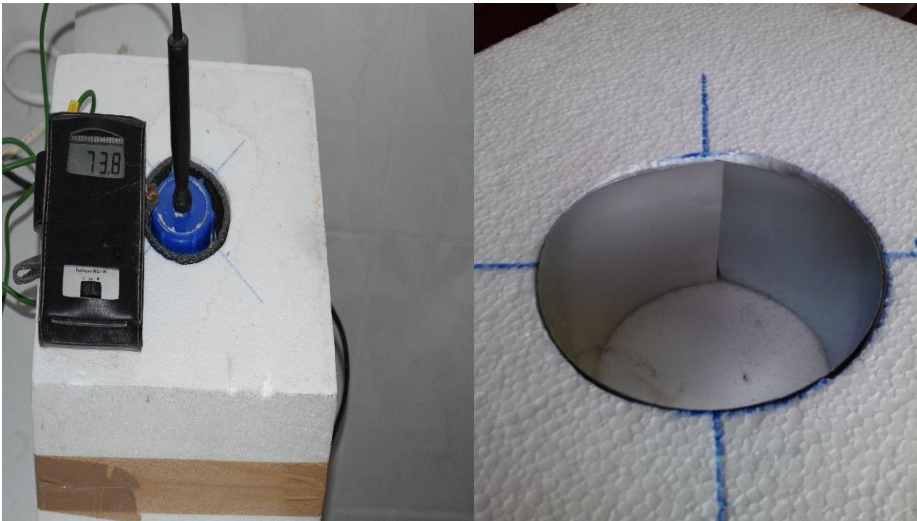


Figure 2. Laboratory model of heat storage

3 Results and Discussion

The values of physical properties (viscosity and electrical conductivity) of prepared base clay.

Tabele 1. Physical properties of prepared base clay

Viscosity (mPa s)	Electrical conductivity κ , mS
1443.8	34.5

Thermal energy storage can be achieved by a combination of water, clay and a material phase change. The gel based on clay allows for continuous change of the temperature and heat transfer, thus increasing the total entropy of the system decreases. The gel based on clay has a high specific heat, while Glauberoba salt thereof, stearic acid and paraffin enable latent heat of phase at different temperature intervals.

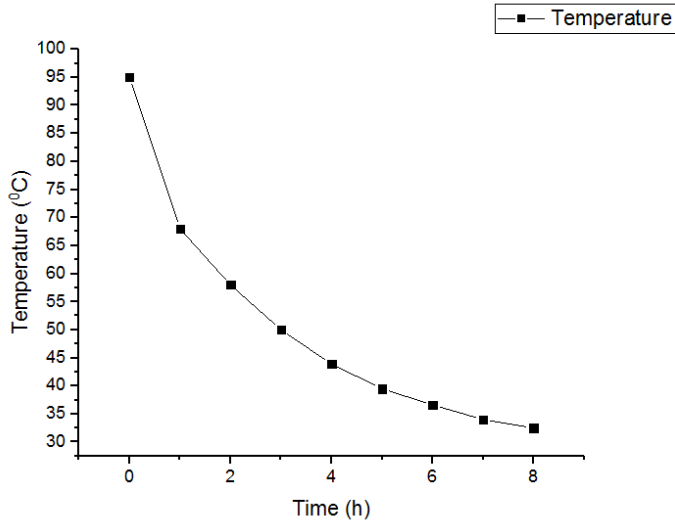


Figure 3. The temperature change of a heterogeneous gel based on clay (100 g of water, 60 g of clay, 5 g of NaOH), 20 g of stearic acid, Glauber's salt 10 g, 10 g of paraffin wax and 5 g of sodium tetraborate.

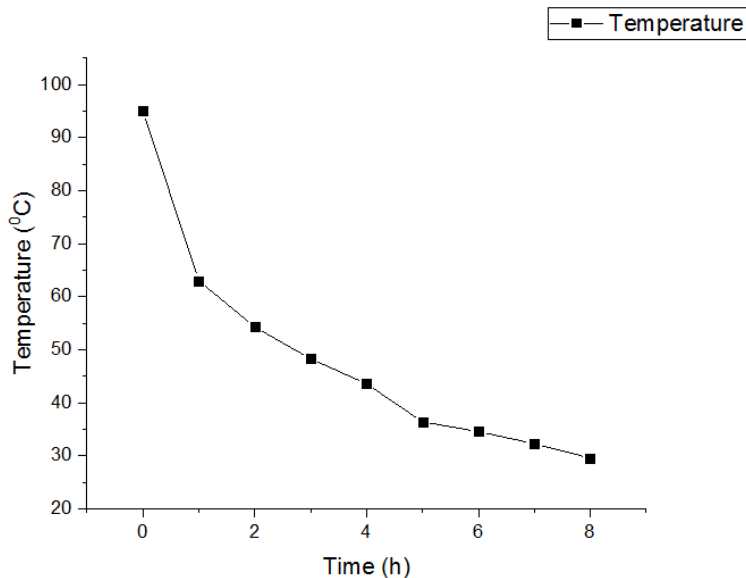


Figure 4. The temperature change of a heterogeneous gel based on clay (100g of water, 60g of clay, 5 g of NaOH), 10 g of stearic acid, Glauber's salt 20 g, 10 g of paraffin wax and 5 g of sodium tetraborate.

Activated carbon provides additional homogenization system and increased accumulation of heat. Water is cooled very slowly even less 10 degrees in a wide temperature range. Water has a high specific heat, but can not be heated at atmospheric pressure above 100°C.

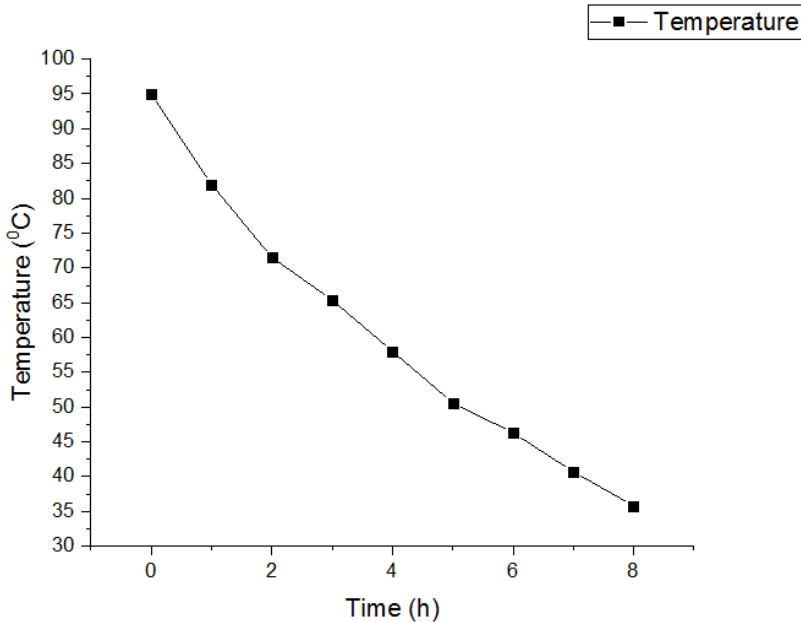


Figure 5. The temperature change of a heterogeneous gel based on clay (100 g of water, 60 g of clay, 5 g of NaOH), 20 g of stearic acid, Glauber's salt 10 g, 10 g and coal assets 5 g of borax.

A sample of active carbon has proven to be more effective because they achieve slower cooling system for heat storage. For 8 hours the temperature heterogeneous mixture dropped from 95°C to 35.8°C. Water as medium storage has good performance when it comes to storage, but there is no possibility of a combination with a phase change material as to prevent phase separation. Further work needs to optimize the amount of water and clay that would allow the accumulation of heat is absorbed easier and easier disclosure.

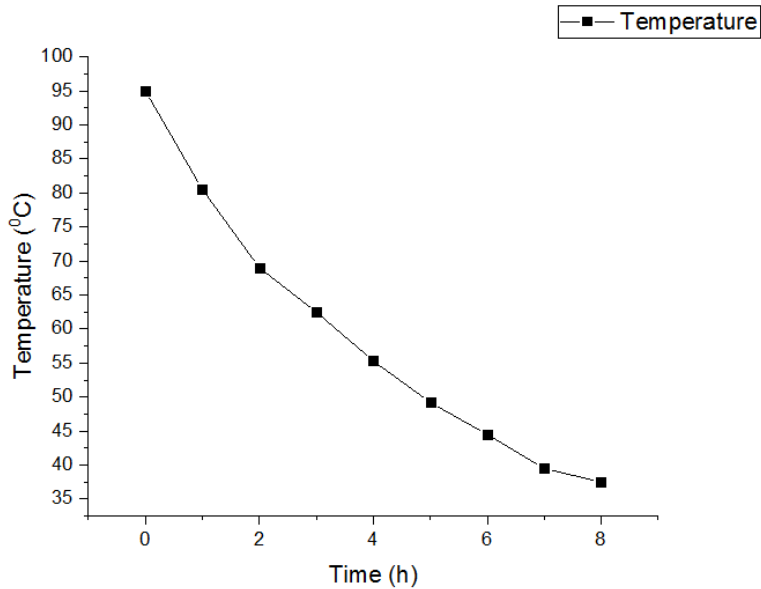


Figure 6. The temperature change of demineralized water

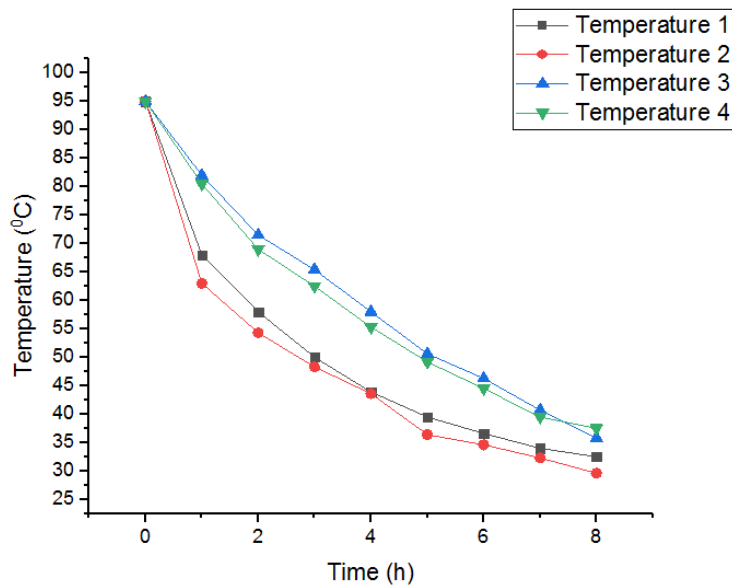


Figure 7. Comparison of temperature change for all four samples. Temperature 1 – Figure 3; Temperature 2 – Figure 4; Temperature 3 – Figure 5; Temperature 4 – Figure 6.

The ratio of Glauber's salt and stearic acid is noted. When it is 1:2 then the effect of the storage temperature is lower for 5 to 10% relative to the 2:1 ratio which can be seen in Fig. 3 and Fig. 4. By increasing the amount of Glauber's salt should be expected more favorable conditions for heat storage.

Acknowledgements

This work was supported by the Ministry of Education, Science and Technological Development of the Republic of Serbia under Project No.III 42006.

References

- [1] Wuttig, M. and Steimer, C., "Phase change materials: From material science to novel storage devices", *Applied Physics a-Materials Science & Processing*, 87:(3), 411-417, 2007.
- [2] Staniša T. Stojiljković, Bratislav Ž. Todorović, *The adsorption-desorption power of bentonite based materials*, LAP LAMBERT Academic Publishing, 2016.
- [3] Olfat M. Sadek, Waffa K. Mekhmer, Na-montmorillonite clay as thermal energy storage material, *Thermochimica Acta* 370, 57–63, 2001.
- [4] Stanisa Stojiljkovic, Role of bentonite clay in the ecology of the human body, XIV International Conference on Medical Geology, GEOMED ,Bari, Italy, 20-25 Sep. 2011.
- [5] Veniale F. The role of microfabric in clay soil stability, *Miner. Petrogr. Acta*, Vol. 29 pp.101-119, 1985.
- [6] Hamdan, M.A., I. Al-Hinti, Analysis of heat transfer during the melting of a phase-change material, *Applied Thermal Engineering* 24 (13),1935–1944, 2004.
- [7] Stanisa Stojiljkovic, Vojkan Miljkovic, Goran Nikolic, Danijela Kostic, Biljana Arsic, Jill Barber, Ivana Savic, Ivan Savic, The influence of the addition of polymers on the physico-chemical properties of bentonite suspensions, *Science of Sintering*, 46(1) 65-73, 2014.
- [8] Biswas Dr. Thermal energy storage using sodium sulphate decahydrate and water. *Solar Energy* 19:99–100, 1977.
- [9] Telkes M. Nucleation of super saturated inorganic salt solution. *Indust Eng Chem* 44:1308, 1952.
- [10] Rupp, J. Interactive textiles regulate body temperature, *International Textile Bulletin* 45 (1),58–59, 1999.
- [11] Pause, B. Development of heat and cold insulating membrane structures with phase change material, *Journal of Coated Fabrics* 25,59–68, 1995.
- [12] Wang, S.X., Y. Li, J.Y. Hu, H. Tokura, Q.W. Song, Effect of phasechange material on energy consumption of intelligent thermalprotective clothing, *Polymer Testing* 25 (5),580–587, 2006.
- [13] Li, Y., The science of clothing comfort. *Textile Progress*, 31,1e135, 2001.
- [14] Mower GD. perceived intensity of peripheral thermal stimuli is independent of internal body temperature. *J comp physiol Psychol.* 90:1152–5, 1976.
- [15] Satinoff E. Behavioural thermoregulation in the cold. In: Fregley MJ, Blatteis cM,editors. *Handbook of physiology (section4: environmental physiology)*. New York, NY, USA: Oxford University press. vol. 1, p. 481–505, 1996.
- [16] Nadel ER, Mitchell GW, Stolwijk JAJ. Differential thermal sensitivity in the human skin. *Pflügers Arch.*, 340:71–6, 1973.

- [17] Crawshaw LI, Nadel ER, Stolwijk JAJ, Stamford BA. Effect of local cooling on sweating rate and cold sensation. *Pflügers Arch.*, 354:19–27, 1975.
- [18] Sharma, A., Tyagi, V.V., Chen, C.R., Buddhi, D.. Review on thermal energy storage with phase change materials and applications, *Renewable and Sustainable Energy Reviews*.13(2) 318-345, 2009.
- [19] Li Z. B., Paraffin/diatomite/multi-wall carbon nanotubes composite phase change material tailor-made for thermal energy storage cement-based composites. *Energy* 72, 371-80, 2014.
- [20] Young, J.O.C. Phase change materials as energy storage media — *Sunworld* 6:169, 1982.

Materials Selection for Thermal Energy Storage: How to Increase the Thermal Conductivity of Phase Change Materials

FLORIAN HENGSTBERGER & CHRISTOPH ZAUNER

Abstract Thermal storages based on phase change materials (PCMs) have a broad spectrum of applications particularly in the field of renewable energy. Unfortunately, the thermal conductivity of the most cost-effective PCMs is notoriously low, which limits the (dis)charging power of these storages and makes large heat exchange areas necessary. Because the heat exchanger is often the main cost driver, increasing the thermal conductivity of the PCM is an option to keep the costs low.

It is well known that PCMs can be improved by adding high thermal conductivity materials in the form of small particles. Since there are many materials to choose from with different characteristics (thermal and mechanical properties, but also price and availability) it is difficult to make an optimum decision without the aid of software. We show that this optimization problem can be solved in a systematic way by formulating a well-defined objective function, which takes the performance increase and the material costs into account, and use the CES Selector materials selection software to choose the best materials.

Keywords: • Thermal energy storage • materials selection • phase change materials • thermal conductivity • CES •

CORRESPONDENCE ADDRESS: Dr. Florian Hengstberger, Scientist, AIT Austrian Institute of Technology GmbH, Center for Energy, Sustainable Thermal Energy Systems, Giefinggasse 2, 1210 Wien, Austria, e-mail: florian.hengstberger@ait.ac.at. Christoph Zauner, Scientist, AIT Austrian Institute of Technology GmbH, Center for Energy, Sustainable Thermal Energy Systems, Giefinggasse 2, 1210 Wien, Austria, e-mail: Christoph.zauner@ait.ac.at.

1 Introduction

For a drastic reduction in CO₂ emissions it is necessary to base the energy system on renewable sources and to use the energy at maximum efficiency. Due to the fluctuating supply of renewable energy and because most of the energy is consumed in the form of heat, thermal energy storages will play a key role in the energy management system of the future. The last years of research on energy storage integration have made clear that no single thermal storage technology will be capable of servicing all demands and that a variety of thermal storage types (temperature level, capacity, discharge time) will be necessary to meet the requirements of a renewable energy system.

Thermal storages based on phase change materials (PCMs) make use of the materials latent heat of fusion: heat is stored by melting and regained by crystallization. Today a large number of possible PCMs are known which cover a wide range of melting temperature and have high energies of fusion [1]. Unfortunately, most of the materials considered today for applications have low thermal conductivity (typically below 1 W/mK [1]). This makes elaborate heat transfer structures (such as finned tubes) necessary which turned out to be a major cost driver. One option to reduce cost of the heat exchanger is to improve the thermal conductivity of the PCM itself, for example by adding high thermal conductivity filler particles.

2 Materials Selection

For the most cost-effective choice of material a trade-off between performance of the filler, i.e. high thermal conductivity, and the amount of filler material has to be made. To attain a certain thermal conductivity of the composite (PCM and filler material) a low percentage of an expensive, high thermal conductivity particle (such as a metal) can be used or a larger amount of a material with lower conductivity.

Because many material families (metals, ceramics, glasses) come into question, the number of potential candidates is very high. Faced with this complexity, it is unlikely that an engineer will make an optimum decision without the aid of software.

Material choices of similar complexity are frequently encountered in mechanical design. In this field, the software CES Selector has evolved, which assists the engineer with material property charts and selection tools [2]. Although focused on mechanical engineering, CES Selector provides also thermophysical properties and material costs. With this information, the problem of selecting the most cost-effective fillers can be tackled in a systematic way.

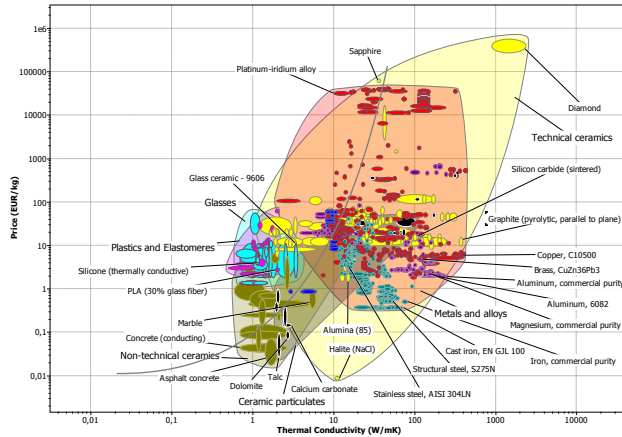


Figure 5 Thermal conductivity vs. price for engineering materials. A trade-off between thermal conductivity and price must be made. The coloured areas indicate the family envelopes. The grey line is the approximate Pareto frontier.

The material property chart in Fig. 1 gives an overview of thermal conductivity and price for a large number of common engineering materials. To generate this plot, the material families of ceramics, ceramic particulates, metals and alloys as well as plastics and elastomers were included. We did not consider any hybrid materials (composites, foams, honeycombs, natural materials).

The chart reveals many important facts. As expected, high material performance comes at a certain price: high thermal conductivity materials are generally more costly. The graph further reveals that prices and thermal conductivities span several orders of magnitudes, which means that very bad (and very good) choices can be made.

It is apparent from the material family envelopes that glasses, plastics and elastomers, with their intermediate price and low thermal conductivity, are bad candidates. In contrast, there are many candidates from (non)-technical ceramics, ceramic particulates and metals which excel either in low price, high thermal conductivity or an attractive combination of both properties. An approximate Pareto frontier (grey line) can be sketched as a guide to the eye.

From this perspective many of the most common engineering metals, which are produced in vast quantities worldwide, are very attractive. Some examples are: C10500 copper (used for electrical contacts), 6082 aluminium (used in heat sinks), CuZn36Pb3 free cutting brass, structural steel and cast iron.

The optimum solution will be close to the Pareto frontier as sketched in Fig. 1. To select the best material, the effect of the filler particles on the thermal conductivity must first be quantified by a thermal model of the composite.

3 Random Dispersed Particles

The general approach for materials selection is to find an objective function and a number of constraints which define the problem in terms of material properties [3]. In this example, one has to minimise the costs C per volume V of storage. This quantity is defined by the volumetric fill factor Φ , the specific costs (per mass) of the filler particles C_f and their density ρ_f :

$$C/V = \Phi C_f \rho_f \rightarrow \min$$

The constraint is given by the condition that a certain thermal conductivity of the composite has to be achieved. For the thermal model of the composite we will revert to the Maxwell model, which is one of the simplest approaches and valid if thermal fields of the filler particles do not interact. Its usage can be justified for small amounts of random dispersed particles (typically not more than roughly 10 %).

The Maxwell model for the thermal conductivity of a composite (λ_c) that consists of a phase change material (λ_p) and an embedded filler material (λ_f) of randomly dispersed particles is:

$$\lambda_c = \lambda_p \frac{\lambda_f + 2\lambda_p + 2\Phi \Delta\lambda}{\lambda_f + 2\lambda_p - \Phi \Delta\lambda}.$$

(Here, $\Delta\lambda = \lambda_f - \lambda_p$ is the difference in thermal conductivity.)

It is now important to discuss some general features of the model. The maximum attainable thermal conductivity for a given fill factor is:

$$\lambda_{c, \max} = \lambda_p \frac{(1 + 2\Phi)}{(1 - \Phi)}.$$

A fill factor of 10 % results therefore in a rather modest increase of about $R = \lambda_{c, \max} / \lambda_p = 4/3$.

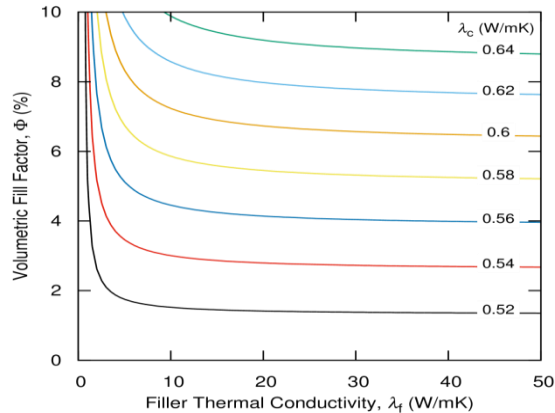


Figure 6 Effect of the thermal conductivity on the fill factor. The contours of λ_c decrease sharply with increasing λ_f and then stagnate. Increasing the thermal conductivity of the filler is ineffective as soon as $\lambda_f \gg \lambda_p = 0.5$ W/mK.

Figure 2 shows contour lines of thermal conductivity of the composite as a function of the fill factor and the filler's thermal conductivity. In order to achieve a specified λ_c (the constraint) one has the freedom to choose between combinations λ_f and Φ as one moves along a contour of constant λ_c . Note, how rapidly the fill factor drops at the beginning. Spending more on the performance of the filler material (higher thermal conductivity) leads to a strong reduction of the fill factor. Investing in thermal conductivity surely pays off in this region. Later however, the contour lines stagnate and even large increases of the thermal conductivity have little effect on the fill factor. Increasing the thermal conductivity cannot be justified.

A physical interpretation for this behaviour is that the filler particles provide thermal shortcuts in the material. As soon as the thermal conductivity of the filler is much greater than that of the PCM ($\lambda_f \gg \lambda_p$), the shortcuts are so effective that the thermal resistance of the filler particles plays no role and the composite's thermal conductivity is defined by the properties of the PCM. (Note, that $\lambda_{c, \max}$ is independent of λ_f .)

For the selection of the optimum material, we have to derive an objective function based on material properties by eliminating the fill factor from the objective function. Solving the Maxwell model for Φ results in

$$\Phi = \frac{(\lambda_f + 2\lambda_p)(R-1)}{\Delta\lambda(2+R)},$$

where R is the desired enhancement in thermal conductivity. The objective function is

$$C/V = \frac{(\lambda_f + 2\lambda_p)(R-1)c_f\rho_f}{\Delta\lambda(2+R)}$$

and can be minimised¹ using the material properties and price information stored in CES Selector.

4 Improved PCMs

As a case study we analyse a PCM with a very low thermal conductivity ($\lambda_p = 0.5$) and specify an improvement in thermal conductivity of $R = 4/3$, which is compatible with the limits of the Maxwell model. The volume specific costs are now a function of the properties of the filler only:

$$C/V = \frac{(\lambda_f + 1)c_f\rho_f}{(\lambda_f - 0.5)10}.$$

The according equation for the fill factor is:

$$\Phi = \frac{(\lambda_f + 1)}{(\lambda_f - 0.5)10}.$$

A plot of these two quantities reveals now the economically best choice for the filler material and the volumetric density needed. The fill factor will of course exceed 10 % for all materials, because this is the limit as λ_c approaches infinity. We will restrict the following analysis to materials which keep $\Phi < 0.15$.

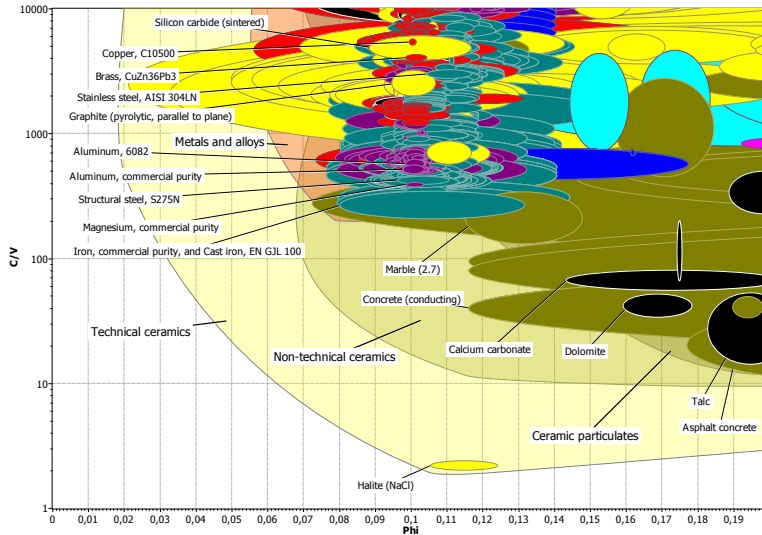


Figure 7 Case study for a PCM with $\lambda_p = 0.5$ W/mK. The surprising result is that table halite (rock salt) is the optimum choice. Other ceramics and many common engineering metals are also cost effective candidates.

The surprising result of this analysis (see Fig. 3) is that halite, i.e. the mineral form of ordinary table salt, performs best due to its exceptionally low price and remarkably high thermal conductivity. CES selector lists a price of less than 10 € per ton and a room temperature thermal conductivity of 10.4 – 11.7 W/mK. Latest literature [4] reports here a considerably lower value of about 6 W/mK. But even with this updated value and a tenfold increase in price, halite still performs exceptionally: $C/V \approx 25$ and $\Phi \approx 0.12$.

CES Selector offers also information on the stability and durability of the material, which are important factor, but cannot be included in the objective function. The maximum service temperature² of halite is 180 °C, which is acceptable at least for low temperature PCMs, but the durability might be an issue, in particular the resistance to water (moisture).

It is important, not to focus too much at optimisation itself and to keep the overall costs in mind. Prices for PCMs are typically around 1000 €/m³ and comparable costs can be accepted for the filler. (Note, that C/V refers to the cost per volume of the total storage.) With this relaxed condition, several other, more intuitive choices, such as the common engineering aluminium, magnesium, and iron and their alloys are viable options.

The fact that ordinary iron wins the contest among the metals and alloys is due to its low price. Any increase from the thermal conductivity of iron ($\lambda > 70$ W/mK) does not pay

off, because this value exceeds that of the PCM already by more than a factor of hundred. Any further increase in filler thermal conductivity leads only to minute changes in Φ , but results (due to the increased specific material costs) in a significant overall increase of the volume specific costs.

5 Outlook

The main limitation of our analysis is the Maxwell model, which allows only small fill factors and consequently only little improvements in thermal conductivity. To deal with higher densities more accurate models are needed. Very specific theories are also necessary when other forms of materials (fibres, platelets) are considered.

Care must also be taken with the price information available in CES Selector, because the actual real market prices might deviate significantly. In addition, we did not take the cost for processing the materials, for example crushing or granulation, into account. Because many of the most common engineering metals are good fillers, it might also be possible to use scrap material, which would reduce the cost for certain metals drastically.

The surprising fact that (under the given model and requirements) table salt is the economically best option for a filler material and that many ceramic particulates also perform well suggests that other rocks or minerals might be included in this search. Here, CES selector has only a few entries and is far from complete.

Author Contributions

F. H. derived the objective function. F. H. and C. Z. conducted the materials selection. F. H. wrote the manuscript and C. Z. commented it.

Acknowledgements

This project has received funding from the Klima- und Energiefonds' programm e!MISSION.at – Energy Mission Austria under the Grant Agreement No. 845 020.

Notes

¹ In materials selection it is common to maximise a performance index. Here, we chose minimisation, because C/V has units of €/m³ which are easy to interpret

² The maximum service temperature depends strongly on the application. In heat storages higher temperatures close to the melting point of the filler can surely be tolerated

References

- [1] F. Agyenim, N. Hewitt, P. Eames, and M. Smyth, “A review of materials, heat transfer and phase change problem formulation for latent heat thermal energy storages (LHTESS)”, *Renewable and Sustainable Energy Reviews*, vol. 14, pp. 615–628, 2010.

- [2] CES Selector 2016 Software, Granta Design Limited, Cambridge, UK. Available from: <http://www.Grantadesign.com>, 2017.
- [3] M. F. Ashby, *Materials selection in mechanical design*, Oxford: Butterworth-Heinemann, 2011.
- [4] A. Urquhart and S. Bauer, „Experimental determination of single-crystal halite thermal conductivity, diffusivity and specific heat from $-75\text{ }^{\circ}\text{C}$ to $300\text{ }^{\circ}\text{C}$ ”, *International Journal of Rock Mechanics & Mining Sciences*, vol. 78, pp. 350–352, 2015.

Improving the Functionality of Resorcinol-Formaldehyde Based Carbon Aerogels as Electrode Material for Supercapacitor Applications

QAISAR ABBAS, MOJTABA MIRZAEIAN & ABRAHAM A. OGWU

Abstract Polymeric carbon and activated carbon aerogels were synthesized through sol-gel polycondensation reaction followed by the pyrolysis at 800 °C under Argon (Ar) and physical activation under CO₂ at different temperatures with different degrees of burn-off. The BET specific surface area (SSA) of the carbons was increased from 537 to 1775 m²g⁻¹ and their total pore volume was increased from 0.24 to 0.94 cm³g⁻¹ during the activation process while the pore size was kept constant around 2nm. Both non-activated and activated carbons were used as electroactive materials in an electrochemical capacitor. The capacitive behaviour of the electrodes was analysed by cyclic voltammetry (CV) and electrochemical impedance spectroscopy (EIS) measurements using 6 M KOH as an electrolyte.

The results of CV measurements showed improved specific capacitance (SC) of 197 Fg⁻¹ of activated carbon as compared to the SC of 136 Fg⁻¹ when non-activated carbon was used as electrode material.

The result of EIS measurements showed low internal resistance indicating that the polymeric carbons possess a highly conductive three dimensional crosslinked structure. Due to their high specific surface area, controlled pore size, high conductivity and desirable capacitive behaviour these materials are preferred as electrode material for electrochemical capacitors.

Keywords: • Carbon aerogels • Physical activation • Cyclic voltammetry (CV) • Electrochemical capacitors (EC's) • electrochemical impedance spectrometry (EIS) •

CORRESPONDENCE ADDRESS: Qaisar Abbas, University of the West of Scotland, School of Engineering and Computing, High St., Paisley PA1 2BE, Scotland UK e-mail: qaisar.abbas@uws.ac.uk. Mojtaba Mirzaeian, PhD, University of the West of Scotland, School of Engineering and Computing, High St., Paisley PA1 2BE, Scotland UK e-mail: mojtaba.mirzaeian@uws.ac.uk. Abraham A Ogwu, PhD, University of the West of Scotland, School of Engineering and Computing, High St., Paisley PA1 2BE, Scotland UK e-mail: Abraham.Ogwu@uws.ac.uk.

1 Introduction

With continuing increase in the contribution of renewable energies to the global energy demands, energy conversion/storage systems such as fuel cells [1], batteries [2] and electrochemical capacitors (EC's) [3] have attracted considerable attentions in recent years. Due to their favourable properties such as superior power density, long cycle life, and excellent charge/discharge capability [4], additional emphasis has been placed on research and development of EC's also known as supercapacitors. However to fill the gap in energy/power continuum when combined with other electrical energy storage devices their low energy densities are yet to be improved. Improving the specific capacitance or operating voltage is considered as common strategy to increase the energy density of ECs. Specific capacitance of an EC can be enhanced by increasing the electrochemically active surface area [5] and controlling the pore size of its electrode material [6], increasing the electrode electrolyte wettability [7] or incorporating the pseudocapacitive components within its electrode [8]. Due to their high specific surface area, exceptionally high porosity and controllable pore size during their synthesis, high electrical conductivity, inertness and interconnected microstructure [9] carbon aerogels are considered as the most promising electrode materials for ECs.

In this study activated carbon aerogels were synthesised through polycondensation reaction between resorcinol (R) and formaldehyde (F) followed by the carbonisation of the gels and finally physical activation of the carbons under CO₂ at different temperatures. Both resultant carbon aerogels and activated carbon aerogels were used as electroactive materials for the fabrication of electrodes for electrochemical capacitors. The effect of specific surface area of the carbon used in the electrode and wettability of the electrode with electrolyte on the specific capacitance of the cell were examined by CV and EIS measurements.

2 Experimental

2.1 Synthesis of RF gels

The RF aerogels were prepared by polycondensation reaction between resorcinol and formaldehyde with a resorcinol to catalyst molar ratio of 100 according to the procedure explained elsewhere [9, 10].

2.2 Carbonization of RF aerogels (RFC)

The dried RF aerogels were carbonized at different temperatures to investigate the effect of pyrolysis conditions on the porous structure of carbon aerogels. A sample of gel in a ceramic boat was placed in the middle of a tubular furnace and purged with Ar at room temperature for 30 min prior to the pyrolysis. The temperature was increased at 5 °C min⁻¹ to 150 °C and maintained for 30 min. The temperature was then increased to 450 °C at 5 °C min⁻¹ and held for 30 min. Finally the temperature was increased to 800 °C at 10 °C

min⁻¹ and the sample was kept at this temperature for 3h before cooling it to the room temperature.

2.3 Activation of RF aerogels (RFCA)

The activated carbon aerogels were prepared by physical activation under CO₂ at different temperatures. Prior to heating, the sample was purged with Ar at room temperature for 30 min. The temperature was then increased at 10 °C min⁻¹ and the gas was switched from Ar to CO₂ once the desired activation temperature was achieved. The sample was kept at this temperature under CO₂ during the activation and then the gas was switched back to Ar and the sample was cooled down to room temperature.

2.4 Characterisation of activated carbon aerogels (RFCA)

The porous structure of carbon (RFC) and activated carbon aerogels (RFCA) was characterized by a Tri-Star adsorption analyser (Micromeritics). Samples were evacuated in a vacuum oven at 80°C at 5 mbar for 24 h and then degassed at 300 °C using a Flowprep system (Micromeritics) prior to the adsorption/desorption measurements. BET method was used for surface area measurements, t-plot method was used for micropore analysis, and BJH method using adsorption branch of the isotherm was used for pore size distribution. The total pore volume was determined from the adsorbed volume of N₂ at P/P₀ = 0.99 [10].

Contact angle measurements were carried out by a CAM 200 goniometer system manufactured by KSV Ltd based on video captured images and automatic image analysis using CAM software. Deionised water, Ethylene glycol and Diiodomethane were used as probe liquid for the determination of contact angles.

Raman spectroscopy was carried out on an “In via Raman microscope (Renishaw, UK)” with 514.5 nm diode laser excitation in the range of 1000 – 3000 cm⁻¹ to evaluate the vibrational properties of the electro-active material.

3 Results and Discussion

3.1 BET analysis of activated aerogels

N₂ adsorption–desorption isotherms of the carbon and activated carbons at different activation temperatures are shown in Figure 1.

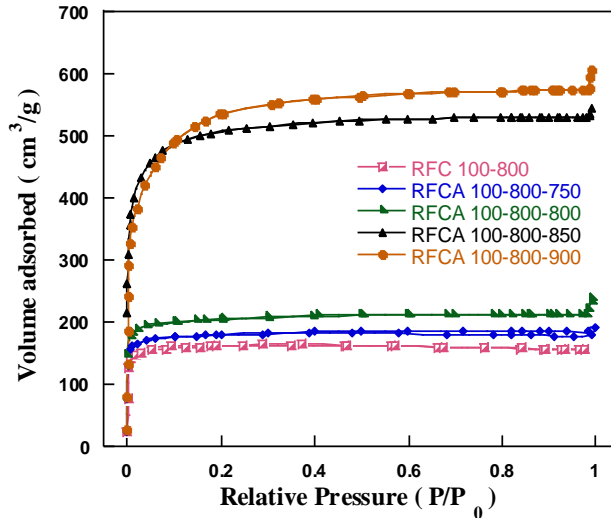


Figure 1 N₂ adsorption–desorption isotherms of activated carbon aerogels at different activation temperatures.

All isotherms show a sharp increase in the amount of gas adsorbed at low pressures in the range of $P/P_0 < 0.01$ indicating the development of microporosity in carbon structure due to the physical activation. This is followed by a hysteresis loop in P/P_0 range 0.4-0.9 which represents the development of mesoporosity within the activated carbon samples [11]. The lower part of the hysteresis loops represent the filling of the mesopores while the upper parts represent the emptying of the mesopores [12]. With the increase in activation temperature the volume of gas adsorbed increases due to the development of porosity in the samples. Table 1 shows a significant increase in pore volume and specific surface area regardless average pore size being the same (i.e. around 2nm).

Table 1 Porosity parameters of activated carbon aerogels activated at different temperatures.

Sample	S_{BET} (m^2g^{-1})	V^{total} (cm^3g^{-1})	V^{micro} %	V^{meso} %	D^{avg} (nm)
RFC 100-800	537	0.2420	90	10	1.80
RFCA 100-800- 750	602	0.2981	79	21	1.99
RFCA 100-800- 800	678	0.3707	72	28	2.19
RFCA 100-800- 850	1687	0.8413	72	28	2.00
RFCA 100-800- 900	1775	0.9394	42	58	2.12

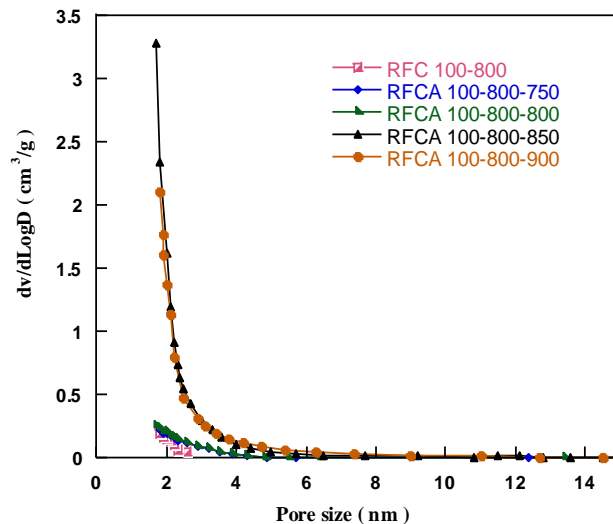


Figure 2 Pore size distribution of activated carbon aerogels at different activation temperatures.

Pore size distribution (PSD) of all the samples is represented in Figure 2 indicating all the samples are predominantly microporous in nature and pore size distribution is centred around 2 nm.

3.2 Contact angle measurement

Contact angle was found to be dependent on the type of substrate (carbon/ activation carbon) and the probing liquid used. The highest contact angle was observed when most polar liquid (water) was used as probing liquid on the carbon substrate. A significant decrease in the contact angle was observed when carbon substrate was substituted with the activated carbon aerogels. When ethylene glycol and Diiodomethane were used as probe liquids similar trends were observed. This decrease in contact angle can be attributed to the activation under CO₂ environment since it modifies the carbon surface by the introduction of oxygen functional groups [13].

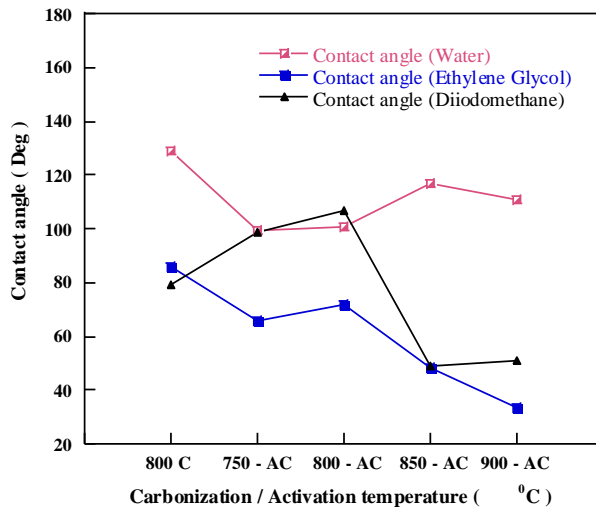


Figure 3 Contact angle measurements of carbon aerogels using different substrate.

3.3 Raman spectroscopy

Figure 4 shows the Raman spectra of carbons activated at different temperatures. Activation results in well-developed porous structure however activation at very high temperatures and at higher degree of burn off, can result in decrease in the degree of graphitization [11]. Peaks shown in Figure 4 around 1340 and 1600 cm⁻¹ are the characteristics peak of such carbon material [14]. The ratio I_D/I_G of the relative intensity of the D and G band is proportional to the number of defect sites in carbon, the higher the ratio is lower the degree of graphitization is [15].

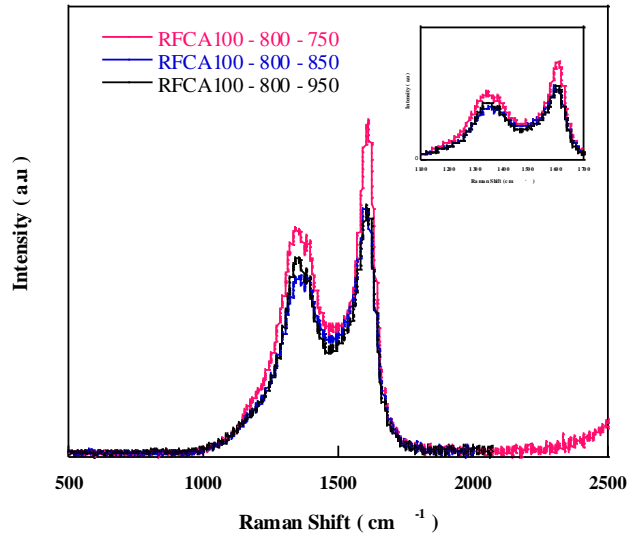


Figure 4 Raman spectra of RFCA 100-800 activated at different temperatures.

Increase in activation temperature increase the I_D/I_G values as listed in Table 2.

Table 2 Raman features of activated carbons.

Sample	Activation Temperature (°C)	D Peak (cm ⁻¹)	G Peak (cm ⁻¹)	I_D / I_G
RFCA 100-800	750	1340	1610	0.67
RFCA 100-800	850	1340	1590	0.72
RFCA 100-800	950	1350	1600	0.78

4 Surface cleaning of activated carbons

To understand the effect of surface functional groups on the performance of electrodes in an electrochemical cell, the surface of activated carbons was further cleaned to remove the oxygen functional group introduced due to CO₂ activation. Table 3 and 4 show the EDX results of the RFC100-800 carbon activated at 800 °C before and after surface cleaning with N₂ at 600 °C. A reduction in oxygen functional groups from 0.71% to 0.41% can be observed.

Table 3 shows the consecrations of various elements in RFCA100-800-800.

Element s	Apparent Concentratio n	Wt%	Wt% Sigma	Atomic %
C	20.19	87.3	0.14	92.24
O	0.71	2.79	0.09	2.21
F	3.38	5.09	0.08	3.40
Na	0.23	0.46	0.03	0.26
Si	1.09	3.13	0.05	1.42
S	0.13	0.40	0.04	0.16
Cl	0.27	0.89	0.05	0.32
Total		100		100

Table 4 shows the consecrations of various elements in RFCA100-800-800 after cleaning at 600⁰C for 1hour.

Element s	Apparent Concentratio n	Wt%	Wt% Sigma	Atomic %
C	17.76	89.3	0.16	92.79
O	0.41	2.35	0.10	1.83
F	3.50	7.65	0.12	5.03
Na	0.15	0.43	0.04	0.24
S	0.07	0.30	0.05	0.12
Total		100		100

5.0 Electrochemical measurements

Electrochemical measurements were conducted using a Voltalab 40 analytical potentiostat. Prior to the electrochemical measurements the cell was place under vacuum for 20 min to enhance the penetration of electrolyte within the porous structure of the electrode. It was then kept under open circuit for 15 min to stabilize. Cyclic Voltammetry (CV) measurements were used for the capacitance calculations with a voltage range between 0.5 to 1.0 V at scan rates of 5, 10, and 15mVs⁻¹.

5.1 Electrochemical characterisation

In this work 6 M KOH solutions was used as electrolyte in sandwich type symmetric capacitor cell. Specific capacitance was calculated from the discharge curve of CV using the following equation;

$$C = \left(\frac{dV}{dt} \right) \quad (1)$$

Where I is the average discharge current and dV/dt is the scan rate. The specific capacitance C_{sp} in Fg^{-1} was calculated by:

$$C_{sp} = 2 \times C / m \quad (2)$$

Where ‘ C ’ is the measured capacitance for two-electrode cell and m is the mass of active material in one electrode.

Table 3 shows the specific capacitance (SC) of polymer based carbons activated at different temperatures. It can be witnessed that carbon activated at 800 °C delivers highest capacitance even showing a lower SSA of 678 m^2g^{-1} when compared with the carbon activated at 900 °C having a SSA of 1775 m^2g^{-1} . Our results show that there is no direct relationship between SSA and capacitance measured. However PSD plays a vital role in capacitor performance where micropores are important for the ion adsorption, whereas the mesopores are essential for ion transportation through bulk of active material [16]. Therefore the optimization of micro/meso-porosity is crucial to achieving the highest SC.

Table5 Specific capacitance of the electrodes at different scan rate in 6M KOH electrolyte

Sample	SSA (m^2g^{-1})	Activation temperatur e (C)	Specific Capacitance (Fg^{-1})		
			Scan rate (mVs^{-1})		
			5	10	15
RFC 100- 800	537	-----	136	71	51
RFCA 100- 800	602	750	144	52	23
RFCA 100- 800	678	800	197	120	42
RFCA 100- 800	678	800	163	44	25
RFCA 100- 800	1687	850	64	18	10
RFCA 100- 800	1775	900	60	36	34

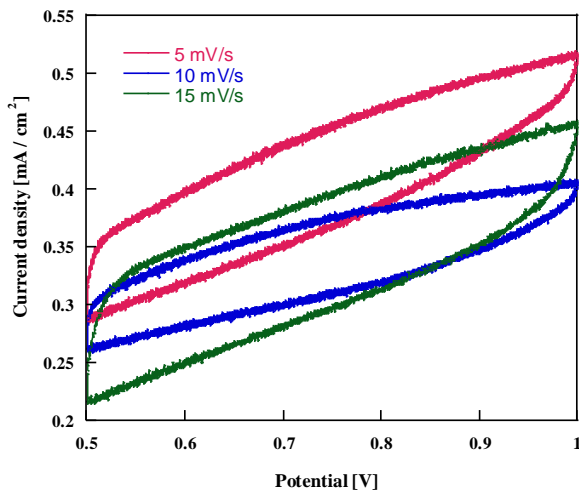


Figure 5 Cyclic Voltammogram of the cell using (RFC100-800-900) activated carbon as the electroactive material at different scan rates.

5.2 Electrochemical impedance spectroscopy (EIS) measurements

EIS measurements were also performed at the AC voltage amplitude of 10mV and the frequency range of 100 KHz to 5 Hz with number of frequencies (per decade) of 5 as shown in figure 6.

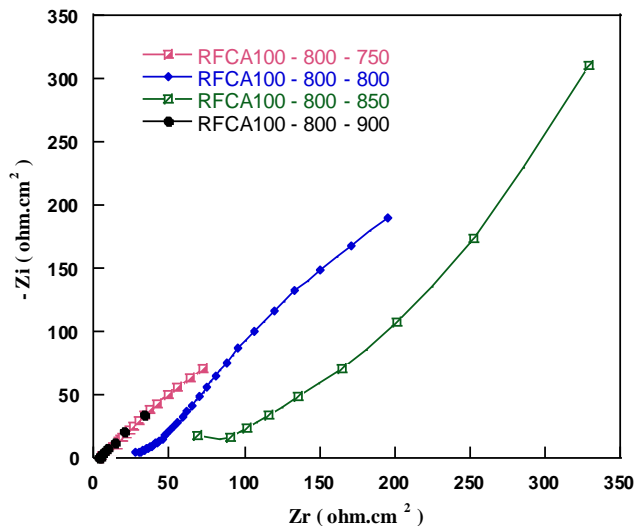


Figure 6 EIS spectra of carbon aerogels with different activation temperature.

4 Conclusions

The effect of the porous structure, wettability and surface functional groups on the specific capacitance of supercapacitor cell has been evaluated. Enhanced wettability and increased specific capacitance was observed due to physical activation of the polymeric carbons based electroactive materials under CO₂ environment. This was achieved due to the increase in specific surface area and introduction of oxygen surface functional group. Highest specific capacitance of 197 Fg⁻¹ at the scan rate of 5mVs⁻¹ was achieved using carbon activated at 800^oC as an electrode material. Reduction in specific capacitance from 197 Fg⁻¹ to 163 Fg⁻¹ was observed after surface cleaning was performed at 600^oC. This might be due to the reduction in oxygen concentration in the carbon sample after surface cleaning.

References

- [1] A. Alaswad, A. Baroutaji, H. Achour, J. Carton, A. Al Makky, and A. Olabi, "Developments in fuel cell technologies in the transport sector," *International Journal of Hydrogen Energy*, vol. 41, pp. 16499-16508, 2016.
- [2] X. Guo, B. Sun, D. Su, X. Liu, H. Liu, Y. Wang, *et al.*, "Recent developments of aprotic lithium-oxygen batteries: functional materials determine the electrochemical performance," *Science Bulletin*, 2017.
- [3] P. J. Hall, M. Mirzaeian, S. I. Fletcher, F. B. Sillars, A. J. Rennie, G. O. Shitta-Bey, *et al.*, "Energy storage in electrochemical capacitors: designing functional materials to improve performance," *Energy & Environmental Science*, vol. 3, pp. 1238-1251, 2010.
- [4] J.-j. Ruan, Y.-q. Huo, and B. Hu, "Three-dimensional Ni (OH) 2/Cu 2 O/CuO porous cluster grown on nickel foam for high performance supercapacitor," *Electrochimica Acta*, vol. 215, pp. 108-113, 2016.
- [5] Y. Zhu, S. Murali, M. D. Stoller, K. Ganesh, W. Cai, P. J. Ferreira, *et al.*, "Carbon-based supercapacitors produced by activation of graphene," *Science*, vol. 332, pp. 1537-1541, 2011.
- [6] J. Chmiola, G. Yushin, Y. Gogotsi, C. Portet, P. Simon, and P.-L. Taberna, "Anomalous increase in carbon capacitance at pore sizes less than 1 nanometer," *Science*, vol. 313, pp. 1760-1763, 2006.
- [7] S. L. Candelaria, B. B. Garcia, D. Liu, and G. Cao, "Nitrogen modification of highly porous carbon for improved supercapacitor performance," *Journal of Materials Chemistry*, vol. 22, pp. 9884-9889, 2012.
- [8] S. Majid, "Effects of Electrodeposition Mode and Deposition Cycle on the Electrochemical Performance of MnO 2-NiO Composite Electrodes for High-Energy-Density Supercapacitors," *PloS one*, vol. 11, p. e0154566, 2016.
- [9] M. Mirzaeian and P. J. Hall, "The control of porosity at nano scale in resorcinol formaldehyde carbon aerogels," *Journal of materials science*, vol. 44, pp. 2705-2713, 2009.
- [10] M. Mirzaeian and P. J. Hall, "Nano structure carbons for energy storage in lithium oxygen batteries," in *Sustainable Power Generation and Supply, 2009. SUPERGEN'09. International Conference on*, 2009, pp. 1-10.

- [11] M. Zhou, F. Pu, Z. Wang, and S. Guan, "Nitrogen-doped porous carbons through KOH activation with superior performance in supercapacitors," *Carbon*, vol. 68, pp. 185-194, 2014.
- [12] S. J. Gregg, K. S. W. Sing, and H. Salzberg, "Adsorption surface area and porosity," *Journal of The Electrochemical Society*, vol. 114, pp. 279C-279C, 1967.
- [13] L.-Z. Fan, S. Qiao, W. Song, M. Wu, X. He, and X. Qu, "Effects of the functional groups on the electrochemical properties of ordered porous carbon for supercapacitors," *Electrochimica Acta*, vol. 105, pp. 299-304, 2013.
- [14] M. Zhou, T. Cai, F. Pu, H. Chen, Z. Wang, H. Zhang, *et al.*, "Graphene/carbon-coated Si nanoparticle hybrids as high-performance anode materials for Li-ion batteries," *ACS applied materials & interfaces*, vol. 5, pp. 3449-3455, 2013.
- [15] M. Liu, L. Gan, W. Xiong, F. Zhao, X. Fan, D. Zhu, *et al.*, "Nickel-doped activated mesoporous carbon microspheres with partially graphitic structure for supercapacitors," *Energy & Fuels*, vol. 27, pp. 1168-1173, 2013.
- [16] L. Zhang, H. Liu, M. Wang, and L. Chen, "Structure and electrochemical properties of resorcinol–formaldehyde polymer-based carbon for electric double-layer capacitors," *Carbon*, vol. 45, pp. 1439-1445, 2007.

Binary Mixtures of Ionic Liquids (ILs) and Aliphatic Nitrile Solvents as Electrolytes for Supercapacitors

FLAVIEN IVOL, JOHAN JACQUEMIN & FOUAD GHAMOISS

Abstract During this work, we report the physical and electrochemical properties of solutions containing the 1-ethyl-3-methylimidazolium bis(trifluoromethylsulfonyl)imide ([EMIM][TFSI]) ionic liquid in mixture with a nitrile-based organic solvent, namely the adiponitrile (ADN), glutaronitrile (GLN) or 2-methylglutaronitrile (MGLN) as a function of composition and temperature. Firstly, the composition which exhibits the highest conductivity for each of the binary mixtures was determined at 25 °C to further formulate original blends for supercapacitors. Then, their thermal and transport properties were investigated to highlight their main advantages and drawbacks in comparisons with benchmark electrolytes. Finally, their electrochemical performances as potential electrolytes were investigated regarding their usage in electrochemical double layer capacitors.

Keywords: • supercapacitors • electrolytes • ionic liquid • binary mixtures • nitrile-based organic solvents

CORRESPONDENCE ADDRESS: Flavien Ivol, Ph.D. student, Laboratoire de Physico-Chimie des Matériaux et des Electrolyte pour l'Energie (EA 6299), Faculté des Sciences et Techniques, Université François Rabelais de Tours, Parc de Grandmont, 37200 Tours, France, e-mail: flavien.ivol@univ-tours.fr. Johan Jacquemin, Ph.D., Senior lecturer, Laboratoire de Physico-Chimie des Matériaux et des Electrolyte pour l'Energie (EA 6299), Faculté des Sciences et Techniques, Université François Rabelais de Tours, Parc de Grandmont, 37200 Tours, France, e-mail: johan.jacquemin@univ-tours.fr. Fouad Ghamouss, Ph.D., Senior lecturer, Laboratoire de Physico-Chimie des Matériaux et des Electrolyte pour l'Energie (EA 6299), Faculté des Sciences et Techniques, Université François Rabelais de Tours, Parc de Grandmont, 37200 Tours, France e-mail: fouad.ghamouss@univ-tours.fr.

1 Introduction

The drive to develop high capacity and high power electrical energy storage devices is a key factor for the practical realization of alternative renewable energy sources which are inherently intermittent in nature. Of the range of developing energy storage systems, including batteries and fuel cells, electrochemical double layer capacitors (EDLCs) have attracted much attention as efficient electrochemical power devices. The key feature of EDLCs is driven by their high-power delivery (up to 10 kW.kg⁻¹), high cyclability (>500 000 cycles) and energy (close to 5 Wh.kg⁻¹). [1] In general, two carbon electrodes and an organic liquid electrolyte compose EDLCs. To date, the industrial benchmark electrolyte is based on the tetraethylammonium tetrafluoroborate (Et₄NBF₄) dissolved in acetonitrile (ACN), which presents low viscosity and high ionic conductivity allowing a high-power density under ambient conditions. However, due to its low boiling point (81.6 °C), high vapor pressure, even at room temperature (9.7 kPa at 20 °C) and high flammability (flash point = 12.8 °C), ACN induces safety issues. Therefore, safer electrolyte must be formulated to improve Risk and Safety by keeping, however, the overall performances of the designed EDLCs. [1] In this particular context, the interest in using an ionic liquid (IL) to formulate the EDLCs' electrolyte has been growing. [1] ILs are a class of molten salts which are liquid at temperature below 100 °C, which are constituted by organic cations and inorganic/organic anions. Due to their purely ionic nature, ILs possess an intrinsic conductivity, and exhibit, generally, good thermal and chemical stability, non-flammability and non-volatility under ambient conditions. [2] For this reason, several recent studies have detailed the use of neat ILs as solvent-free electrolyte systems in EDLCs. [3-4] However ILs are very viscous and expensive compounds in comparison with classical solvents and/or molten salts. To solve such issues, two main strategies are reported in the literature; firstly, by designing and testing novel IL structures with effectively reduced viscosity and improved transport properties; [5-6] and secondly, by formulating novel electrolytes containing an ionic liquid mixed with a molecular solvent. In this later context, the most popular organic solvents used for the preparation of these blends are the propylene carbonate (PC) [7], γ -butyrolactone (GBL) [8], and acetonitrile (ACN). [4] Recently, the aliphatic dinitriles solvents ((NC(CH₂)_nCN)), such as adiponitrile (ADN), glutaronitrile (GLN) and 2-methylglutaronitrile (MGLN), have attracted a great attention for the formulation of safer electrolytes due to their high boiling points, high flash points and inherent low vapor pressure in comparison with analogous acetonitrile-based electrolytes. [9-10] In addition, these commercially available dinitriles exhibit also good solvating properties due to the presence of -CN groups and are relatively cheap even within a high degree of purity. For these reasons, we decided to further investigate the advantages and drawbacks of the adiponitrile (ADN), glutaronitrile (GLN) and 2-methylglutaronitrile (MGLN) as potential technological solvents for EDLCs. Furthermore, to formulate electrolytes, we selected the 1-ethyl-3-methylimidazolium bis(trifluoromethylsulfonyl)imide, [EMIM] [TFSI], as it is a very commonly used and well understood IL which has been already reported as an electrolyte component for EDLCs in several publications owing to its reasonable viscosity and high operating voltage (at 20 °C, σ = 8.8 mS.cm⁻¹, η = 34 mPa.s and EW = 4.3 V). [9] In this study, the formulation of the selected electrolytes has been carried-out by determining

firstly the conductivity of each binary mixture as a function of the composition at 25 °C. From this determination, each electrolyte formulation was then selected by taking the exact composition giving the maximum of conductivity in each case. Then, we report on the thermal and physical-chemical characterization of selected electrolytes as a function of the temperature. Afterwards the electrochemical performances of EDLCs containing these innovative electrolytes have been assessed at 25 °C using activated carbon electrodes.

2 Experimental/Methodology

2.1 Materials

The commercially available [EMIM][TFSI] was purchased from Solvionic (electrochemical grade 99.9%, H₂O < 30 ppm). During this work, this IL was used after drying under high vacuum (1 Pa) at 60 °C overnight and was then stored under nitrogen atmosphere to avoid water contamination from atmosphere. After this treatment, the water content in the [EMIM][TFSI] was below 10 ppm. Selected nitriles, *i.e.* adiponitrile (99%), glutaronitrile (99%), and 2-methylglutaronitrile (99%) were purchased from Aldrich. Prior to be used, the dinitriles were redistilled under reduced pressure until their water content was below 20 ppm, as measured by Karl-Fischer technique. To avoid further contamination with moisture from the atmosphere, the selected IL and nitrile solvents were stored in a glovebox (MBraun) under an argon atmosphere with a moisture and oxygen content below 1 and 3 ppm, respectively. A porous Whatman® GF/C membrane (thickness η = 265 μ m and pore diameter \varnothing = 16 mm) filled with the electrolyte solution was used as the separator during electrochemical measurements, while the two electrodes were both based on activated carbon with 3.6 mg of active material (10 mm diameter).

2.2 Electrolytes formulation

As mentioned previously, the formulation of the selected electrolytes has been carried-out by determining firstly the conductivity of each binary mixture as a function of the composition at 25 °C. Herein, the conductivity measurements were performed inside a glove box under N₂ by using a Crison GLP31 digital multi-frequencies conductometer between (1000 and 5000) Hz. The temperature control from 10 to 80 °C is ensured within \pm 0.2 °C by means of a JULABO thermostated bath. The conductometer was first calibrated with standard solutions of known conductivity (*i.e.* (0.1 and 0.02) mol.dm⁻³ KCl aqueous solutions). Each conductivity was recorded when its stability was better than 1 % within 2 min, and the uncertainty of reported conductivities did not exceed \pm 2 %. Figure 1 shows the variation of the conductivity of selected binary mixtures as a function of the IL weight fraction, w_{IL} at 25 °C. As expected, the conductivity of each mixture increases and then decreases with the quantity of IL added into the mixture. In other words, for each selected dinitrile, the conductivity of the solution reaches a maximum for a composition, denoted $C\sigma_{max}$, close to $w_{IL} = 0.75$, and 0.80 for ADN, and GLN or MGLN, respectively.

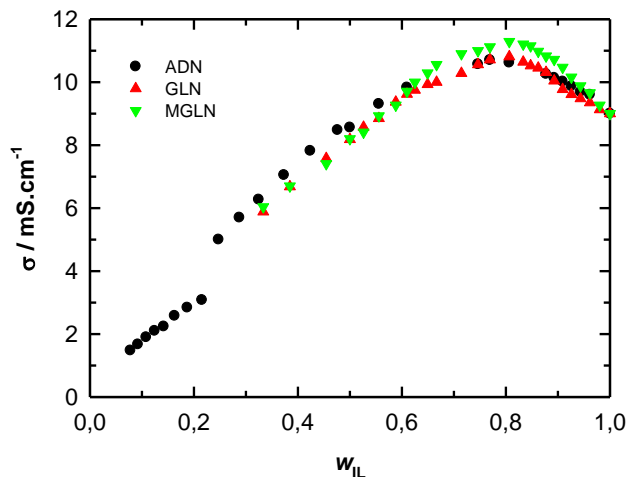


Figure 1. Conductivity, σ , of the three selected binary mixtures as a function of the weight fraction of IL, w_{IL} at 25.0 ± 0.2 °C

Furthermore, as shown in Figure 1, at the maximum of each curve, the conductivity of MGLN-based mixture (11.29 mS.cm^{-1} at $w_{IL} = 0.80$ or $x_{IL} = 0.5352$) seems to be higher than those observed using ADN (10.70 mS.cm^{-1} at $w_{IL} = 0.75$ or $x_{IL} = 0.4792$) or GLN (10.81 mS.cm^{-1} at $w_{IL} = 0.80$ or $x_{IL} = 0.5005$). Each electrolyte at the maximum of conductivity, $C\sigma_{max}$, was then simply prepared in mass with an accuracy of $\pm 1.10^{-4}$ g using an OHAUS pioneerTM balance by mixing at ambient temperature known quantities of the IL and the dinitrile under a dry atmosphere in a glove box under N_2 .

2.3 Methods

Differential scanning calorimetric measurements were performed with a Perkin-Elmer DSC 4000 coupled with an Intracooler SP VLT 100. The instrument was calibrated with cyclohexane (solid–solid phase transition at -87.06 °C, melt transition (T_m) at 6.54 °C) and indium (T_m at 156.60 °C). From this study, the uncertainty of reported thermal properties did not exceed ± 1 °C and ± 2 %. The measuring (containing around 10 mg of studied material) and the reference cells were filled with inert aluminum pans. Each sample stability was measured under a N_2 atmosphere, and its DSC thermogram has been recorded with a scan rate of 5 °C.min^{-1} during a cooling from 20 °C to -60 °C, followed by a heating from -60 °C to 80 °C. An Antoon Paar rolling-ball viscometer Lovis 2000 M/ME was used to determine the viscosity of the pure liquid compounds and selected electrolytes from 5 to 80 °C within ± 0.02 °C. The viscosity standard (ASTM Oil Standard S600 of CANNON, 1053 mPa.s at 25 °C) and ultra-pure water were used to calibrate the viscometer. From this study, the uncertainty of reported viscosity measurements did not exceed ± 1 %. Electrochemical measurements were carried-out on a Versatile Multichannel Potentiostat (Biologic S.A) piloted by the EC Lab V11.10 interface.

Galvanostatic charge-discharge experiments and cyclic voltammetry were conducted using a Teflon Swagelok[®]-type system with a two-electrode cell with activated carbon as the working and counter electrodes.

3 Results and Discussion

3.1 Physical properties of selected blends

Based on our preliminary work devoted on the conductivity of investigated mixtures, electrolytes within an IL molar fraction, x_{IL} close to 0.4792, 0.5005 and 0.5332 for the ADN-, GLN- and MGLN-based blends, respectively, have been identified as interesting electrolytes for EDLCs. For the realization of high performance EDLCs, the use of electrolytes presenting a large temperature range (*i.e.* presenting a low melting and a high decomposition temperature), a low viscosity and high conductivity is in fact crucial. By considering these recommendations, the thermal properties of selected blends have been determined as shown in Figures 2 and 3, while transport properties data are shown in Figures 4 and 5.

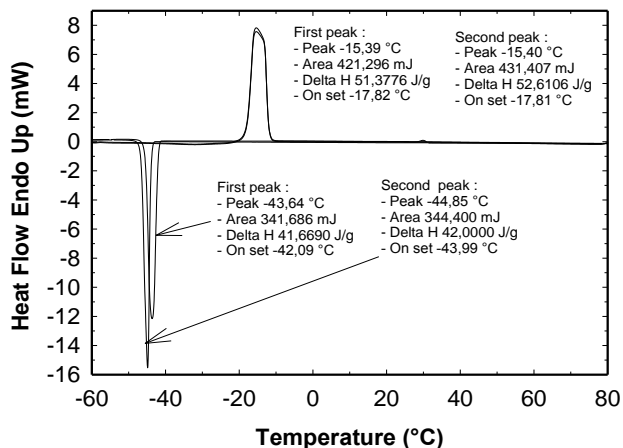


Figure 2. Example of DSC thermograph in the case of the pure IL

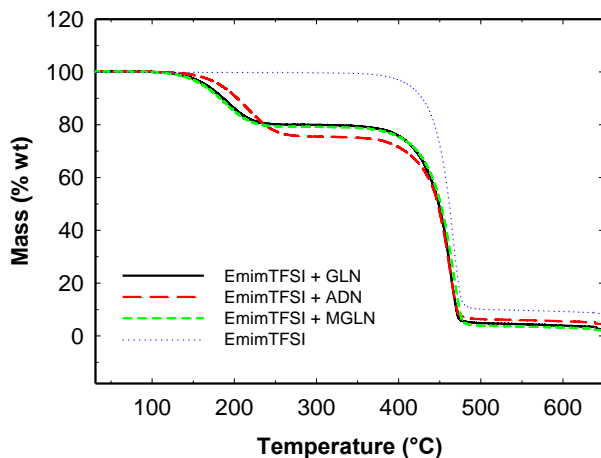


Figure 3. TGA curves for the pure IL and selected blends

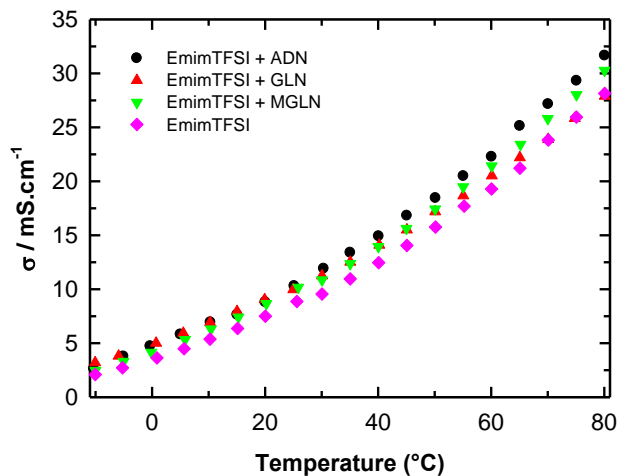


Figure 4. Temperature dependence of the conductivity of the selected blends

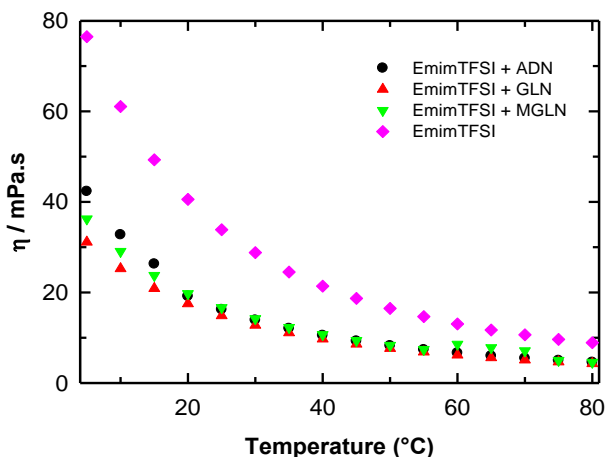


Figure 4. Temperature dependence of the viscosity of the selected blends.

As shown in Figures 2-3, the [EMIM][TFSI] show a melting point close to $-17.8\text{ }^{\circ}\text{C}$ (Figure 2), and a decomposition temperature close to $373\text{ }^{\circ}\text{C}$ (Figure 3). By mixing a dinitrile with this IL, a lower melting temperature is observed for each investigated blend. This behavior is driven by the melting point of each dinitrile $T_m = 1\text{ }^{\circ}\text{C}$, $-29\text{ }^{\circ}\text{C}$, and $-45\text{ }^{\circ}\text{C}$ for ADN, GLN and MGLN, respectively and more importantly by the formation of an eutectic in each case, as already reported by our group previously. [9] However, TGA curves clearly show that the presence of the dinitrile decreases the thermal stability of blends in comparison of the pure IL. According to the formulation of selected blends, it is obvious to point out that the first decomposition, observed at temperature close to $125\text{ }^{\circ}\text{C}$, is due to the evaporation of the dinitrile solvent as a mass loss close to 20wt% and 25wt% is observed for GLN- or MGLN- and ADN-based electrolytes, respectively. According to Figure 3, one can note also that ADN-based electrolyte is slightly more stable than the two others mainly due to its lower volatility. [9] In other words, selected electrolytes seem to be in a stable liquid state from $-16\text{ }^{\circ}\text{C}$ to $125\text{ }^{\circ}\text{C}$. This liquid range temperature is large enough to be used for EDLCs. As expected and shown in Figures 4 and 5, by increasing the temperature, the conductivity increases and the viscosity decreases for all investigated electrolytes. All investigated blends have better transport properties than the pure IL, as the presence of the solvent increases the conductivity and decreases the viscosity as also expected. At low temperature, *i.e.* lower than $25\text{ }^{\circ}\text{C}$, GLN-based electrolyte seems to have better transport properties than MGLN or ADN blends. For example, at $20\text{ }^{\circ}\text{C}$ conductivity and viscosity values are close to (8.80, 9.04, and 8.67) $\text{mS}\cdot\text{cm}^{-1}$ and (19.17, 17.50, and 19.75) $\text{mPa}\cdot\text{s}$ for the ADN, GLN and MGLN solutions, respectively. However, such tendency seems to be strongly affected by the temperature as at $T > 30\text{ }^{\circ}\text{C}$, the conductivity of ADN blend is higher than the two other solutions. For example, at $60\text{ }^{\circ}\text{C}$ conductivity and viscosity values are close to (22.27, 20.52, and 21.42) $\text{mS}\cdot\text{cm}^{-1}$ and (6.62, 6.17, and 8.57) $\text{mPa}\cdot\text{s}$ for the ADN, GLN and MGLN solutions, respectively. However, such transport properties are considerable lower than

those reported for the state-of-the-art electrolytes, *i.e.* the 1 mol.dm⁻³ Et₄NBF₄ in ACN (at 25 °C 55 mS.cm⁻¹ and 0.6 mPa·s) or 1 mol.dm⁻³ Et₄NBF₄ in PC (at 25 °C 13 mS.cm⁻¹ and 2.6 mPa·s). [1] In other words, it is obvious to highlight that the selected [EMIM][TFSI]-dinitrile blends reported herein work cannot compete with the ACN-based electrolyte. However, their transport properties are within the same order of magnitude of those reported for the 1 mol.dm⁻³ Et₄NBF₄ in PC especially taking into account the difference on the ionic concentration in solution in each case.

3.2 Electrochemical Behavior of Selected Electrolytes

Electrochemical performances of studied electrolytes were investigated in EDLC configuration at 25 °C. As shown in Figure 6, the cyclic voltammetry was performed for each electrolyte to investigate the voltammetric response obtained at 25 °C under a full cell voltage of 2.7 V and as a function of the scan rates from 5 mV.s⁻¹ to 200 mV.s⁻¹. As shown in Figure 6, no faradaic reaction is observed for the investigated electrolytes. It can be seen that the EDLC (referred to the total active materials) displayed the typical capacitive behavior in this operative voltage. As expected, regardless of the blend and operating voltages employed all electrolytes show an increase in distortion from the typical rectangular shape for the CVs for higher scan rates; however, the Coulombic efficiency of the charge-discharge process was always near 100 %. In other words, all investigated systems exhibit a typical capacitive behavior and nearly rectangular shape of the voltammetric response. However, at high scan rate (*e.g.* 100 mV.s⁻¹), the voltammetric response of each EDLC exhibits a strong deviation from the capacitor-like behavior. This strong deviation can be mainly attributed to different contributions from parallel resistances due to diffusion of solvated ions in the pores of the electrode material. In fact, a decrease of capacitance is achieved by increasing the scan rate. For example, the measured specific capacities at 20 mV.s⁻¹ and 100 mV.s⁻¹ are close to (32.2 and 22.0) F.g⁻¹, (38.3 and 22.5) F.g⁻¹, and (37.1 and 17.0) F.g⁻¹ for ADN, GLN and MGLN blends, respectively. Besides, the better electrochemical performances observed in the case of the GLN blend can be attributed to its better transport properties as its ionic conductivity is higher than those measured for the ADN or MGLN mixtures.

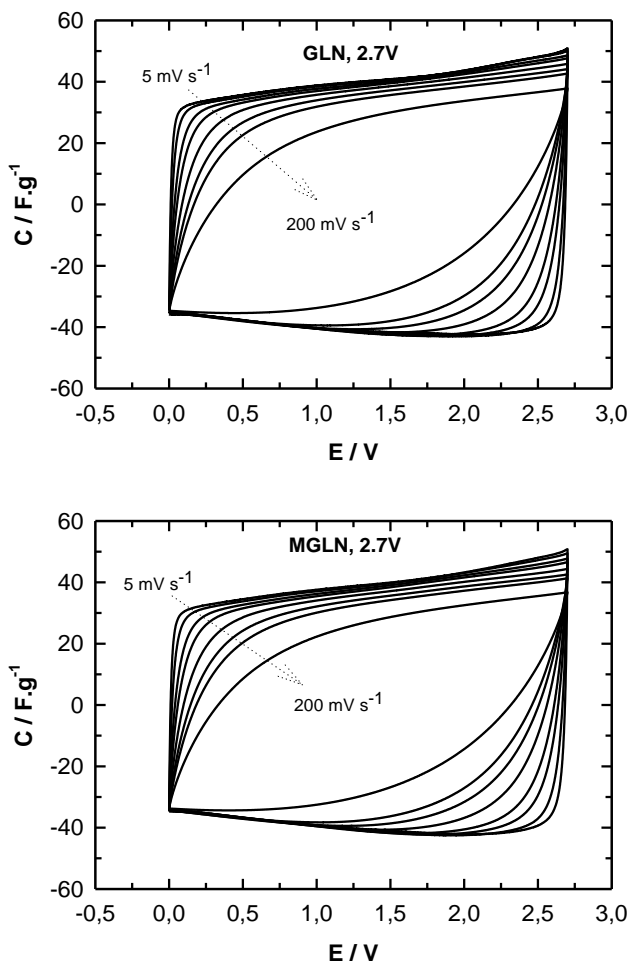


Figure 6. Cyclic voltammograms of the investigated blends as a function of the scan rates from 5 mV.s⁻¹ to 200 mV.s⁻¹

By contrast, the ADN-based electrolyte, which is more viscous at 25 °C (*i.e.* less ionic), leads to a lower specific capacitance. Taking into account the results reported herein, all investigated nitrile-based electrolytic solutions appear to be suitable as electrolytes in EDLCs. However, it is also obvious that these electrolytes are not outperforming the conventional benchmark but they are very promising especially by taking into account their better thermal properties than ACN-based electrolyte.

4 Conclusion

In this manuscript, we have reported about the use of blends of dinitriles, namely ADN, GLN and MGLN mixed with the [EMIM][TFSI] in EDLCs. Herein, their physical (liquid range temperature, conductivity, viscosity) and electrochemical (CV, specific capacitance) properties configuration are reported. The results show clearly that these blends can be regarded as new class of electrolytes for EDLCs. Based on the results of the conductivity and viscosity measurements, the GLN blend has the superior transport properties with higher conductivity ($9.04 \text{ mS}\cdot\text{cm}^{-1}$ at $20 \text{ }^\circ\text{C}$) and lower viscosity ($17.50 \text{ mPa}\cdot\text{s}$ at $20 \text{ }^\circ\text{C}$) than the ADN and MGLN blends. In fact, these values are close to those reported for the commonly used organic solvent based electrolyte of $1 \text{ mol}\cdot\text{dm}^{-3} \text{ Et}_4\text{NBF}_4$ in PC ($13 \text{ mS}\cdot\text{cm}^{-1}$ and $2.6 \text{ mPa}\cdot\text{s}$ at $25 \text{ }^\circ\text{C}$, respectively). As a matter of fact, using these electrolytes it is possible to realize EDLCs which are able to deliver energy and power values among the highest reported so far for devices containing non-conventional electrolyte. Such GLN-based mixture can provide an efficient and safer electrolyte with similar performances (high capacitance) to the classical PC-based electrolyte. These results confirm that the use of blends of organic solvent and ionic liquid represent a good strategy for the design of EDLCs. Thereafter, it is also crucial to further evaluate the safety behavior of these electrolytes, especially when they are put in the contact with a flame, for example. Study is still in progress, and more detailed and comparative physical and electrochemical results will be presented soon.

References

- [1] Béguin, F.; Presser, V.; Balducci, A.; Frackowiak, E. Carbons and Electrolytes for Advanced Supercapacitors. *Adv. Mater. (Weinheim, Ger.)* 2014, *26*, 2219-2251.
- [2] Aparicio, S.; Atilhan, M.; Karadas, F. Thermophysical Properties of Pure Ionic Liquids: Review of Present Situation. *Ind. Eng. Chem. Res.* 2010, *49*, 9580-9595.
- [3] Balducci, A.; Dugas, R.; Taberna, P. L.; Simon, P.; Plée, D.; Mastragostino, M.; Passerini, S., High Temperature Carbon–Carbon Supercapacitor Using Ionic Liquid as Electrolyte. *J. Power Sources* 2007, *165*, 922-927.
- [4] Abdallah, T.; Lemordant, D.; Claude-Montigny, B., Are Room Temperature Ionic Liquids Able to Improve the Safety of Supercapacitors Organic Electrolytes without Degrading the Performances? *J. Power Sources* 2012, *201*, 353-359.
- [5] Coadou, E.; Timperman, L.; Jacquemin, J.; Galiano, H.; Hardacre, C.; Anouti, M., Comparative Study on Performances of Trimethyl-Sulfonium and Trimethyl-Ammonium Based Ionic Liquids in Molecular Solvents as Electrolyte for Electrochemical Double Layer Capacitors. *J. Phys. Chem. C* 2013, *117*, 10315-10325.
- [6] Coadou, E.; Goodrich, P.; Neale, A. R.; Timperman, L.; Hardacre, C.; Jacquemin, J.; Anouti, M. Synthesis and Thermophysical Properties of Ether-Functionalized Sulfonium Ionic Liquids as Potential Electrolytes for Electrochemical Applications. *ChemPhysChem* 2016, *17*, 3992-4002.
- [7] Pohlmann, S.; Olyschläger, T.; Goodrich, P.; Vicente, J. A.; Jacquemin, J.; Balducci, A., Mixtures of Azepanium Based Ionic Liquids and Propylene Carbonate as High Voltage Electrolytes for Supercapacitors. *Electrochim. Acta* 2015, *153*, 426-432.

- [8] Dagousset, L.; Nguyen, G. T. M.; Vidal, F.; Galindo, C.; Aubert, P.-H. Ionic liquids and γ -Butyrolactone Mixtures as Electrolytes for Supercapacitors Operating Over Extended Temperature Ranges. *RSC Adv.* 2015, 5, 13095-13101.
- [9] Ghamouss, F.; Brugère, A.; Jacquemin, J. Physicochemical Investigation of Adiponitrile-Based Electrolytes for Electrical Double Layer Capacitor. *J. Phys. Chem. C* 2014, 118, 14107-14123.
- [10] Schütter, C.; Neale, A. R.; Wilde, P.; Goodrich, P.; Hardacre, C.; Passerini, S.; Jacquemin, J.; Balducci, A., The Use of Binary Mixtures of 1-Butyl-1-Methylpyrrolidinium Bis{(Trifluoromethyl)Sulfonyl}Imide and Aliphatic Nitrile Solvents as Electrolyte for Supercapacitors. *Electrochim. Acta* 2016, 220, 146-155.

Electrochemical Model Development and Overcharging Investigation of the Vanadium Redox Flow Battery

KITTIMA NGAMSAI & AMORNCHAI ARPORNWICHANOP

Abstract The electrochemical cell is an important component of vanadium redox flow battery (VRB) systems for power generation. A comprehensive understanding of the cell components and behavior results in the improved performance and efficient operation of the VRB. In this study, a simplified electrochemical model of VRB is developed to predict the potential of an actual cell, and the model is employed to investigate the performance of the electrochemical cell. The results of the predicted cell potential are beneficial to determining a usable voltage range for the system, which can be used to define the properties of connecting devices. In addition, overcharging in the cell is studied with respect to key operating parameters, such as the flow rate of the electrolyte solution, the current density and the inlet state of charge. The results obtained can be used to operate the system without overcharging in the VRB cell.

Keywords: • vanadium redox flow battery • electrochemical model • actual potential • overcharging • Nernst equation •

CORRESPONDENCE ADDRESS: Kittima Ngamsai, Ph.D., Researcher, Chulalongkorn University, Faculty of Engineering, Department of Chemical Engineering, Bangkok 10330, Thailand, e-mail: kittimajaaom@hotmail.com. Amornchai Arpornwichanop, Ph.D., Assistant Professor, Chulalongkorn University, Faculty of Engineering, Department of Chemical Engineering, Computational Process Engineering Research Unit, Bangkok 10330, Thailand, e-mail: Amornchai.a@chula.ac.th.

<https://doi.org/10.18690/978-961-286-052-3.11>

ISBN 978-961-286-052-3

© 2017 University of Maribor Press

Available at: <http://press.um.si>.

1 Introduction

Energy storage plays an important role in the development of renewable energy systems. It can solve the problems of the uncertainty and intermittency of renewable energy. Vanadium redox flow batteries (VRBs) are an important potential technology that can be utilized to store energy [1]. The redox reactions of vanadium are used in both the positive and negative half-cells. Therefore, cross-contamination between the ions from either half-cell is eliminated [2]. In addition, the key advantage of a VRB system is the independent design of its power and energy because the system power is determined by the electrochemical cell stack, whereas the system energy depends on the amount of active species in the electrolyte solution [3].

The VRB system is composed of many sub-components such as the VRB cell, electrolyte storage tank and electrical conversion unit. Modeling and simulation tools are a low-cost and less time-consuming way to study and understand the complex behavior of VRBs [4]. In general, the electrochemical model and mechanical model of the VRB system are employed to explain the electrochemical cell and the electrolyte flow of the system, respectively [5]. The mass, charge, energy and momentum transport and conservation have been considered to investigate the cell behavior [6]. Moreover, the design of the appropriate flow rate within the cell has been studied [7]. Specifically, the flow through fiber electrodes was simulated to study the effect of flow characteristics on cell performance [8]. To date, although the different models of the VRB cell have been proposed and developed, they are sensitive to model parameters that are varied by a change in the operating conditions and need to be study.

To more precisely understand the VRB system, the fundamental VRB electrochemical cell is briefly described in this study to comprehend the operation of the VRB cell. A simple electrochemical model of VRB is explained, and this model is used to study the behavior of a VRB cell. In addition, experiments of the VRB cells are carried out and the obtained data are used to compared with the model prediction. The model can then be used to predict the cell voltage of the same cell system in other conditions. In this study, losses within the cell during operation are studied to comprehend the effect of cell components on the cell voltage of the VRB system. The effect of operating conditions on overcharging in a VRB cell is studied considering three factors, flow rate of electrolyte solution, current density and the inlet state of charge.

2 Cell Configuration

A single cell VRB shown schematically in Figure 1 is used in this study. The cell consists of three components: (1) current collectors, (2) fiber electrodes and (3) an ion exchange membrane. Electrolyte solutions are flowed through the fiber electrodes of the cell, which are sandwiched between the current collector and the ion exchange membrane in both half-cells. The reactions that occur in positive and negative half-cells are presented in Equations (1) and (2), respectively.



3 Electrochemical Model

3.1 Nernst Equation

The Nernst equation is used to describe the cell voltage without current flow, which is called the open circuit voltage (OCV). The Nernst equation indicates the existing energy in the system, which is the state of charge (SOC) of the system. The correlation of the SOC and the OCV is presented in Equation (3). The SOC can be written in terms of the vanadium concentration in Equation (4).

$$\text{OCV} = E_{\text{total}}^0 + \frac{RT}{nF} \ln \left(\frac{\text{SOC}}{1-\text{SOC}} \right)^2 \quad (3)$$

$$\text{SOC} = \frac{C_{\text{V}^{2+}}}{C_{\text{total}}} = \frac{C_{\text{VO}_2^+}}{C_{\text{total}}} \quad (4)$$

The standard potential of the cell is equal to 1.390 V when an electrolyte solution is employed with a vanadium concentration of 1.5 mol L⁻¹ and a sulfuric acid concentration of 3 mol L⁻¹. However, this potential depends on the ingredients of the electrolyte solution. In the charging process, the actual potential is equal to the OCV plus its losses, whereas in the discharging process, the actual potential is equal to the OCV minus its losses. The losses of the charging and discharging processes are different.

3.2 Actual Potential

The actual potential is the voltage of the cell during operation which current flows through the cell.

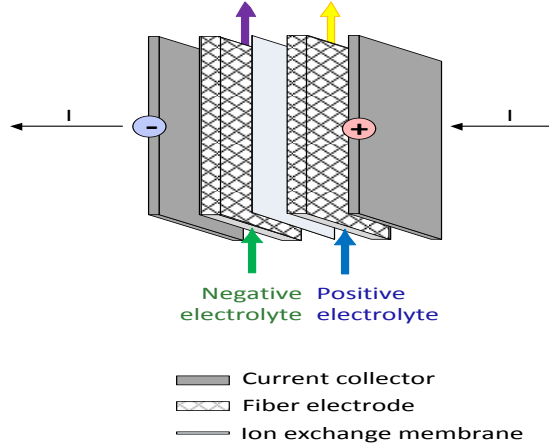


Figure 1. A VRB single cell

The activation loss (η_{act}) can be calculated from Equation (5), which indicates that the activation loss depends on the operating current, flow rate, operating temperature, concentration of protons in the electrolyte solution and the electrode material for the cell.

$$\eta_{act} = \frac{RT}{\alpha n F} \ln \left(\frac{I}{I_0} \right) \quad (5)$$

The concentration overpotential arises from the difference between the ion concentrations in the bulk solution (b) and at the electrode surface (s). The concentration difference depends on the uniformity and the speed of the flow rate within the cell, which result from the fiber electrode configuration, the flow channel design and the pump power. The concentration loss (η_{con}) can be calculated from Equation (6).

$$\eta_{conc} = \frac{RT}{F} \ln \left\{ \frac{C_{VO_2^+}(b) C_{H^+}(b)^2 C_{V^{2+}}(b)}{C_{VO^{2+}}(b) C_{V^{3+}}(b)} \times \frac{C_{VO^{2+}}(s) C_{V^{3+}}(s)}{C_{VO_2^+}(s) C_{H^+}(s)^2 C_{V^{2+}}(s)} \right\} \quad (6)$$

The ohmic overpotential is the resistance to electron flow. Electrons travel from the low voltage electrode where the oxidation reaction occurs toward the high voltage electrode where the reduction reaction occurs. Therefore, this loss involves the resistances of the

current collector ($R_{\text{collector}}$) and the fiber electrode ($R_{\text{electrode}}$). The ohmic loss (η_{ohm}) can be calculated from Equation (7).

$$\eta_{\text{ohm}} = (R_{\text{electrode}} + R_{\text{collector}}) \cdot I \quad (7)$$

The ionic overpotential is the voltage loss from ion diffusion resistance. Therefore, it consists of the ion exchange membrane resistance (R_{membrane}) and the electrolyte solution resistance ($R_{\text{electrolyte}}$). The ionic loss (η_{ion}) can be calculated by Equation (8).

$$\eta_{\text{ion}} = (R_{\text{membrane}} + R_{\text{electrolyte}}) \cdot I \quad (8)$$

Consequently, the actual potentials in the charging and discharging processes can be calculated by Equations (9) and (10), respectively.

$$U_{\text{ch}} = \text{OCV} + \eta_{\text{act}} + \eta_{\text{con}} + \eta_{\text{ohm}} + \eta_{\text{ion}} \quad (9)$$

$$U_{\text{dch}} = \text{OCV} - \eta_{\text{act}} - \eta_{\text{con}} - \eta_{\text{ohm}} - \eta_{\text{ion}} \quad (10)$$

The correlations of the SOC and the actual potential (cell voltage) in the charging and discharging processes obtained from the above equations are illustrated in Figure. 2. The parameters used in the simulation are presented in Table 1.

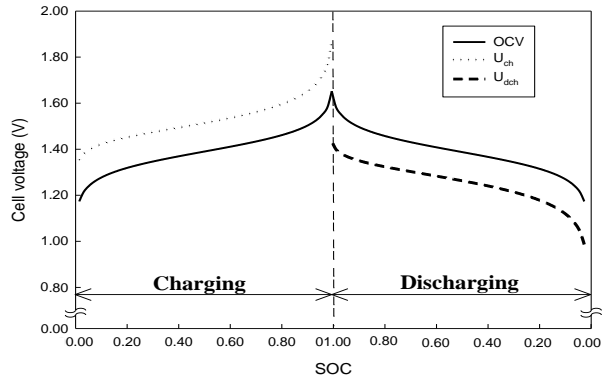


Figure 2. Cell voltage in charging and discharging processes using the constant current mode

Table 1. The parameters used in the simulation of the actual potential

A	0.014 m ²
C_{total}	1.5 mol L ⁻¹
E^0_{total}	1.39 V
F	96,485 A s mol ⁻¹
k^0_{ch}	3.2 x 10 ⁻⁶ m s ⁻¹
k^0_{dch}	3.3 x 10 ⁻⁶ m s ⁻¹
n	1
R	8.314 J mol K ⁻¹
$R_{\text{collector}}$	6 x 10 ⁻⁶ Ω m ²
$R_{\text{electrode}}$	8 x 10 ⁻⁶ Ω m ²
R_{membrane}	4.8 x 10 ⁻⁵ Ω m ²
T	298 K
V_c	0.0378 L
V_{sol}	0.28 L
α	0.57

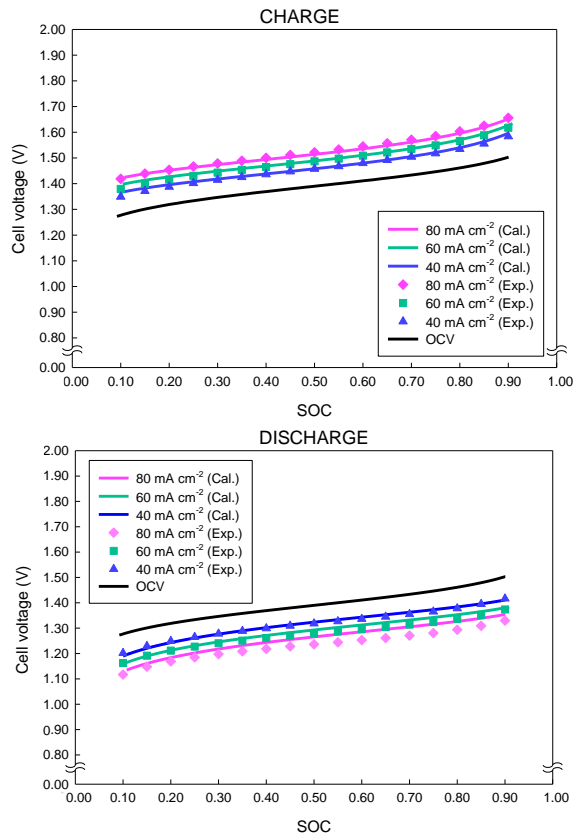


Figure 3. Effect of the SOC on cell voltage: Comparison between the experimental data and data calculated from the electrochemical model at various current densities.

4 Results and Discussion

4.1 Model validation

The electrochemical models that are discussed above are simulated to study the effects of current density on the voltage efficiency of the VRB system at three different current densities, 80 mA cm^{-2} , 60 mA cm^{-2} and 40 mA cm^{-2} . Experiments with the same constant currents were also performed. A cell with an effective area of 0.014 m^2 and an electrolyte solution with a vanadium concentration of 1.5 mol L^{-1} were employed to validate the simulations. The results of the charging and discharging processes with varying current densities are illustrated in Figure (3).

The results show that during the charging process, at the highest current density (80 mA cm⁻²), the highest voltage is obtained (i.e., the largest difference from the OCV) for all SOC regions. In the discharging process, the results show that at the highest current, the lowest voltage is obtained. For the charging process, the calculated data agree reasonably well with the experimental data. However, for the discharging process, the calculated and experimental data are significantly different.

4.2 Effect of the operating conditions on overcharging in a VRB cell

Overcharging is occurred when the input power is higher than the limitation of the obtainable power. For the VRB system, overcharging is because the amount of vanadium active species in the cell is insufficient for the input charge. The excess charge will generate heat, and side reactions occur, i.e., oxygen and hydrogen evolution reactions in the positive and negative half-cells, respectively. In addition, overcharging leads to electrolyte imbalance, electrode damage and flow obstruction from the gases. The factors that affect overcharging are the flow rate of the electrolyte solution, which affects the retention time of the active species in the cell, the inlet SOC (SOC_{in}) and the charging current (or current density), which is the rate of charge input. In addition, the important factor that reveals the occurrence of overcharging is the outlet SOC (SOC_{out}). In regular systems, the outlet SOC must be less than 1. The outlet SOC is the amount of active species ($C_{V^{2+}}$ and $C_{VO_2^+}$) at the cell outlet divided by the amount of all vanadium species (C_{total}). Therefore, $C_{V^{2+}}$ and $C_{VO_2^+}$ at the cell outlet must be less than or equal to in a non-overcharging system.

Overcharging is initially considered from $C_{V^{2+}}$ and $C_{VO_2^+}$, which are the amount of active species in the negative and positive sides, respectively. During charging and discharging operations, $C_{V^{2+}}$ and $C_{VO_2^+}$ are always changing. The concentration changes depend on operating conditions, including the current density, the flow rate and the inlet SOC.

Effect of the Flow Rate

The correlation of the flow rate within the cell and the outlet SOC is illustrated in Figure 4. A current density of 80 mA cm⁻², an inlet SOC of 0.5 and a cell with effective area of 100 cm² are used in the simulation. The result shows that more change in the outlet SOC is found when the flow rate is less than 20 cm³ min⁻¹, which indicates that a small change in the flow rate has a large effect on the outlet SOC. This flow rate region is called the region of critical flow rate. Therefore, the flow rate should be higher than the region of critical flow rate in practical operation. Figure 4 also implies that the cell is overcharged at a flow rate of less than 6 cm³ min⁻¹ because the outlet SOC is greater than 1.

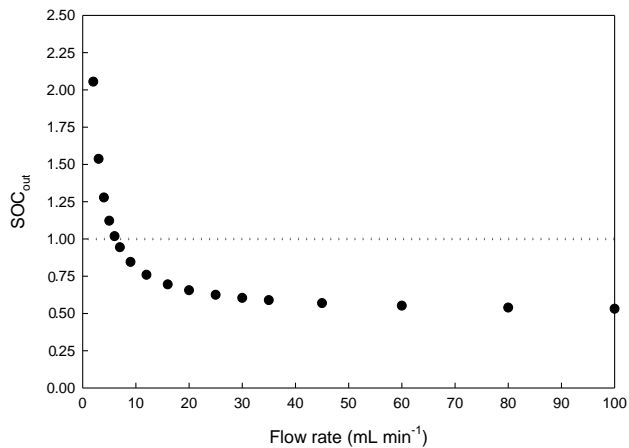


Figure 4. Correlation between the flow rate and the outlet SOC (an inlet SOC of 0.5 and a current density of 80 mA cm⁻²)

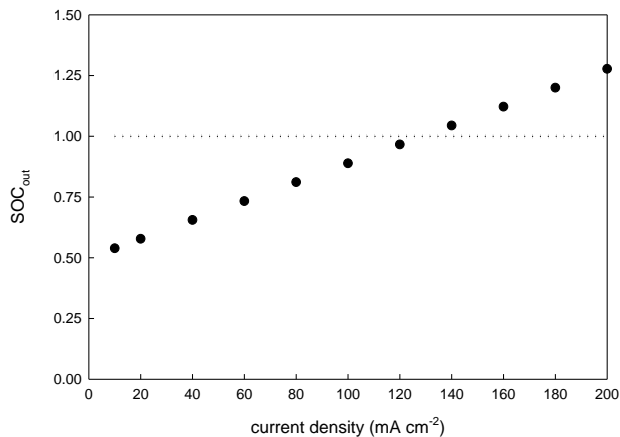


Figure 5. Correlation between the current density and the outlet SOC (an inlet SOC of 0.5 and a flow rate of 10 cm³ min⁻¹).

Effect of the Current Density

To compare the performance of this system with other systems, the operating current of the system is preferably calculated with respect to the effective area (the current density). The correlation of the current density and the outlet SOC at an inlet SOC of 0.5, a flow rate of 10 cm³ min⁻¹ and in a cell with an effective area of 100 cm² is illustrated in Figure 5. Using a current density higher than 120 mA cm⁻² leads to overcharging in this condition.

Effect of the Inlet SOC

The SOC is preferably measured at the inlet and the outlet of the cell. The SOC at the cell inlet indicates the existing energy in the electrolyte solution coming from the reservoir, while the SOC at the cell outlet indicates the existing energy in the electrolyte solution with charging and discharging effects. The outlet SOC is the indicator of overcharging. The correlation of the inlet and outlet SOCs at a flow rate of $10 \text{ cm}^3 \text{ min}^{-1}$ and a current density of 80 mA cm^{-2} in a cell with an effective area of 100 cm^2 is illustrated in Figure 6. The cell overcharge at an inlet SOC of approximately 0.7. At this point, the cell needs to be stopped or the conditions need to be adjusted to protect the cell from overcharging. The alteration of the conditions should consider three factors together to effectively utilize the system. The details of these considerations are presented below.

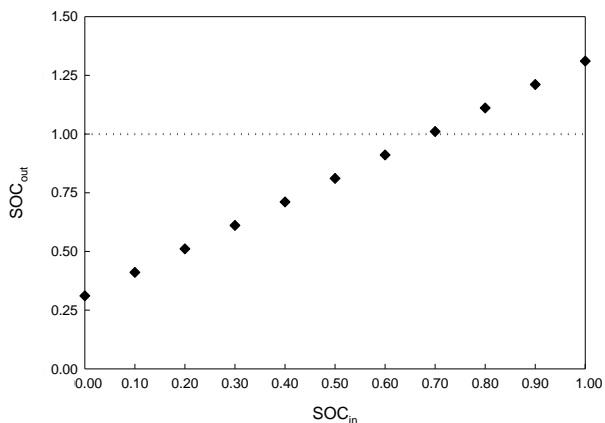


Figure 6. Correlation between the inlet and outlet SOCs

5 Conclusions

In this study, the electrochemical models for a VRB cell is developed and used to explain the actual potential of the cell. Initially, the Nernst equation is used to explain OCV, which is the cell voltage without current flow (idle mode). The actual potential can be determined by considering voltage losses (i.e., activation loss, concentration loss, ohmic loss and ionic loss) in the charging and discharging processes. The simulation of the current density effect indicates that a high current density results in a high loss. Furthermore, the effect of the flow rate of the electrolyte solution within the cell on any losses is studied. In addition, overcharging within the VRB cell is studied. Three factors are investigated, including the flow rate, current density and inlet SOC. The parameter that is used to indicate overcharging is the outlet SOC. The results show that the three factors need to be considered together to indicate overcharging within the cell. These results can be used to operate and design the controller to eliminate overcharging within VRB cells.

Acknowledgements

Support from Chulalongkorn Academic Advancement into Its 2nd Century Project is gratefully acknowledged.

References

- [1] D. Chen, S. Wang, M. Xiao, Y. Meng, Synthesis and properties of novel sulfonated poly(arylene ether sulfone) ionomers for vanadium redox flow battery, *Energy Conversion and Management*, 51 (2010) 2816-2824.
- [2] M. Kazacos, M. Cheng, M. Skyllas-Kazacos, Vanadium redox cell electrolyte optimization studies, *Journal of Applied Electrochemistry*, 20 (1990) 463-467.
- [3] H. Al-Fetlawi, A.A. Shah, F.C. Walsh, Non-isothermal modelling of the all-vanadium redox flow battery, *Electrochimica Acta*, 55 (2009) 78-89.
- [4] A.A. Shah, H. Al-Fetlawi, F.C. Walsh, Dynamic modelling of hydrogen evolution effects in the all-vanadium redox flow battery, *Electrochimica Acta*, 55 (2010) 1125-1139.
- [5] C. Blance, Modeling of a vanadium redox flow battery electricity storage system, Polytechnic school Federal of Lausanne, 2009.
- [6] A.A. Shah, M.J. Watt-Smith, F.C. Walsh, A dynamic performance model for redox-flow batteries involving soluble species, *Electrochimica Acta*, 53 (2008) 8087-8100.
- [7] J. Escudero-González, P.A. López-Jiménez, Methodology to optimize fluid-dynamic design in a redox cell, *Journal of Power Sources*, 251 (2014) 243-253.
- [8] Q. Xu, T.S. Zhao, P.K. Leung, Numerical investigations of flow field designs for vanadium redox flow batteries, *Applied Energy*, 105 (2013) 47-56.

A Comprehensive Review of Solar Thermal Energy Storage

IOAN SARBU & CALIN SEBARCHIEVICI

Abstract Thermal energy storage (TES) is a technology that stocks thermal energy by heating or cooling a storage medium so that the stored energy can be used at a later time for heating and cooling applications and power generation. This paper is focused on the analysis of TES technologies that provide a way of valorising solar heat and reducing the energy demand of buildings. The principles of several energy storage methods and calculation of storage capacities are described. Sensible heat storage technologies including the use of water, underground, and packed-bed are briefly reviewed. Latent-heat storage systems associated with phase-change materials for use in solar heating and cooling of buildings, solar water-heating and heat-pump systems, and thermochemical heat storage are also presented. Finally, cool thermal energy storage is also briefly reviewed.

Keywords: • sensible heat storage • latent heat storage • phase change materials • thermochemical storage • cool thermal energy storage •

CORRESPONDENCE ADDRESS: Ioan Sarbu, Ph.D., Professor, Polytechnic University of Timisoara, Department of Building Services Engineering, Piata Victoriei 2A, 300006 Timisoara, Romania, e-mail: ioan.sarbu@upt.ro. Calin Sebarchievici, Ph.D., Lecturer, Polytechnic University of Timisoara, Department of Building Services Engineering, Piata Victoriei 2A, 300006 Timisoara, Romania, e-mail: calin.sebarchievici@upt.ro.

<https://doi.org/10.18690/978-961-286-052-3.12>

ISBN 978-961-286-052-3

© 2017 University of Maribor Press

Available at: <http://press.um.si>.

1 Introduction

One of the main aspects of solar systems is storage. Thermal energy storage (TES) systems are used particularly in buildings and industrial processes. Advantages of using thermal energy storage in an energy system are the increase of the overall efficiency and better reliability, but it can also lead to better economics, reducing investment and running costs, and less pollution of the environment and less carbon dioxide (CO₂) emissions [1].

In Europe, it has been estimated that around 1.4 million GWh/year could be saved and 400 million tons of CO₂ emissions avoided, in the building and industrial sectors by more extensive use of heat and cold storage [2].

Storage density, in terms of the amount of energy per unit of volume or mass, is an important issue for applications in order to optimise a solar ratio, efficiency of the appliances (solar thermal collectors and absorption chillers), and room consumption. For these reasons, it is worth to investigate the possibility of using phase-change materials (PCMs) in solar system applications. The potential of PCMs is to increase the energy density of small-sized water storage tanks, reducing solar storage volume for a given solar fraction or increasing the solar fraction for a given available volume [3].

It is possible to think of thermal storage in the hot and/or in the cold side of the plant. The former allows the storage of hot water from the collectors (and from the auxiliary heater) to be supplied to the generator of the absorption chiller (in cooling mode) or directly to the users (in heating mode). The latter allows the storage of cold water produced by the absorption chiller to be supplied to the cooling terminals inside the building. While heat storages in the hot side of solar plants are always present because of heating and/or domestic hot water (DHW) production, cold storages are justified in bigger size plants. Cold storages are used not only to get economic advantages from the electricity tariffs (in case of electric compression chiller) depending on the time-of-the-day but also to lower cooling power installed and to allow more continuous operation of the chiller [4].

This paper is focused on the analysis of TES technologies that provide a way of valorising solar heat and reducing the energy demand of buildings. The principles of several energy storage methods and calculation of storage capacities are described. Sensible heat storage (SHS) technologies including the use of water, under-ground and packed-bed are briefly reviewed. Additionally, latent-heat storage (LHS) systems associated with PCMs for use in solar heating and cooling of buildings, solar water-heating and heat-pump systems, and thermochemical storage (TCS) are presented. Finally, cool thermal energy storage is also briefly reviewed.

2 Classification and Characteristics of Storage Systems

The main types of thermal energy storage of solar energy are presented in Fig. 1. An energy storage system can be described in terms of the following characteristics:

capacity, power, efficiency, storage period, charge and discharge times, and cost of the storage system. Capacity, power and discharge time are interdependent variables, and in some storage systems, capacity and power can also depend on each other.

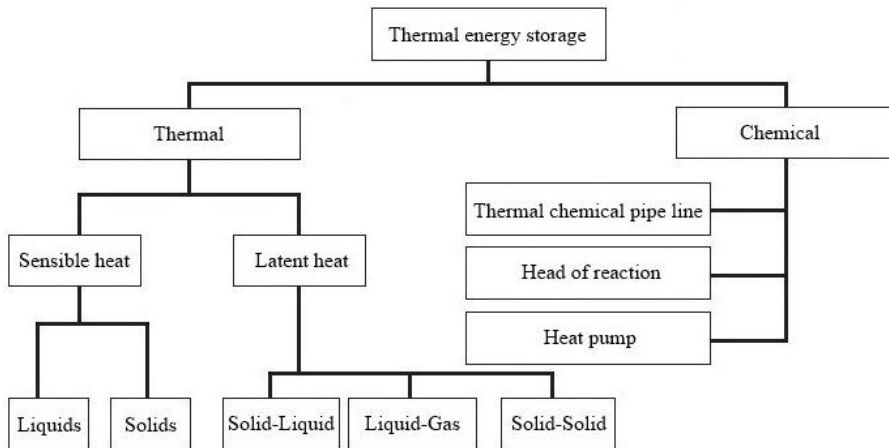


Figure 1. Types of Thermal Energy Storage of Solar Energy

Typical parameters for TES systems are shown in Table 1 [5], including capacity, power, efficiency, storage period, and cost. High-energy storage density and high power capacity for charging and discharging are desirable properties of any storage system. It is well known that there are three methods for TES at temperatures from $-40\text{ }^{\circ}\text{C}$ to more than $400\text{ }^{\circ}\text{C}$: sensible heat, latent heat associated with PCMs, and thermochemical heat storage associated with chemical reactions (Fig. 2) [6].

Table 1. Typical Parameters of TES Systems

TES System	Capacity (kWh/t)	Power (MW)	Efficiency (%)	Storage Period	Cost (€/kWh)
Sensible (hot water)	10-50	0.001-10	50-90	days/months	0.1-10
PCM	50-150	0.001-1	75-90	hours/months	10-50
Chemical reactions	120-250	0.01-1	75-100	hours/days	8-100

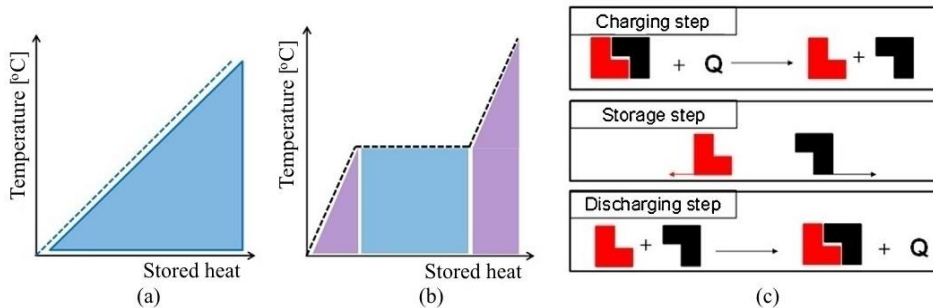


Figure 2. Methods of Thermal Energy Storage: (a) sensible heat; (b) latent heat; (c) thermochemical reactions

The choice of storage medium depends on the nature of the process. For water heating, energy storage as sensible heat of stored water is logical. If air-heating collectors are used, storage in sensible or latent heat effects in particulate storage units is indicated, such as sensible heat in a pebble-bed heat exchanger. In passive heating, storage is provided as sensible heat in building the elements. If photovoltaic or photo-chemical processes are used, storage is logically in the form of chemical energy.

3 Sensible Heat Storage

Sensible heat storage (SHS) (Fig. 2a) is the simplest method based on storing thermal energy by heating or cooling a liquid or solid storage medium (e.g., water, sand, molten salts, or rocks), with water being the cheapest option.

SHS system utilises the heat capacity and the change in temperature of the storage medium during the process of charging and discharging. The amount of heat stored depends on the specific heat of the medium, the temperature change, and the amount of storage material [7].

$$Q_s = \int_{t_i}^{t_f} mc_p dt = mc_p (t_f - t_i) \quad (1)$$

where: Q_s is the quantity of heat stored, in J; m is the mass of heat storage medium, in kg; c_p is the specific heat, in J/(kg·K); t_i is the initial temperature, in °C; t_f is the final temperature, in °C.

3.1 Water tank storage

The use of hot-water tanks is a well-known technology for thermal energy storage. Hot-water tanks serve the purpose of energy saving in water heating systems based on solar

energy and in co-generation (i.e., heat and power) energy supply systems. A typical system in which a water tank is used is shown in Fig. 3.

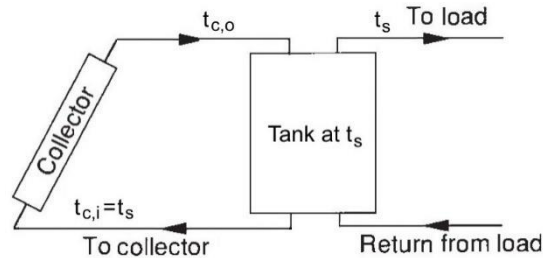


Figure 3. A Typical System Using Water Tank Storage

The energy storage capacity of a water (or other liquid) storage unit at uniform temperature (i.e., fully mixed, or no stratified) operating over a finite temperature difference is given by Eq. (1) redefined as

$$Q_s = mc_p \Delta t_s \quad (2)$$

where Q_s is the total heat capacity for a cycle operating through the temperature range Δt_s and m , c_p is the mass and the specific heat, respectively of water in the unit. The temperature range over which such a unit can operate is limited at the lower extreme for most applications by the requirements of the process. The upper limit may be determined by the process, the vapour pressure of the liquid, or the collector heat loss.

Hot water storage systems used as buffer storage for DHW supply are usually in the range of 500 L to several cubic meters (m³). This technology is also used in solar thermal installations for DHW combined with building heating systems (combisystems).

3.2 Underground storage

Underground thermal energy storage (UTES) is also a widely used storage technology, which makes use of the ground (e.g., the soil, sand, rocks, and clay) as a storage medium for both heat and cold storage.

Means must be provided to add energy to and remove it from the medium. This is done by pumping heat transfer fluids (HTFs) through pipe arrays in the ground. The pipes may be vertical U-tubes inserted in wells (*boreholes*) that are spaced at appropriate intervals in the storage field or they may be horizontal pipes buried in trenches. These storage systems are usually not insulated, although insulation may be provided at the ground surface.

Aquifer storage is closely related to ground storage, except that the primary storage medium is water, which flows at low rates through the ground. Water is pumped out of and into the ground to heat it and extract energy from it. Water flow also provides a mechanism for heat exchange with the ground itself. As a practical matter, aquifers cannot be insulated. Only aquifers that have low natural flow rates through the storage field can be used.

Cavern storage and pit storage are based on large underground water reservoirs created in the subsoil to serve as TES systems. Caverns are the same in their principles of operation as the tanks discussed in previously section. Energy is added to or removed from the store by pumping water into or out of the storage unit. The major difference will be in the mechanisms for heat loss and possible thermal coupling with the ground. These storage options are technically feasible, but applications are limited because of the high investment costs.

3.3 Pebble-bed storage

A pebble-bed (packed-bed) storage unit uses the heat capacity of a bed of loosely packed particulate material to store energy. A fluid, usually air, is circulated through the bed to add or remove energy. A variety of solids may be used, rock and pebble being the most widely used materials.

A pebble-bed storage unit is shown in [8]. In operation, flow is maintained through the bed in one direction during addition of heat (usually downward) and in the opposite direction during removal of heat. Note that heat cannot be added and removed at the same time; this is in contrast to water storage systems, where simultaneous addition to and removal from storage is possible.

A major advantage of a packed-bed storage unit is its high degree of stratification. The pebbles near the entrance are heated, but the temperature of the pebbles near the exit remains unchanged and the exit-air temperature remains very close to the initial bed temperature. As time progresses a temperature front passes through the bed. When the bed is fully charged, its temperature is uniform.

Many studies are available on the heating and cooling of packed beds. The first analytical study was by Schumann [9].

4 Latent-Heat Storage

The energy storage density increases and hence the volume is reduced, in the case of LHS (Fig. 2b). The heat is mainly stored in the phase-change process (at a quite constant temperature) and it is directly connected to the latent heat of the substance. The use of a LHS system using PCMs is an effective way of storing thermal energy and has the advantages of high-energy storage density and the isothermal nature of the storage process.

LHS is based on the heat absorption or release when a storage material undergoes a phase change from solid to liquid or liquid to gas or vice versa. The storage capacity Q_s , in J, of the LHS system with a PCM medium [7] is given by

$$Q_s = \int_{t_i}^{t_m} mc_p dt + mf\Delta q + \int_{t_m}^{t_f} mc_p dt \quad (3)$$

$$Q_s = m \left[c_{ps} (t_m - t_i) + f\Delta q + c_{pl} (t_f - t_m) \right] \quad (4)$$

where t_m is the melting temperature, in °C; m is the mass of PCM medium, in kg; c_{ps} is the average specific heat of the solid phase between t_i and t_m , in kJ/(kg K); c_{pl} is the average specific heat of the liquid phase between t_m and t_f , in J/(kg K); f is the melt fraction; and Δq is the latent heat of fusion, in J/kg. For example, Glauber's salt ($\text{Na}_2\text{SO}_4 \cdot 10\text{H}_2\text{O}$) has $c_{ps} \approx 1950$ J/(kg·°C), $c_{pl} \approx 3550$ J/(kg·°C), and $\Delta q = 2.43 \times 10^5$ J/kg at 34 °C.

The measurement techniques presently used for latent heat of fusion and melting temperature of PCMs are: (1) differential thermal analysis (DTA), and (2) differential scanning calorimeter (DSC). In DSC and DTA techniques, sample and reference materials are heated at constant rate. The temperature difference between them is proportional to the difference in heat flow between the two materials and the record is the DSC curve. The recommended reference material is alumina (Al_2O_3). Latent heat of fusion is calculated using the area under the peak and melting temperature is estimated by the tangent at the point of greatest slope on the face portion of the peak.

Morrison and Abdel-Khalik [10] developed a model applicable to PCMs in small containers.

4.1 Characteristics of PCMs

A large number of PCMs (organic, inorganic, and eutectic) are available in any required temperature range. PCMs are classified as different groups depending on the material nature (paraffin, fatty acids, salt hydrates, etc.) (Fig. 4).

Considering real applications in thermal energy store, the most widespread materials are paraffin's (organics), hydrated salts (inorganic), and fatty acids (organics). In cold storage, ice water is quite used as well. Table 2 shows some of the most relevant PCMs in different temperature ranges with their melting temperature, enthalpy, and density.

Table 2. Phase Change Material Properties

PCM	Melting Temperature (°C)	Melting Enthalpy (kJ/kg)	Density (g/cm ³)
Ice	0	333	0.92
Na-acetate trihidrate	58	250	1.30
Paraffin	-5–120	150–240	0.77
Erythritol	118	340	1.30

4.2 PCMs used for energy storage in buildings

Storage concepts applied to the building sector have been classified passive or active systems [11].

Passive Technologies

The use of TES as passive technology has the objective to provide thermal comfort with the minimum use of heating, ventilation and air-conditioning (HVAC) energy.

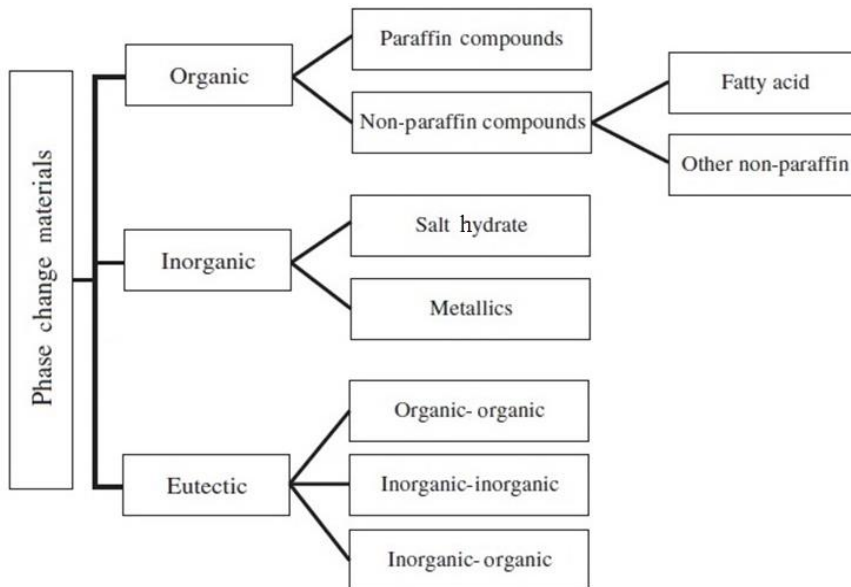


Figure 4. Classification of PCMs

When high thermal-mass materials are used in buildings, passive sensible storage is the technology that allows the storage of high quantity of energy, giving thermal stability

inside the building. Materials typically used are rammed earth, alveolar bricks, concrete, or stone.

Standard solar walls, also known as Trombe walls, and solar water walls also use sensible storage to achieve energy savings in buildings [12]. Trombe wall (Fig. 5) is a wall with high thermal capacity, shielded by a glass pane. A greenhouse effect is created, reducing thermal losses from the wall, heating the air between wall and glass that can be introduced into the room with a natural draught due to the chimney effect of the heated air.

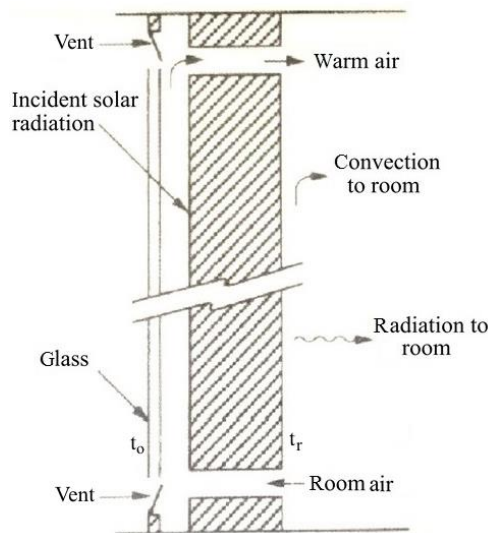


Figure 5. Schematics of a storage Trombe wall

PCM can be incorporated in construction materials using different methods, such as direct incorporation, immersion, encapsulation, micro-encapsulation, and shape-stabilisation. Traditionally, wallboards have been studied as one of the best options to incorporate PCM to building walls. A new approach in PCM-wallboards is the addition of an aluminium honeycomb in containing a microencapsulated PCM wallboard (Fig. 6) [13]. Another approach to incorporate PCM in building walls is to mix it with insulation materials. In masonry wall, the PCM incorporation can be, for example, within clay bricks [14].

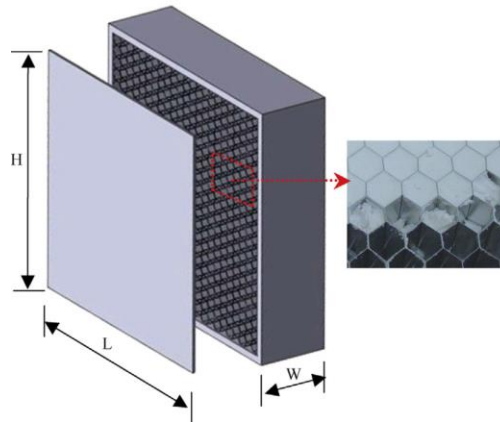


Figure 6. Microencapsulated PCM honeycomb wallboard

Active Technologies

The use of TES in building active systems is an attractive and versatile solution for several applications for new or retrofitted buildings, such as the implementation of renewable energy sources in the HVAC for space heating/cooling, the improvement in the performance of the current installations or the possible application of peak load-shifting strategies [15].

Furthermore, TES have been used in building solar systems to convert an intermittent energy source and meet the heating and DHW demand. The most popular solar TES building systems is extended to integrate solar air collectors in building walls or use PCM in ventilated facades (Fig. 7) [16].

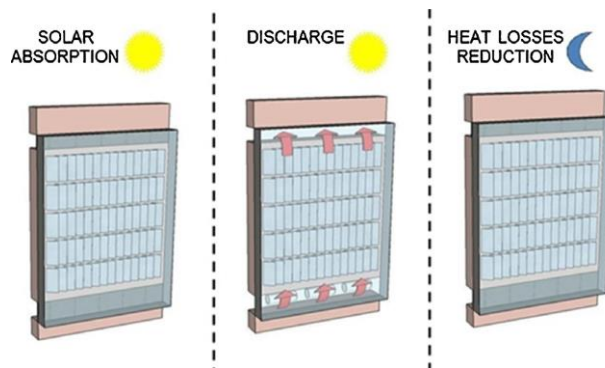


Figure 7. Operational mode of the ventilated façade with PCM

Thermal energy storage has very big potential as a key technology to reduce the energy demand of buildings and/or to improve the energy efficiency of their energy systems.

4.3 Advantages and Disadvantages of PCMs

The main advantages and drawbacks of PCM versus water SHSs are [17]:

- the possibility to reduce the tank volume for a given amount of energy stored, that is, true only if storage is operated in a very narrow temperature range around phase-transition temperature;
- less on-off cycles of auxiliary heaters (for plants with storage in the hot side) and chillers (for plants with storage in the cold side);
- higher investment costs; and
- higher risks due to leak of stability and erosion of material encapsulating PCMs.

5 Chemical Energy Storage

The TCS use thermochemical materials (TCM) which store and release heat by a reversible endothermic/exothermic reaction process (Fig. 2c). During the charging process, heat is applied to the material A, resulting in a separation of two parts B+C. The resulting reaction products can be easily separated and stored until the discharge process is required. Then, the two parts B+C are mixed at a suitable pressure and temperature conditions and energy is released.

The products B and C can be stored separately, and thermal losses from the storage units are restricted to sensible heat effects, which are usually small compared to heats of reaction.

Thermal decomposition of metal oxides for energy storage has been considered by Simmons [18].

Energy storage by thermal decomposition of $\text{Ca}(\text{OH})_2$ has been extensively studied by Fujii et al. [19]. The reaction is $\text{Ca}(\text{OH})_2 \leftrightarrow \text{CaO} + \text{H}_2\text{O}$. The forward reaction will proceed at temperatures above about 450 °C; the rates of reaction can be enhanced by the addition of zinc or aluminium. The product CaO is stored in the absence of water. The reverse exothermic reaction proceeds easily.

Thermochemical reactions, such as adsorption, can be used to store heat and cold, as well as to control humidity. The high storage capacity of sorption processes also allows thermal energy transportation.

6 Cool Thermal Energy Storage

Cool thermal energy storage (CTES) has recently attracted increasing interest in industrial refrigeration applications, such as process cooling, food preservation, and building air-conditioning systems. CTES appears to be one of the most appropriate methods for correcting the mismatch that occurs between the supply and demand of energy. Cool energy storage requires a better insulation tank as the energy available in the cool state is expensive, compared to the heat available in a hot storage tank. Cheralathan et al. [20] investigated the performance of an industrial refrigeration system integrated with CTES. The authors have indicated significant savings in capital and operating cost, in thermal storage-integrated systems. The size of the PCM-based CTES system was also considerably reduced when compared with that of a chilled water system.

The sorption phenomenon can also be applied for TES. In that case, a heat source promotes the dissociation (endothermic process) of a working pair, whose substances can be stored separately. When they come into contact again, heat is released (exothermic process). Therefore, the energy can then be stored with virtually no loss because the heat is not stored in a sensible or latent form but rather as potential energy, as long as the substances are kept separate.

Typical applications involve adsorption of water vapour to silica-gel or zeolites (i.e., micro-porous crystalline alumina-silicates). Of special importance for use in hot/humid climates or confined spaces with high humidity are open sorption systems based on lithium-chloride to cool water and on zeolites to control humidity.

The adsorption cycle has already been used in several research projects to promote TES. Hauer [21] presented a seasonal adsorption TES system, working with the silica-gel/water pair (Fig. 8). During the summer, while the system is charging, the heat from the solar collectors is conducted to three adsorbent beds, promoting the desorption stage. In the winter, the low temperatures in the solar collector promote the evaporation of the water in the evaporators/condensers, and the heat of adsorption is released to the building heating system.

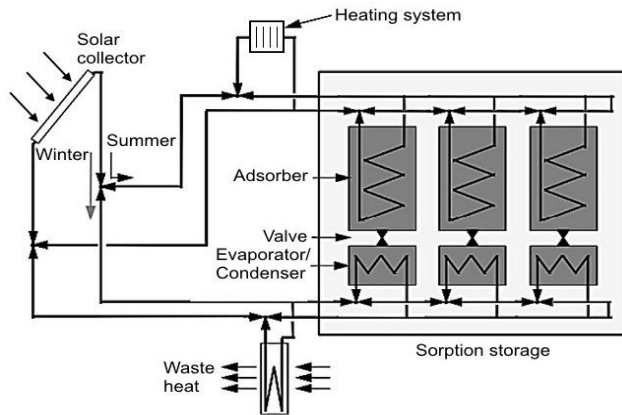


Figure 8. Seasonal adsorption thermal storage system

A cascade storage system offers vast potential for the improvement of a solar cooling-system performance. In a cascaded storage system, PCMs with different melting temperatures are arranged in a series to store heat in different temperatures. A cascaded multiple PCM-based storage system would improve solar collecting efficiency as the lower temperature at the bottom of the tank is connected to the inlet of the solar collector. The numerical results from the parametric study investigated by Shaikh and Lafdi [22] indicated that the total energy charged rate can be significantly enhanced by using composite PCMs as compared to the single PCM.

7 Conclusions

Figure 9 shows the different TES technologies: sensible heat (i.e., water as an example); latent heat (i.e., different materials); and thermo-chemical (i.e., sorption and chemical reactions).

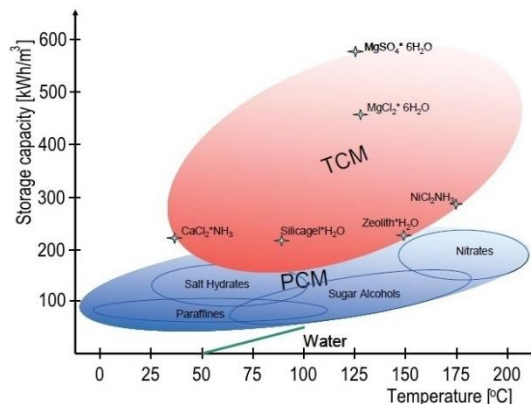


Figure 9. Storage capacity depending on temperature for TES

SHS is applicable to domestic systems, district heating and industrial needs. The most popular and commercial heat storage medium is water, which has a number of residential and industrial applications. Underground storage of sensible heat in both liquid and solid media is also used for typically large-scale applications. However, TES systems based on SHS offer a storage capacity that is limited by the specific heat of the storage medium.

PCMs can offer a higher storage capacity that is associated with the latent-heat of the phase-change. PCMs also enable a target-oriented discharging temperature that is set by the constant temperature of the phase-change.

TCS can offer even higher storage capacities. Thermochemical reactions such as adsorption can be used to accumulate and discharge heat and cold on demand, as well as to control humidity in a variety of applications using different chemical reactants.

At present, TES systems based on sensible heat are commercially available while TCS and PCM-based storage systems are mostly under development and demonstration.

References

- [1] I. Dincer and M.A. Rosen, *Thermal energy storage: systems and application*. Chichester, UK: John Wiley & Sons, 2002.
- [2] IEA IRENA, The energy technology systems analyses programme (ETSAP): technology brief E17, www.irena.org/publications, 2013
- [3] M. Medrano, M.O. Yilmaz, M. Nogue's, I. Martorell, J. Roca, and L.F. Cabeza, Experimental evaluation of commercial heat exchangers for use as PCM thermal storage systems, *Applied Energy*, vol. 86, pp. 2047-2055, 2009.
- [4] R. Lazzarin, Solar cooling plants: how to arrange solar collectors, absorption chillers and the load, *International Journal of Low Carbon Technology*, vol. 2, no. 4, pp. 376-390, 2007.
- [5] A. Hauer, Storage technology issues and opportunities, International Low-Carbon Energy Technology Platform, Strategic and Cross-Cutting Workshop "Energy Storage – Issues and Opportunities", Paris, France; 2011.
- [6] A. de Garcia and C.F. Cabeza, Phase change materials and thermal energy storage for buildings, *Energy and Buildings*, vol. 103, pp. 414-419, 2015.
- [7] G.A. Lane, *Solar heat storage-latent heat materials*, vol. I. Boca Raton, FL: CRC Press, 1983.
- [8] I. Sarbu and C. Sebarchievici, *Solar heating and cooling systems: fundamentals, experiments and applications*, Oxford: Elsevier, 2016.
- [9] T.E.W. Schumann, Heat transfer: A liquid flowing through a porous prism, *Journal of Franklin Institute*, vol. 208, pp. 405-416, 1929.
- [10] D.J. Morrison and S.I. Abdel-Khalik, Effects of phase-change energy storage on the performance of air-based and liquid-based solar heating systems, *Solar Energy*, vol. 20, pp. 57-67, 1978.
- [11] R. Parameshwaran, S. Kalaiselvam, S. Harikrishnan, and A. Elayaperumal, Sustainable thermal energy storage technologies for buildings: a review, *Renewable and Sustainable Energy Reviews*, vol. 16, pp. 2394-2433, 2012.

- [12] O. Saadatian, K. Sopian, C.H. Lim, N. Asim, and M.Y. Sulaiman, Trombe walls: a review of opportunities and challenges in research and development, *Renewable and Sustainable Energy Reviews*, vol. 16, pp. 6340-6351, 2012.
- [13] C. Lai and S. Hokoi, Thermal performance of an aluminum honeycomb wallboard incorporating microencapsulated PCM, *Energy and Buildings*, vol. 73, pp. 37-47, 2014.
- [14] T. Silva, R. Vicente, N. Soares, and V. Ferreira, Experimental testing and numerical modelling of masonry wall solution with PCM incorporation: a passive construction solution, *Energy and Buildings*, vol. 49, pp. 235-245, 2012.
- [15] Y. Sun, S. Wang, F. Xiao, and D. Gao, Peak load shifting control using different cold thermal energy storage facilities in commercial buildings: a review, *Energy Conversion and Management*, vol. 71, pp. 101-114, 2013
- [16] A. de Gracia, L. Navarro, A. Castell, A. Ruiz-Pardo, S. Alvarez, and L.F. Cabeza, Experimental study of a ventilated facade with PCM during winter period, *Energy and Buildings*, vol. 58, pp. 324-332, 2012.
- [17] L.A. Chidambaram, A.S. Ramana, G. Kamaraj, and R. Velraj, Review of solar cooling methods and thermal storage options, *Renewable and Sustainable Energy Reviews*, vol. 15, pp. 3220-3228, 2011.
- [18] J.A. Simmons, Reversible oxidation of metal oxides for thermal energy storage, *Proceedings of the International Solar Energy (ISES) Meeting*, 1976, vol. 8, pp. 219.
- [19] I. Fujii, K. Tsuchiya, M. Higano, and J. Yamada, Studies of an energy storage system by use of the reversible chemical reaction: $\text{CaO} + \text{H}_2\text{O} \leftrightarrow \text{Ca}(\text{OH})_2$, *Solar Energy*, vol. 34, pp. 367-377, 1985.
- [20] M. Cheralathan, R. Verlaaj, and S. Renganarayanan, Performance analysis on industrial refrigeration system integrated with encapsulated PCM-based cool thermal energy storage system, *International Journal of Energy Research*, vol. 31, pp. 1398-1413, 2007.
- [21] A. Hauer, *Adsorption systems for TES – Design and demonstration projects*. In: H.O. Paksoy (editor), *Thermal energy storage for sustainable energy consumption*, Netherlands: Springer, 2007.
- [22] S. Shaikh and K. Lafdi, Effect of multiple phase change materials (PCMs) slab configurations on thermal energy storage, *Energy Conversion and Management*, vol. 47, pp. 2103-2117, 2006.

Greener Synthesis of 1,2-Butylene Carbonate from CO₂ Using Graphene-Inorganic Nanocomposite Catalysis

VICTOR ONYENKEADI, SUELA KELLICI & BASU SAHA

Abstract The synthesis of 1,2 butylene carbonate (BC) from cycloaddition reaction of 1,2 butylene oxide (BO) and carbon dioxide (CO₂) was investigated using several heterogeneous catalysts in the absence of organic solvent. Continuous hydrothermal flow synthesis (CHFS) has been employed as a rapid and cleaner route for the synthesis of highly efficient graphene-inorganic heterogeneous catalyst, represented as Ce–La–Zr/GO nanocomposite. The graphene-inorganic heterogeneous catalyst has been characterised using transmission electron microscopy (TEM) and X-ray photoelectron spectroscopy (XPS), while X-ray powder diffraction (XRD) and Brunauer–Emmett–Teller (BET) methods have been used for the surface area measurements. Ceria, lanthana, zirconia doped graphene nanocomposite catalyst has shown high catalytic activity as compared to other reported heterogeneous catalysts in the absence of any organic solvent with a selectivity of 76% and 64% yield of 1,2 butylene carbonate at the reaction conditions of 408 K, 75 bar in 20 h.

Keywords: • 1,2 butylene carbonate (BC) • carbon dioxide (CO₂) • continuous hydrothermal flow synthesis (CHFS) • ceria-lanthana-zirconia and graphene oxide nanocomposite (Ce-La-Zr/GO) • heterogeneous catalysis •

CORRESPONDENCE ADDRESS: Victor Onyenkeadi, Ph.D., London Southbank University, School of Engineering, SE1 0AA, United Kingdom, e-mail: onyenkev@lsbu.ac.uk. Suela Kellici, Ph.D., Senior Lecturer, London Southbank University, School of Engineering, SE1 0AA, United Kingdom, e-mail: kellicis@lsbu.ac.uk. Basu Saha, Ph.D., Professor of Chemical and Process Engineering London Southbank University, School of Engineering, SE1 0AA, United Kingdom, e-mail: b.saha@lsbu.ac.uk.

<https://doi.org/10.18690/978-961-286-052-3.13>

ISBN 978-961-286-052-3

© 2017 University of Maribor Press

Available at: <http://press.um.si>.

1 Introduction

The global emission of carbon dioxide (CO₂) into the atmosphere has reached an unsustainable level that has resulted in climate change and therefore there is the need to reduce the emission of CO₂ [1]. Recently, there has been a tremendous interest in the use of CO₂ as an environmentally benign building block in the chemical industry due to its chemical and physical properties such as chemical inert, stability, non-flammability, non-toxicity and therefore it can be considered as an attractive green replacement of toxic reactants such as isocyanates and phosgene [2, 3]. CO₂ is regarded as a stable compound due to its carbon covalently bonded to two oxygen atoms, although the thermodynamic stability of CO₂ requires a significant amount of energy to be decomposed [4]. The reactions of CO₂ with epoxides are exothermic and generate an organic carbonate such as cyclic and polycyclic carbonates [5].

Organic carbonates such as acyclic, cyclic and polycyclic carbonates are widely used chemicals in agriculture, automobile, cosmetic, lithium battery, paint and pharmaceutical industries [1, 5-8].

1,2-butylene carbonate is a valuable chemical of great commercial interest. It is an excellent reactive intermediate material used in industry for the production of plasticisers, surfactant, and polymers and can also be used as a solvent for degreasing, paint remover, wood binder resins, foundry sand binders, lubricants as well as lithium battery because of its high polarity property [5].

The use of continuous hydrothermal flow synthesis (CHFS) reactors has been considered for catalyst preparation in order to improve the catalyst stability and enhance performance.

2 Experimental

2.1 Materials

Natural graphite powder, hydrochloric acid, sulphuric acid, sodium nitrate, potassium hydroxide pellet, hydrogen peroxide, acetone, octane and potassium permanganate were purchased from Fisher Scientific UK Ltd. Methanol, cerium(III) nitrate hexahydrate, Lanthanum (III) nitrate hexahydrate, zirconium (IV) oxynitrate hydrate, 1,2-butylene oxide, 1,2-butylene carbonate were purchased from Sigma–Aldrich Co. LLC, UK. The catalysts used for the experiments were magnesium oxide, titanium silicate, zirconium oxide, cerium oxide, lanthana oxide, lanthana doped zirconia, lithium doped zirconia, zirconium doped hydrotalcite, ceria doped zirconia and ceria, lanthana doped zirconia were supplied by MEL Chemicals Company except for magnesium oxide and titanium silicate which were purchased from Sigma Aldrich. The liquid CO₂ cylinder (99.9%) equipped with a dip tube was purchased from BOC Ltd., UK. All chemicals were used without further pre-treatment or purification.

2.2 Preparation and characterisation of ceria-lanthana-zirconia/graphene inorganic nanocomposite synthesis via CHFS

CHFS experiments were conducted using a reactor, basic design that has been reported elsewhere [6-10]. CHFS reactor consists of three high performance pressure pumps used for delivery aqueous solution of reagents. The catalyst was successfully prepared and characterised by Adeleye et al (2015). The properties of the prepared ceria-lanthana-zirconia/graphene inorganic nanocomposite catalyst via CHFS are given in Table 1.

Table 1: Physical and chemical properties of graphene oxide (GO) and ceria, lanthana, zirconia/graphene(Ce-La-Zr/GO)

Catalyst properties	Graphene based catalyst of ceria, lanthana and zirconia	
	GO	Ce-la-zr/Go
Physical form	Black powder	Black powder
% Atomic composition(XPS)	O: 24.64 C:75.36	Ce: 2.98 La:1.19 O: 34.99 C: 47.29 K: 0.8 Zr: 12.75
Mean particle size (nm)	-	5.78±3.9
BET surface area (m ² g ⁻¹)	124	115
Pore volume (cm ³ g ⁻¹)	0.049	0.047
Average pore diameter (nm)	2.37	2.16

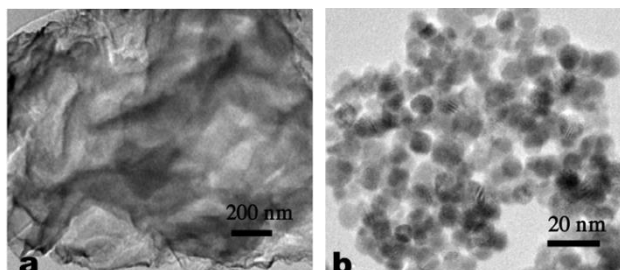


Figure 8. Transmission electron microscopy (TEM) images of graphene oxide and ce-la-zr/GO catalyst assessed for the synthesis of 1,2 butylene carbonate

a: grapheme oxide) and b: (Ce-La-Zr/GO as prepared via CHFS).

2.3 Experimental procedure for the synthesis of 1,2 butylene carbonate

The synthesis of 1,2 butylene carbonate was carried out in a 25 mL stainless steel high pressure reactor equipped with a stirrer, thermocouple and a heating mantle and controller. The reactor was charged with a required amount of BO and catalyst. The reactor was heated to the required temperature and continuously stirred at a known stirring speed. Supercritical fluid pump was used to pump CO₂ at a desired pressure from the cylinder to the reactor and left for a specified time. After the reaction, the reactor was cooled down to room temperature using an ice bath. The reactor was depressurized and the reaction mixture was filtered. The recovered catalyst was washed with acetone and dried

in an oven while the products were analysed using a gas chromatography (GC) equipped with a flame ionization detector (FID) with a capillary column using octane as an internal standard. The effect of various parameters such as catalyst types, catalyst loading, CO₂ pressure, reaction temperature and reaction time was studied for the optimization of the reaction conditions. Catalyst reusability studies were also conducted to assess the stability of the catalyst for synthesis of BC.

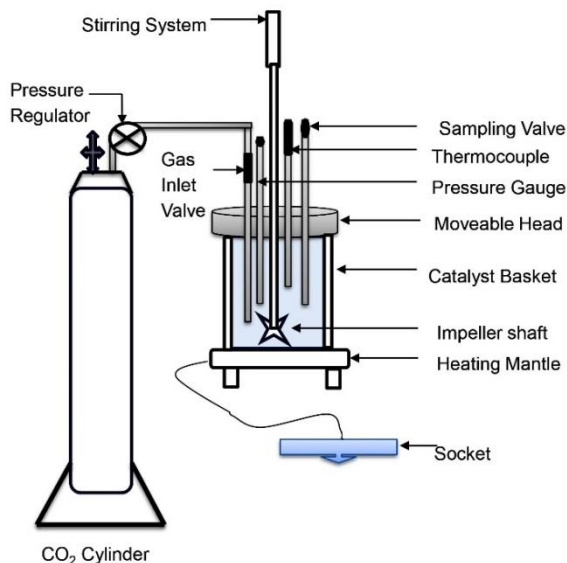


Figure 2. Schematic of a high pressure reactor.

3 Results and Discussion

3.1 Proposed reaction mechanism

The synthesis of 1,2 butylene carbonate through cycloaddition reaction of carbon dioxide to 1,2 butylene oxide in the presence of Ce-La-Zr/GO inorganic nanocomposite catalyst can be seen in Figure 3a and 3b.

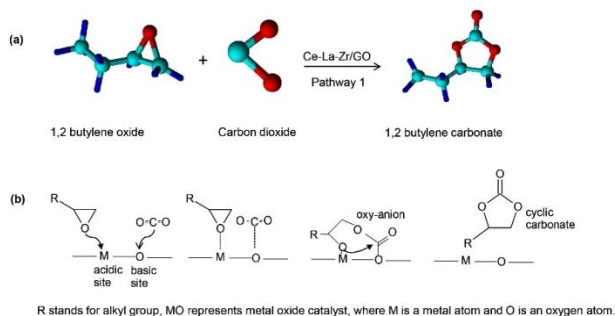


Figure 3. Reaction scheme and pathway for synthesis of 1,2 butylene carbonate.

3.2 Effect of different heterogeneous catalysts

The detailed study of various heterogeneous catalysts were conducted in order to ascertain the best performing metal oxide or mixed metal oxide catalyst for the synthesis of 1,2 butylene carbonate through cycloaddition reaction of carbon dioxide to 1,2 butylene oxide using a high pressure reactor (Figure 2). Figure 4 shows the results of different heterogeneous catalysts and also the corresponding improvement of Ce-La-ZrO using graphene oxide as a base catalyst decorated with Ce-La-Zr in 1:1 ratio via CHFS route on the conversion of 1,2 butylene oxide, the yield and selectivity of 1,2 butylene carbonate using the optimum reaction conditions. Ce-La-Zr/GO catalyst gave an improved conversion of BO (84%) and highest BC yield (64%) and selectivity (76%) at optimum reaction 408 K temperature, CO₂ pressure 75 bar, reaction time 20 h, stirring speed 300 rpm and catalyst loading of 10% (w/w).

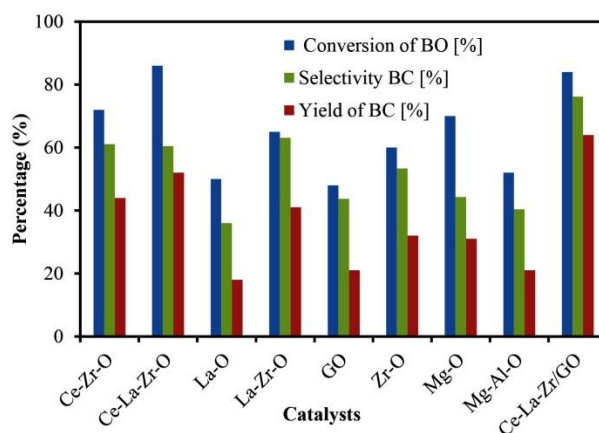


Figure 4. Effect of different heterogeneous catalysts

3.3 Effect of reaction temperature

The heterogeneous catalytic reaction of 1,2 butylene oxide and CO₂ were carried out at different reaction temperature from 368 K to 443 K in order to study its effect on 1,2 butylene oxide conversion and of 1,2 butylene carbonate yield and selectivity. The reaction conditions for this study were set at 10% catalyst loading, 75 bar CO₂ pressure and duration for 20 h. As it was expected, the higher the temperature, the more the conversion of 1,2 butylene oxide into carbonates isomers and oligomers. Figure 5 shows the temperature dependence on the yield and selectivity of 1,2 butylene carbonate.

It was observed from Figure 5 that there was a corresponding increase in conversion of 1,2 butylene oxide, 1,2 butylene carbonate yield and selectivity as temperature increases from 368 K to 408 K but further increase of temperature from 408 K to 443 K, there was slight drop of 1,2 butylene carbonate yield from 64% to 60% whilst its respectively 1,2 butylene oxide conversion increases from 84% to 90%.

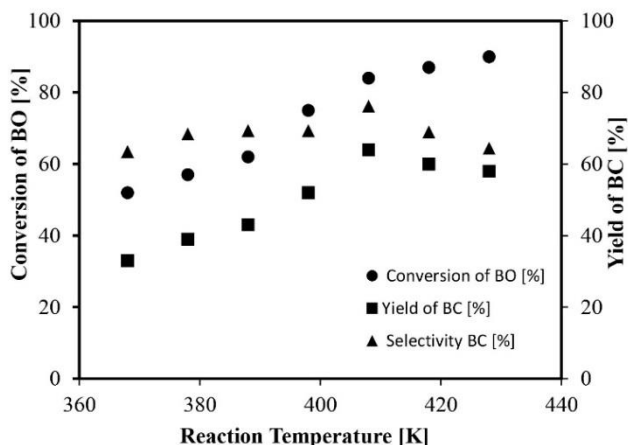


Figure 5. Effect of reaction temperature

3.4 Effect of CO₂ pressure

The application of CO₂ pressure is very significant in the synthesis of 1,2 butylene carbonate through the reaction of 1,2 butylene oxide and CO₂. The use of supercritical state of CO₂ reaction system can cause an increase in mass transfer efficiency of the reactants and lead to a shift in the reaction equilibrium to open up the thermodynamic limitation of this reaction [8, 11]. The effect of CO₂ pressure on 1,2 butylene conversion and 1,2 butylene carbonate yield was studied in order to ascertain the optimum CO₂ pressure for the reaction of cycloaddition of CO₂ to 1,2 butylene oxide. The experiments were carried out in a high pressure reactor at 408 K with CO₂ pressure ranging from 55 bar to 105 bar for 20 h and the results are shown in Figure 6. It can be seen in Figure 6, that an increase in CO₂ pressure from 55 bar to 75 bar increases the 1,2 butylene oxide conversion and the yield of 1,2 butylene carbonate, but beyond 75 bar there were further

increase in 1,2 butylene oxide conversion but no significant increase in the yield of 1,2 butylene carbonate rather a slight decrease in the yield.

At a CO₂ pressure of 75 bar, 1,2 butylene oxide conversion and 1,2 butylene carbonate yield were of 84% and 64% respectively. Beyond 75 bar, there was a slight drop in 1,2 butylene carbonate yield and that might be as a result of decomposition of 1,2 butylene carbonate to form oligomers. Therefore, it can be concluded that the optimum CO₂ pressure for this reaction is 75 bar. This study shows an improvement in polarity and solubility of 1,2 butylene oxide conversion at supercritical condition of CO₂ as the reaction pressure increases.

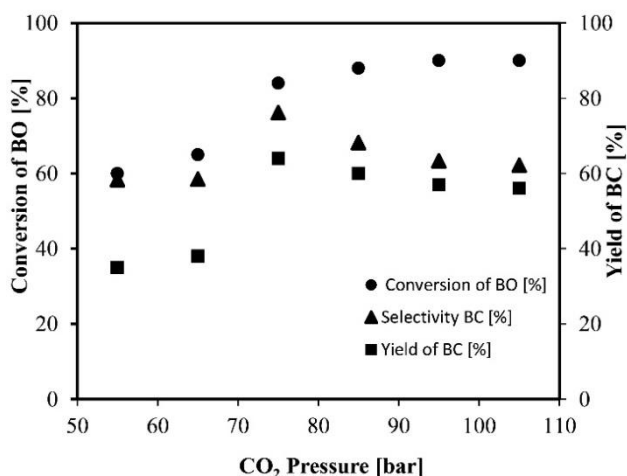


Figure 6. Effect of CO₂ pressure

3.5 Catalyst reusability studies

The heterogeneous catalyst reusability experiments were conducted to investigate the catalytic activity of the best performed heterogeneous catalyst. Ceria, lanthana, zirconia with graphene inorganic nanocomposite reusability study was investigated in order to obtain its performance in different runs. The experiments were carried out in a high pressure reactor at optimum reaction conditions of 408 K temperature, 75 bar pressure, fresh 10% (w/w) catalyst loading of Ce-La-Zr/GO for 20 h. The catalyst was used for 6 runs and as it can be seen in Figure 7 that the conversion of 84% and yield of 64% were remain unchanged. Therefore, it can be concluded that Ce-La-Zr/GO catalysts can be reused several times and still maintain its high catalytic activity.

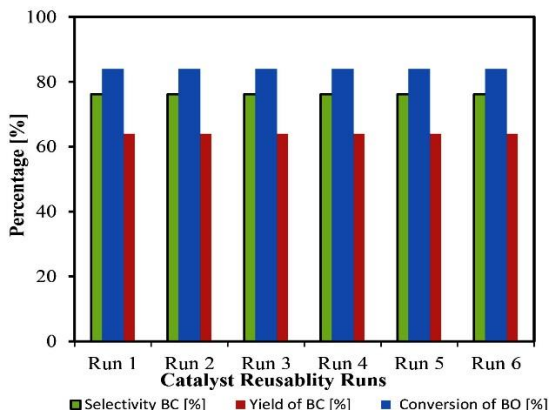


Figure 7. Catalyst reusability studies

4 Conclusions

The synthesis of 1,2 butylene carbonate through cycloaddition reaction of carbon dioxide and 1,2 butylene oxide was successfully carried out using a high pressure reactor in the presence of various heterogeneous catalysts without any organic solvent. Among the used heterogeneous catalysts ceria, lanthana, zirconia/graphene inorganic nanocomposite catalyst (Ce-La-Zr/GO) was found to be the best performed catalyst and the optimum reaction condition was found at 408 K, 75 bar CO₂ pressure, 10% (w/w) catalyst loading and 20 h reaction. Ce-La-Zr/GO catalyst was easily recycled and reused several times without any reduction in its catalytic performance.

Acknowledgements

We would like to acknowledge Magnesium Elektron Limited (MEL) Chemicals, UK for supplying the catalysts for this work. Special thanks to School of Engineering LSBU and PATIB Venture for their financial supports.

References

- [1] M. Aresta and A. Dibenedetto, "14 - Industrial utilization of carbon dioxide (CO₂)", vol. 2, pp. 377-410, 2014.
- [2] M. Aresta, A. Dibenedetto and A. Angelini, "Catalysis for the Valorization of Exhaust Carbon: from CO₂ to Chemicals, Materials, and Fuels. Technological Use of CO₂," *Chem.Rev.*, vol. 114, pp. 1709-1742, 2012.
- [3] W. Dai, S. Luo, S. Yin and C. Au, "The direct transformation of carbon dioxide to organic carbonates over heterogeneous catalysts," *Applied Catalysis A-General*, vol. 366, pp. 2-12, 2015.
- [4] W. Wang, Y. Himeda, J.T. Muckerman, G.F. Manbeck and E. Fujita, "CO₂ Hydrogenation to Formate and Methanol as an Alternative to Photo- and Electrochemical CO₂ Reduction," *Chem.Rev.*, vol. 115, pp. 12936-12973, 2009.

- [5] A. Shaikh and S. Sivaram, "Organic carbonates," *Chem.Rev.*, vol. 96, pp. 951-976, 1996.
- [6] A.I. Adeleye, D. Patel, D. Niyogi and B. Saha, "Efficient and Greener Synthesis of Propylene Carbonate from Carbon Dioxide and Propylene Oxide," *Ind Eng Chem Res*, vol. 53, pp. 18647-18657, 2014.
- [7] A.I. Adeleye, S. Kellici, T. Heil, D. Morgan, M. Vickers and B. Saha, "Greener synthesis of propylene carbonate using graphene-inorganic nanocomposite catalysts," *Catalysis Today*, vol. 256, pp. 347-357, 2015.
- [8] R. Saada, S. Kellici, T. Heil, D. Morgan and B. Saha, "Greener synthesis of dimethyl carbonate using a novel ceria-zirconia oxide/graphene nanocomposite catalyst," *Applied Catalysis B-Environmental*, vol. 168, pp. 353-362, 2015.
- [9] Lin, T., Kellici, S., Gong, K., Thompson, K., & Darr, J. A., "The Rapid Automated Materials Synthesis Instrument (RAMSI): A High Throughput Combinatorial Robot for Nanoceramics Discovery.", no. *Advances in Science and Technology*, 62, pp. 215-220, 2010.
- [10] V. Middelkoop, C.J. Tighe, S. Kellici, R.I. Guar, J.M. Perkins, S.D.M. Jacques, P. Barnes and J.A. Darr, "Imaging the continuous hydrothermal flow synthesis of nanoparticulate CeO₂ at different supercritical water temperatures using in situ angle-dispersive diffraction," *The Journal of Supercritical Fluids*, vol. 87, pp. 118-128, 2014.
- [11] E.J. Beckman, "Supercritical and near-critical CO₂ in green chemical synthesis and processing," *The Journal of Supercritical Fluids*, vol. 28, no. 2–3, 3, pp. 121-191, 2004.

Sugar Alcohols and Synthetic Derivatives as Phase Change Materials

YAGO MAGAN MONTOTO, DANIEL LAGER, CHRISTOPH ZAUNER, ULF STRIJOWSKI, JÖRG KOWALCZYK, FLORIAN HENGSTBERGER & MICHAEL SCHNÜRCH

Abstract Phase-change materials (PCMs) are able to absorb a high amount of energy during a phase change, for example at the time of melting and release it upon recrystallization. Organic compounds as PCMs are very interesting due to their relatively high storage capacity, safety and low cost. Additionally, they are able to cover an interesting range of melting temperatures. There is a large number of PCMs that change their phase in the range of 80 °C to 200 °C. Thus, the use of latent heat storage systems using organic PCMs has a promising future for industrial applications at medium temperatures.

The main focus of this study was sugar alcohols and their thermophysical properties were investigated. Based on these results, the parent compounds were synthetically modified using standard organic synthesis methods with the goal to obtain alternative materials for thermal storage devices regarding different melting temperatures and to improve their melting energy and thermal stability among other properties. By studying and comparing the modified structures with the parent compounds it is possible to identify trends and general guidelines for identifying ever more efficient materials. Within this contribution, we show an enthalpy and melting temperature comparison for sugar alcohols and the synthesized derivatives based on their structure and DSC measurements combined with thermal stability TGA analysis.

Keywords: • sugar alcohols • phase-change material (PCM) • organic • differential Scanning calorimetry (DSC) • melting •

CORRESPONDENCE ADDRESS: Yago Magan Montoto, MSc, Project Assistant, TU Wien, Institute of Applied Synthetic Chemistry, Getreidemarkt 9, 1060 Vienna, Austria, e-mail: yago.montoto@tuwien.ac.at. Daniel Lager, MSc, AIT Austrian Institute of Technology GmbH, Center for Energy, Sustainable Thermal Energy Systems, Giefinggasse 2, 1210 Wien, Austria, e-mail: daniel.lager@ait.ac.at. Christoph Zauner, MSc, AIT Austrian Institute of Technology GmbH, Center for Energy, Sustainable Thermal Energy Systems, Giefinggasse 2, 1210 Wien, Austria, e-mail: christoph.zauner@ait.ac.at. Ulf Strijowski, Südzucker AG, Central Department Research, Development and Services, Wormser Str. 11, 67283 Obrigheim/Pfalz, Germany, e-mail: Ulf.Strijowski@suedzucker.de. Jörg Kowalczyk, Ph.D, Südzucker AG, Central Department Research, Development and Services, Wormser Str. 11, 67283 Obrigheim/Pfalz, Germany, e-mail: Joerg.Kowalczyk@suedzucker.de. Florian Hengstberger, DI Dr., AIT Austrian Institute of Technology GmbH, Center for Energy, Sustainable Thermal Energy Systems, Giefinggasse 2, 1210 Wien, Austria, e-mail: Florian.Hengstberger@ait.ac.at. Michael Schnürch, Associate Prof. Dipl.-Ing. Dr.techn, TU Wien, Institute of Applied Synthetic Chemistry, Getreidemarkt 9, 1060 Vienna, Austria, e-mail: michael.schnuerch@tuwien.ac.at.

1 Introduction

Out of well-known reasons, there is a global trend in energy supply towards the development of efficient, more economical, and more environmentally benign methods. Storing excess energy rather than releasing it unused into the surroundings surely fits well into these considerations. Amongst others, thermal energy storage (TES) systems are an interesting method which could help to increase energy efficiency and to put the spotlight on renewable energies for a sustainable future.

TES systems can be classified in three types: sensible, latent and thermo-chemical heat storages. This paper is focused on the way of storing heat by using the latent heat of a substance. In this particular case, we are interested in solid to liquid phase transition. Materials used for this purpose are known as phase change materials (PCMs) and they can be divided into two groups, organic and inorganic compounds [1]

As advantages of organic PCMs may be considered that they are typically non-corrosive and display often only low supercooling (meaning that a compound is still a liquid in a temperature below its melting point), whereas inorganic compounds typically have a larger phase enthalpy but are eventually corrosive and display problems with supercooling. [2, 3, 4]

As can be seen in Figure 1, organic and inorganic compounds cover different ranges regarding melting energy and melting points as well. Inorganics typically cover melting temperatures >400 °C, whereas organic compounds melt typically below 250 °C. Hence, the two classes are complementary in their potential applications, the organics suitable for “low temperature” applications.

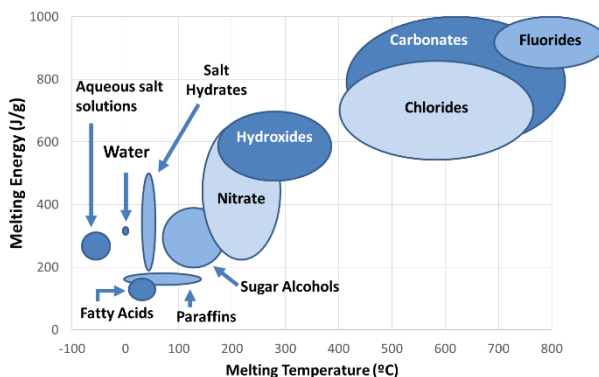


Figure 1. Classification of PCM with their melting temperature and enthalpy

Within this contribution, we will discuss the thermophysical properties of sugar alcohols and some synthetic derivatives thereof, which were prepared in our laboratory. Most

importantly, differential scanning calorimetry (DSC) and thermogravimetric analysis (TGA) measurements have been used to describe the potential of a given compound as PCM. These data will be analysed and compared and our conclusions for future developments will be discussed.

2 Results and Discussion

On the basis that several industrial processes might be carried out in boiling water as solvent (or heated by water steam), a target temperature range for our organic PCMs was defined, starting a bit below 100 °C. Additional prerequisites considering the costs of the materials were specified as well. Since in the end the PCMs should be used in TES devices of industrial scale, a typical volume might be around 10 m³. Hence, the material needs to be cheap and synthetic modifications via multi-step routes cannot be used. Facile syntheses with minimal work-up and purification steps are mandatory. Furthermore, our product must be stable too. An intended lifetime of 10 years with a daily phase transition would end up in 3650 melting/crystallization cycles upon which the material cannot decompose to a significant extent, since otherwise the storage capacity would suffer.

Due to all these project requirements, this study is oriented to temperatures between 80 to 300 °C where a wide range of organic compounds have their melting points. Due to literature precedence [2, 4], sugar alcohols were our first candidate to be investigated.

Moreover, chemical modifications of these organic compounds were undertaken in order to influence the melting points and ideally get to higher latent energies.

With this approach, new application temperatures within a given compound class would become available. This would be highly interesting, since then organic materials could be modified in order to fit the required temperature range for a given process.

2.1 Sugars and derivatives

Sugars and their derivatives are nowadays one of the most studied groups in PCM research [2, 8]. They usually show fitting phase change temperatures for medium temperature storage, with temperatures between 69 to 189 °C, and offer high melting energy capacity, favourable safety and low cost.

For all these reasons, it was our main target group and the screening study was focused on sugar alcohols and different simple modifications of the aforementioned.

Sugar alcohols

Considering all the sugars, sugar alcohols represent the most interesting group in terms of phase change material behaviour.

They are able to absorb and release a big amount of energy due to their hydroxy groups which allow efficient hydrogen bonding. In a first series of experiments we conducted simultaneous thermal analysis (STA) measurements of commercially available sugar alcohols. STA measurements, which combines both DSC and TG, were carried out on a STA 449 F1 JUPITER Netzsch under nitrogen atmosphere. 10 mg samples were heated up with a 10 K/min rate.

It was found that most of the tested compounds have suitable melting points and they offer well-defined peaks in their DSC with a big gap between melting and degradation, as can be seen from Table 1 and Figure 2.

At this stage, we observed outstanding phase energies for our aliphatic sugar alcohols, as mannitol, sorbitol and dulcitol, because of their structural symmetry. That distribution of the hydroxy groups favoured an effective hydrogen bonding which results in higher latent energies. Only the complex sugar alcohols are not appropriate for the PCM's applications.

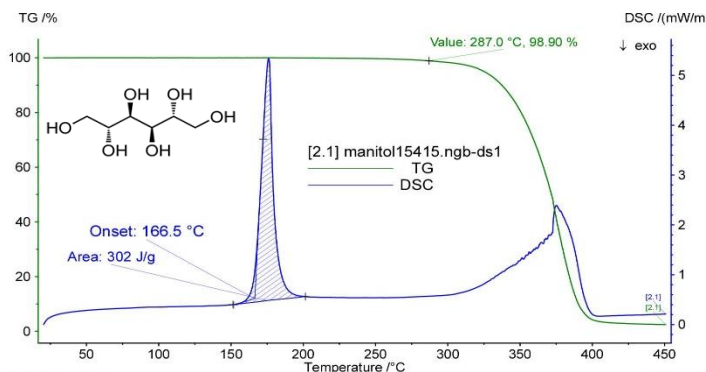
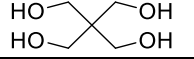
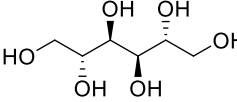
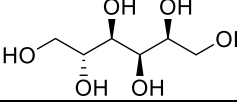
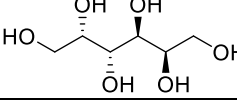
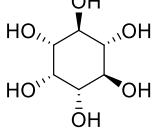
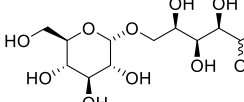
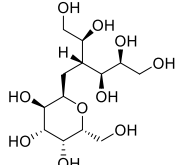
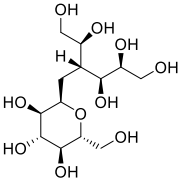


Figure 2. Mannitol simultaneous thermal analysis (STA) data

Lactitol, maltitol and isomalt show a low melting energy. Moreover, isomalt could only recrystallize in the presence of water which limits its applicability in industrial settings.

Table 1. Sugar alcohols experimental data

Compound	Structure	MW (g/mol)	MP T (°C)	ΔH (kJ/kg)	Degradation (TGA)
Pentaerythritol		136,15	187	321.3	238.5
Mannitol		182.172	166.5	307	287.0
Sorbitol		182.172	99.9	265.7	293.3
Dulcitol		182.172	187.8	409.2	318.5
Myo-Inositol		180.16	224.5	270.7	341.3
Isomalt		344.31	147.6	113.7	285.1
Lactitol		344.31	-	142(lit)	-
Maltitol		344.31	150	200.3	274

At this stage, we observed outstanding phase energies for our aliphatic sugar alcohols, as mannitol, sorbitol and dulcitol, because of their structural symmetry. That distribution of the hydroxy groups favoured an effective hydrogen bonding which results in higher latent energies. Only the complex sugar alcohols are not appropriate for the PCM's applications.

Even if most of these sugar alcohols fit well to our requirements, thermal stability tests have to be done. For example, mannitol experienced supercooling and degradation after several cycles because of the oxidation of the material in oxygen atmosphere. This problem is easily solved using an inert atmosphere [6, 7].

For others, such as dulcitol, poor cycle stability was observed [8]

Regarding supercooling, it has been observed that the addition of some nucleation agents can overcome this problem. [3]

In order to improve cycle stability, chemical modifications could also be beneficial in order to get to less reactive and hence more stable compounds. In this regard, acetylation reactions on sugar alcohols are the natural first choice since these reactions are typically high yielding and only use inexpensive starting materials, which is important for the large quantity application we have in mind. Additionally, these reactions are often used to block reactive hydroxy groups in sugar chemistry [9].

Acetylation leads of course to the loss of hydrogen bonding, which would lead to a (desired) decrease in melting point and also melting energy. On the other hand, the molecular weight is significantly increased, which typically has the exact opposite effect. So it had to be seen, which of the two parameters is of greater importance, possibility for hydrogen bonding or molecular weight. In our hands, all investigated acetylations have shown quantitative yields for all the sugars that were modified. A typical procedure for acetylation used the following conditions:

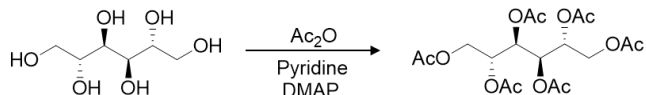


Figure 3. Reaction scheme for a mannitol acetylation

For example, 500mg of mannitol and 5 ml pyridine were placed in an oven-dried 8 ml vial with a magnetic stirring bar. 4-Dimethylaminopyridine (DMAP) as catalyst and acetic acid were added, the vial was closed and the reaction mixture was stirred at room temperature for 75 minutes. For purification, toluene was added in order to co-evaporate pyridine under vacuum. Via this method, 1.19g of product was obtained, which corresponds to 99% yield.

With the acetylated sugars in hand again STA analyses were performed. The acetylation of sugars provides a product with lower melting point and lower melting energy than the starting material due to the absence of hydrogen bonding possibilities. showing that this is the dominant effect.

Table 2. Acetylated derivatives experimental data

Compound	MP T (°C)	ΔH (kJ/kg)	Degradation (TGA)
Acetylated Mannitol	122.7	164	232.3
Acetylated Sorbitol	97.3	162.4	171.7
Acetylated Dulcitol	170.4	200.7	200.7
Acetylated Myo-Inositol	212.6	Dec.	210.8
Acetylated Pentaerythritol	75.3	139.9	142.9

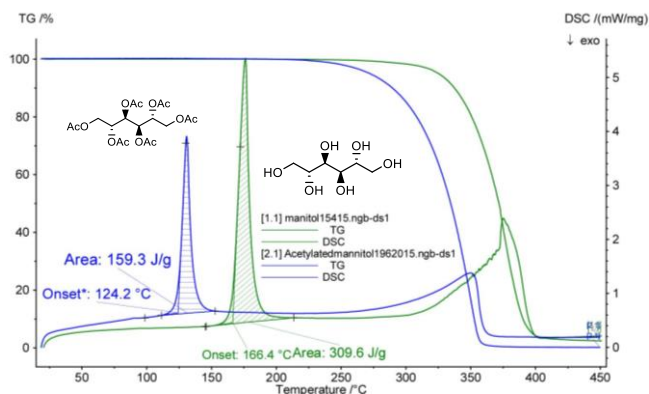


Figure 4. Mannitol and its acetylated derivative properties comparison

Table 3. Comparison of the melting properties of sugar alcohols and their acetylated derivatives

Compound	Sugar alcohol			Acetylated derivative		
	MP T (°C)	ΔH (KJ/kg)	Degradation (TGA)	MP T (°C)	ΔH (KJ/kg)	Degradation (TGA)
Mannitol	166.5	307	287.0	122.7	164	232.3
Sorbitol	99.9	265.7	293.3	97.3	162.4	171.7
Dulcitol	187.8	409.2	318.5	170.4	200.7	200.7
Myo-Inositol	224.5	270.7	341.3	212.6	Dec.	210.8
Pentaerythritol	187	321.3	238.5	75.3	139.9	142.9

Our goal of obtaining a lower melting point was achieved but, unfortunately, once the hydroxy groups are substituted by acetyl groups the properties of the material decline regarding latent energy. Considering all this points, acetylations do not improve the overall properties of sugar alcohols as PCMs.

3 Conclusion

As a result of our chemical modifications in sugar alcohols we could confirm how important is hydrogen bonding regarding further improvements in latent energy. The effect of higher molecular weights does not outbalance the loss of this relatively strong intermolecular interaction. In the case of acetylations, our melting energies decrease approximately by half even though the molecular weight has been more than doubled in comparison to the sugar alcohol starting materials.

New development lines have to be set up in order to find proper patterns to raise melting energies in a wide range of temperatures.

Acknowledgements

The research leading to these results has been part of the TES4SET project (Thermal energy storage for sustainable energy technologies) and received funding from the Austrian Research Promotion Agency (FFG).

References

- [1] A. Sharma, V.V. Tyagi, C.R. Chen, D. Buddhi "Review on thermal energy storage with phase change materials and applications" *Renewable and Sustainable Energy Reviews*, vol. 13, pp 318-345. 2009
- [2] L. F. Cabeza, A. Castell, C. Barreneche, A. de Gracia, A. I. Fernández "Materials used as PCM in thermal energy storage in buildings: A review" *Renewable and Sustainable Energy Reviews*, vol. 15, pp 1675-1695. 2011
- [3] A. Solé, H. Neumann, S. Niedermaier, I. Martorell, P. Schossig, L. F. Cabeza "Stability of sugar alcohols as PCM for thermal energy storage" *Solar Energy Materials & Solar Cells*, Vol. 126, pp. 125-134, 2014
- [4] H. Medling, L.F. Cabeza. Heat and Cold storage with PCM, Springer, Berlin, 2008.
- [5] C. Rathgeber, L. Miró, L. F. Cabeza, S. Hiebler "Measurement of enthalpy curves of phase change material via DSC T-History: When are both methods needed to estimate the behaviour of the bulk material in applications?" *Thermochimica Acta*, Vol. 596. pp. 79-88. 2014
- [6] H. Neumann, S. Niedermaier, A. Solé, P. Schossig "Thermal stability of D-mannitol as phase change material (PCM)" *Eurotherm Seminar*, #99.
- [7] A. Solé, H. Neumann, S. Niedermaier, L. F. Cabeza, E. Palomo "Thermal stability test of sugar alcohols as phase change materials for medium temperature energy storage application" *Energy Procedia*, Vol. 48. pp. 436-439. 2014
- [8] S. N. Gunasekara, R. Pan, J. N. Chiu, V. Martin "Polyols as phase change materials for surplus thermal energy storage" *Applied Energy*, Vol. 162. pp. 1439-1452. 2016 G. Ferrer, A. Solé, C. Barreneche, I. Martorell, L. F. Cabeza "Review on the methodology used in

- thermal stability characterization of phase change materials" *Renewable and Sustainable Energy Reviews*, vol. 50, pp 665-685. 2015
- [9] Peterson V. L.; West E.S.; *The Journal of biological chemistry* vol. 74(2), pp. 3358-3359. 1927

Methane Production from Atmospheric Carbon Dioxide Utilizing Renewable Energy

JANNA VESELOVSKAYA, ANTON LYSIKOV, OLGA NETSKINA, LIDIYA KIBIS & ALEKSEY OKUNEV

Abstract The methanation catalyst 4% Ru/Al₂O₃ has been synthesized by impregnation of the mesoporous support with an aqueous solution of Ru(OH)Cl₃ followed by NaBH₄ treatment. Activation of the catalyst has been studied in a gaseous mixture of CO₂ and H₂ (1:4) at 300°C. XPS analysis has demonstrated that the supported component upon activation has been reduced from Ru⁴⁺ surface species to Ru⁰ particles. The novel process, combining direct CO₂ capture from ambient air using K₂CO₃/Al₂O₃ composite sorbent and CO₂ methanation via Sabatier reaction in the presence of the ruthenium catalyst, has been performed in a cyclic mode. The thermal regeneration of the composite sorbent in these cycles has been carried out in H₂ atmosphere at T = 325°C with the gas flow going straight from the adsorber outlet to the preheated catalytic reactor. Performance of the ruthenium catalyst in CO₂ methanation process has improved upon cycling, apparently due to in situ activation of the supported component. It has been demonstrated that the use of the activated catalyst makes it possible to transform the desorbed carbon dioxide to methane with conversion >98 % at T = 325-400°C.

Keywords: • carbon dioxide • direct air capture • Sabatier reaction • heterogeneous catalysis • power-to-gas •

CORRESPONDENCE ADDRESS: Janna Veselovskaya, Ph.D., Researcher, Boreskov Institute of Catalysis, Akademika Lavrentieva av. 5, 630090 Novosibirsk, Russian Federation, e-mail: lyanig@catalysis.ru, e-mail: jvv@catalysis.ru. Anton Lysikov, Ph.D., Researcher, Boreskov Institute of Catalysis, Akademika Lavrentieva av. 5, 630090 Novosibirsk, Russian Federation, e-mail: lyanig@catalysis.ru. Olga Netskina, Ph.D., Senior Researcher, Boreskov Institute of Catalysis, Akademika Lavrentieva av. 5, 630090 Novosibirsk, Russian Federation, e-mail: netskina@catalysis.ru. Lidiya Kibis, Ph.D., Researcher, Boreskov Institute of Catalysis, Akademika Lavrentieva av. 5, 630090 Novosibirsk, Russian Federation, e-mail: kibis@catalysis.ru, Aleksey Okunev, Ph.D., Prorector, Novosibirsk State University, Pirogova str. 1, 630090 Novosibirsk, Russian Federation, e-mail: okunev@nsu.ru.

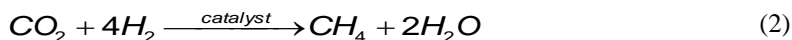
1 Introduction

Carbon dioxide is the major greenhouse gas, which is emitted into the atmosphere by power generation plants, industries and transport vehicles burning fossil fuels. The conventional approach for lowering the CO₂ emissions is carbon capture from flue gases at large stationary sources, such as fossil-fuel based power stations and industrial plants. Direct CO₂ capture of from atmospheric air, also known as Direct Air Capture (DAC), is considered as an alternative path for managing CO₂ emissions [1-4], offering more flexibility compared to conventional source point capture because of widespread availability of air.

Carbon dioxide, captured from ambient air, can be either stored in geological formations or utilized for production of fuels or other valuable chemical products using renewable energy. One of perspective approaches for CO₂ conversion is renewable methane production by the two-step Power-to-Gas (P2G) process [5-7]. The first step of this process is hydrogen generation through electrolysis of water utilizing electrical energy produced by renewables:



The second step is Sabatier reaction between generated hydrogen and carbon dioxide:



Thus, excess power or off-peak power generated by wind generators or solar arrays can be stored in a form of methane, which is a well-known energy carrier and can be used as fuel for numerous industrial applications.

Potential combination of DAC and P2G technologies offers an opportunity to use ambient air as a feedstock for production of renewable methane. In order to achieve this result, atmospheric CO₂ needs to be captured from air by a regenerable sorbent and then thermally desorbed in H₂ flow in the presence of a heterogeneous catalyst accelerating Sabatier process.

Due to the ultradilute nature of atmospheric CO₂, chemical sorbents with strong CO₂-binding affinities are typically employed for DAC [4]. Recently, a composite sorbent based on potassium carbonate (K₂CO₃) and porous gamma-alumina (γ-Al₂O₃), has been proposed for application in DAC [8]. Potassium carbonate is a well-known solid inorganic chemisorbent which reacts with atmospheric CO₂ in the presence of water vapor forming potassium bicarbonate (KHCO₃):



Another reaction involving CO₂, which takes place inside alumina pores due to interaction between the components of the composite, leads to formation of potassium dawsonite (KAlCO₃(OH)₂) crystalline phase. It was shown that thermal regeneration of K₂CO₃/γ-alumina composite material at 300°C results in thermal decomposition of potassium dawsonite and leads to augmentation of CO₂ absorption capacity in temperature-swing adsorption (TSA) cycles [9]. K₂CO₃/γ-Al₂O₃ composite sorbents are regarded as promising materials for DAC [8-11] because of their ability to absorb CO₂ directly from ambient air without any pretreatment (such as drying) and good thermal stability in multiple TSA cycles.

The general aim of our study was to implicate the Direct Air Capture/Methanation (DACM) process using K₂CO₃/γ-alumina composite sorbent for capturing CO₂ from ambient air and Ru/γ-alumina catalyst for accelerating Sabatier reaction. The composite sorbent and the methanation catalyst have been synthesized and then tested in the experimental set-up, consisted of two continuous-flow reactors, connected in series. Additionally, we have studied activation of the catalyst in reductive atmosphere and its effect on CO₂ conversion to methane in the consecutive DACM cycles.

2 Materials and methods

2.1 Synthesis of materials

Composite sorbent K₂CO₃/γ-Al₂O₃ for capturing CO₂ from ambient air

The composite sorbent was prepared by dry impregnation method, described in detail in our previous work [8]. Granular mesoporous γ-Al₂O₃ (produced by JSC «Angarsk Catalysts and Organic Synthesis Plant», Russia) was used as a host matrix. Cylindrical alumina granules were fractured to obtain particles with characteristic grain size of 1-2 mm, which were filled with 40 wt. % aqueous solution of K₂CO₃, then dried at 90 °C for 24 h and calcinated at 300 °C for 2 h. According to atomic absorption spectroscopy potassium loading in the composite sorbent was 12.5 wt. %, which is equivalent to 22.1 wt. % of K₂CO₃.

Ru/Al₂O₃ catalyst for Sabatier reaction

Ruthenium catalyst of methanation was synthesized using mesoporous γ-alumina (produced by JSC “Catalyst”) as a support. Before the synthesis the alumina granules with characteristic size of 0.25-0.50 mm were calcined at 500°C. The specific area of alumina after calcination was determined to be 175 m²/g according to Brunauer-Emmett-Teller (BET) method applied to N₂ adsorption isotherms measured at 77 K.

The ruthenium catalyst was prepared by incipient-wetness impregnation of the support with an aqueous solution of Ru(OH)Cl₃ (produced by JSC “Aurat”). The material was air-dried under infrared lamp at 50-60 °C and then in the oven at 130 °C for 2 hours.

Reduction of the catalyst was carried out at room temperature in an aqueous solution of sodium borohydride with molar ratio Ru : NaBH₄ being 1 : 5. Then the catalyst was washed with distilled water and dried in the oven at 130 °C for 2 hours. Ru loading in the catalyst was determined to be 4 wt. % according to X-ray fluorescence method using a ARL-Advant'x spectrometer with Rh anode X-ray tube.

2.2 Characterization of Ru/Al₂O₃ catalyst samples

X-ray photoelectron spectroscopy

Surface chemistry of the Ru/Al₂O₃ catalyst samples was characterized by means of X-ray photoelectron spectroscopy (XPS) method. XPS experiments were carried out using a KRATOS ES300 photoelectron spectrometer. Spectra were collected with a non-monochromatized MgK α radiation (photon energy 1253.6 eV). The spectrometer calibration was performed with core-level Au4f_{7/2} line set at binding energy 84.0 eV. The Al2p core-level line was used for an internal calibration of the samples. The E_b(Al2p)=74.7 eV was employed in accordance with the literature data for γ -Al₂O₃ [12]. To control the composition of the samples the survey spectra were acquired at the analyzer transmission energy of 50 eV and step of 1.0 eV. The charging states of the elements were analyzed with the narrow spectral regions recorded at an analyzer transmission energy of 25 eV and step of 0.1 eV. The experimental curves were fitted with a combination of Gaussian and Lorentzian peaks after the Shirley background subtraction procedure.

High-resolution transmission electron microscopy

High resolution transmission electron microscope (HRTEM) images for the samples of Ru/alumina were obtained using a JEM-2010 electron microscope (JEOL, Japan) with a lattice-fringe resolution of 0.14 nm at an accelerating voltage of 200 kV. The samples for the HRTEM study were prepared on perforated carbon film mounted on a copper grid.

2.3 Direct air capture/methanation (DACM) experiment

The DACM process was studied in a cyclic mode using the experimental set-up, consisted of two reactors, connected in series [13]. The composite sorbent K₂CO₃/Al₂O₃ was placed into a cylindrical fixed-bed stainless-steel reactor (adsorber) with the inner diameter of 19 cm. The mass of the composite sorbent inside the adsorber was 4.58 g. The methanation catalyst (0.57 g) was placed inside a cylindrical quartz reactor with outer diameter of 10 mm. The inlet of the catalytic reactor was connected to the outlet of the adsorber.

Both the adsorber and the catalytic reactor were located inside cylindrical electrical heaters. Heating control of the adsorber and the reactor was carried out automatically by a proportional–integral–derivative (PID) controller Termodat-13K2 connected to K-type thermocouples which were located inside the outer electrical heaters. The heater

temperatures for the adsorber (T_a) and the reactor (T_r) were recorded throughout the experiment, as well as temperatures measured inside the sorbent layer in the adsorber (T_s) and the methanation catalyst layer in the reactor (T_c).

Key parameters of DACM cyclic experiments are summarized in Table 1. During the first step of each cycle the composite sorbent was saturated with CO₂ as indoor air was pumped through the adsorber using a gas pump (YW Fluid, China). Relative humidity of the inlet air was 20 - 30 %.

Following the CO₂ capture step, the adsorber was purged with hydrogen at room temperature, while the catalytic reactor was preheated up to a preset temperature ($T_r = 300; 325; 350; 375$ or 400°C).

Thermal regeneration of the composite sorbent was carried out by heating the adsorber in hydrogen flow. Inlet H₂ flow rate was controlled by the gas flow regulator RRG-12-36 with an accuracy of ± 1 mL/min. The gas flow from the outlet of the adsorber was going directly into the preheated catalytic reactor. Outlet concentrations of CO₂ and CH₄ were measured each second of the thermal regeneration/methanation step using non-dispersive infrared (NDIR) sensors (produced by Dynament, UK). To avoid moisture entering the sensors water condenser was installed at the outlet of the catalytic reactor.

Table 1. Parameters of the DACM cycles

№	Description of a step	Parameter	Value
1	CO ₂ absorption from air	Duration	8 h
		Inlet air flow rate	1300 mL/min
		Adsorber temperature	20-25°C
2	H ₂ purge/ catalytic reactor preheating	Duration	10 min
		Inlet H ₂ flow rate	100 mL/min
		Adsorber temperature	20-25°C
		Catalytic reactor temperature	300-400°C
3	Thermal regeneration/ methanation	Duration	2 h
		Inlet H ₂ flow rate	100 mL/min
		Adsorber temperature	325°C
		Catalytic reactor temperature	300-400°C
4	Cooling down (no purge)	Duration	2 h

3 Results and discussion

3.1 Effects of Ru/ γ -Al₂O₃ catalyst activation on its structural properties

The as-synthesized catalyst ($m_c = 0.60$ g) was activated in the catalytic reactor using CO₂/H₂ mixture (20 vol. % CO₂, 80 vol. % H₂) at $T_r = 300^\circ\text{C}$, which is a stoichiometric mixture for Sabatier reaction: molar ratio N(CO₂):N(H₂) = 1:4. Flow rate of gaseous mixture at the inlet of the reactor was 100 ml/min. Outlet CO₂ and CH₄ concentrations measured during the activation process are presented in Figure 1a. One can see that at first the outlet CO₂ concentration is close to the inlet one (20 vol. %), but it continuously decreases with time. Meanwhile, the outlet CH₄ concentration slowly rises and reaches 20 vol. % after 5 h of CO₂/H₂ activation procedure. Figure 1b shows that temperature inside the reactor (T_c) increases symbatically with outlet CH₄ concentration due to exothermic effect of Sabatier reaction ($\Delta H = -164$ kJ/mol).

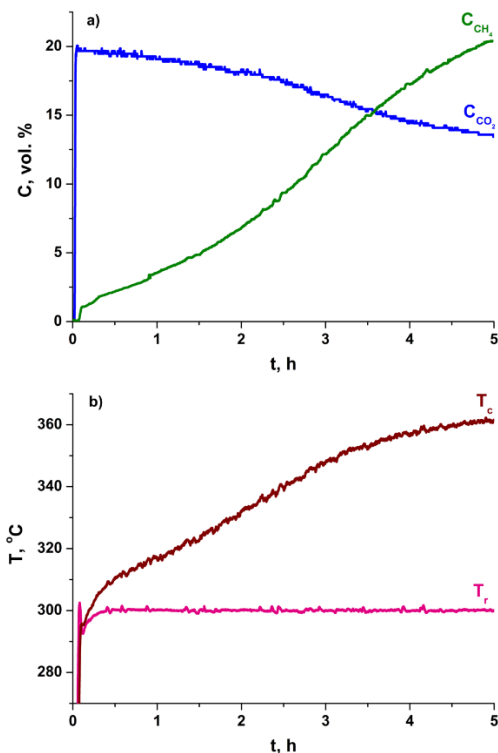


Figure 1. Activation of Ru/alumina catalyst in CO₂/H₂ gaseous mixture: a) outlet CO₂ and CH₄ concentrations; b) temperature of the reactor heater (T_r) and temperature inside the catalyst layer (T_c)

XPS and PEM methods were used to study the structural transformations of the supported component as a result of reductive activation of the catalyst. Hereinafter, the as-synthesized and the activated catalyst samples will be referred to as Ru/Al₂O₃-1 and Ru/Al₂O₃-2, correspondingly.

The analysis of the ruthenium charging states based on Ru3d spectra is complicated due to the overlapping of Ru3d and C1s spectral regions [14]. Therefore, the analysis of the Ru 3p_{3/2} line was performed for interpreting Ru state in the samples. Figure 2 shows Ru3p_{3/2} spectra for initial sample and sample after reaction.

According to the Ru3p_{3/2} spectrum main ruthenium states in the initial sample are characterized by the binding energy (E_b) values of Ru3p_{3/2} 463.7 eV and 467.2 eV typical for oxidized Ru⁴⁺ species in a composition of RuO₂, RuO₂·xH₂O and/or RuOCl₂ [14, 15]. The peak with $E_b(\text{Ru}3p_{3/2})=461.1$ eV is related to the metallic Ru⁰ [14]. After the reaction the intensity of metallic Ru⁰ component with $E_b(\text{Ru}3p_{3/2})=461.6$ eV increases (see Figure 2b) pointing to a substantial reduction of ruthenium.

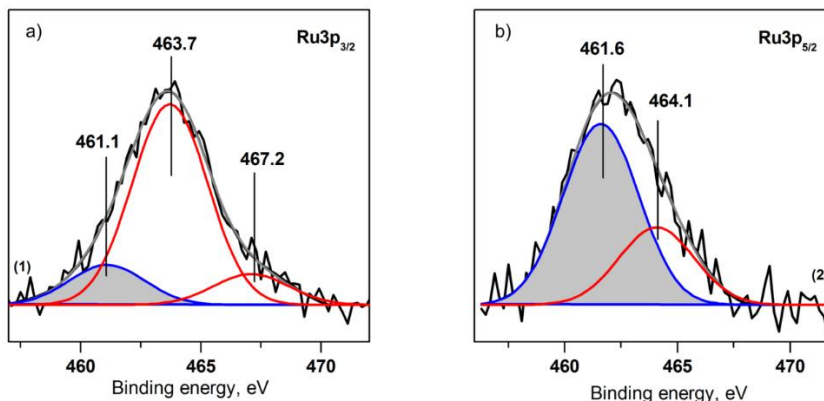


Figure 2. Ru3p_{3/2} XPS spectra of a) Ru/Al₂O₃-1 sample and b) Ru/Al₂O₃-2 sample

The catalyst samples were also characterized by transmission electron microscopy. Analysis of multiple TEM images showed that the supported component in Ru/Al₂O₃-1 sample is represented by small dots, which sizes are less than 2 nm. Taking into account the results of XPS analysis, these dispersed particles should be attributed to oxidized Ru⁴⁺ species. Reductive activation by stoichiometric mixture at 300°C resulted in formation of supported particles with sizes from 1 to 20 nm in Ru/Al₂O₃-2 sample, indicating partial sintering of the supported component. The interplanar spacings of about 0.21 nm, which correspond to (101) plane of hexagonal metallic Ru, were indicated in particles of the supported component in Ru-Al₂O₃-2 sample, which is in accordance to XPS results. Thus,

it can be concluded that the activation of the catalyst using H₂/CO₂ mixture at 300-360°C leads to reduction of Ru⁴⁺ species to active Ru⁰ metallic phase.

3.2 Atmospheric CO₂ methanation in the DACM cycles

To assess feasibility of the DACM process, the composite sorbent and the methanation catalyst were tested in consecutive cycles (Table 1) using two-reactor experimental set-up, described in section 2.3. The catalyst and the composite sorbent were used as synthesized without any additional treatment, such as activation.

Figure 3 shows gas flows for the methanation step of the first DACM cycle, as well as temperatures measured inside the adsorber and the catalytic reactor. While the adsorber heater temperature was set at $T_a = 325^\circ\text{C}$, the sorbent layer was heated up to $T_s = 300^\circ\text{C}$, according to the thermocouple located inside the adsorber. Thermal regeneration of the composite sorbent in hydrogen flow resulted in the release of CO₂, which was mostly converted into methane inside the catalytic reactor preheated up to $T_r = 400^\circ\text{C}$. It should be noted that CO₂ and CH₄ gas flow peaks recorded at the outlet of the catalytic reactor are accompanied by the peak of temperature measured inside the catalytic reactor (Figure 3), which is similar to the thermal effect observed during the catalyst activation experiment (Figure 1).

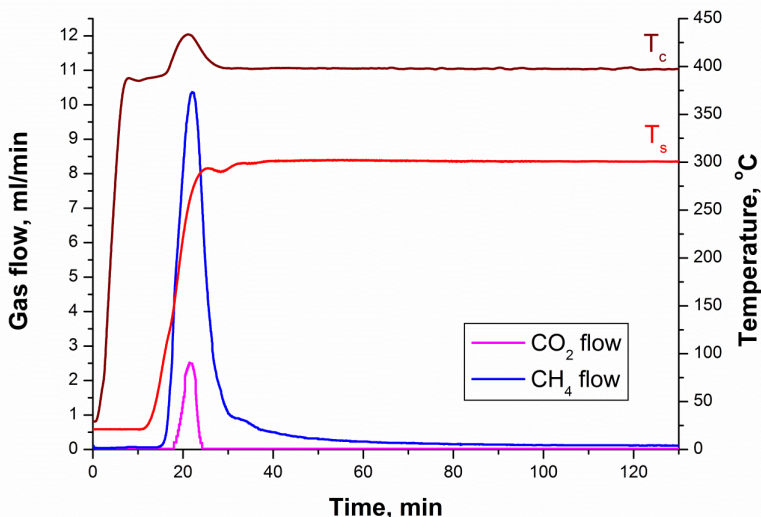


Figure 3. Outlet CO₂ and CH₄ flows and temperatures of the composite sorbent and the catalyst (T_s and T_c) in the course of thermal regeneration/methanation step of the first DACM cycle

Total volumes of CO₂ and CH₄ released during each methanation step of the DACM process (V(CO₂) and V(CH₄), respectively) were obtained by integrating experimental gas flows. Carbon dioxide conversion to methane (X) was calculated as follows:

$$X = \frac{V(\text{CH}_4)}{V(\text{CH}_4) + V(\text{CO}_2)} \cdot 100\%, \quad (4)$$

Figure 4 shows evolution of X in the consecutive DACM cycles. Although the operating conditions for cycles № 1-5 were the same as for cycles № 7-11, correspondingly, it did not result in the same values of CO₂ conversion X was 91.6-94.3 % in the cycles № 1-3 with T_r = 350-400°C and then sharply decreased down to 67.7 % at T_r = 300°C (cycle №5). However, upon further cycling CO₂ conversion to methane was improved: X was 98.2-99.8 % in DACM cycles № 7-10 (T_r = 325-400°C) and 90.2% in cycle №11 (T_r = 300°C). The results obtained can be attributed to above-mentioned slow activation of Ru/Al₂O₃ catalyst in the course of the experiment (see section 4.1), which should be taken into account upon further development of DACM process.

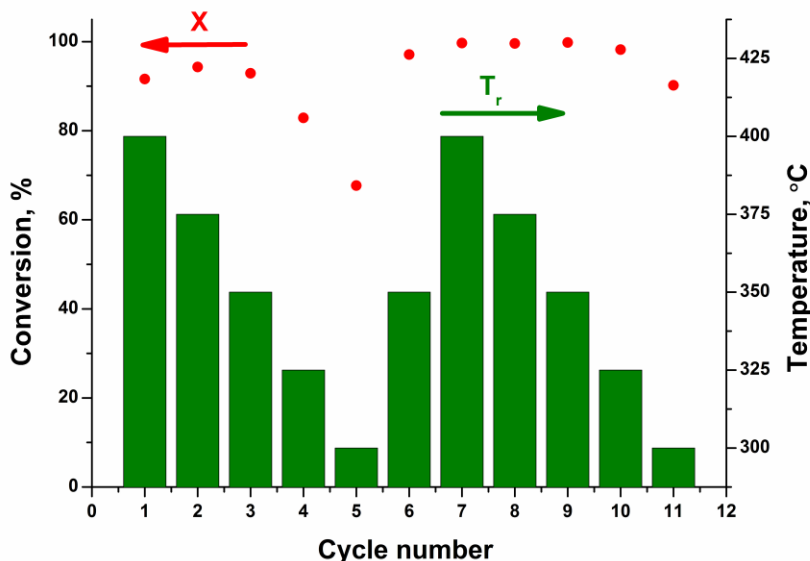


Figure 4. CO₂ conversion to CH₄ (X) in consecutive DACM cycles with different T_r.

4 Conclusions

The methanation catalyst 4 wt. % Ru/Al₂O₃ was synthesized using the insipient wetness impregnation method. Structural properties of the catalyst before and after activation by a stoichiometric gas mixture of CO₂ and H₂ (1 : 4) at 300°C were studied by XPS and

TEM methods. It was revealed that after air oxidation the surface of supported component particles is covered by oxidized Ru⁴⁺ species. The activation in CO₂/H₂ gas mixture at 300°C resulted in partial reduction of the supported component to Ru⁰ state and also led to coarsening of the supported component particles.

The novel DACM process was implemented in continuous-flow system with two separate reactors for 1) CO₂ capture/desorption utilizing K₂CO₃/Al₂O₃ sorbent and 2) Sabatier reaction over 4 wt. % Ru/Al₂O₃ methanation catalyst. It was demonstrated that slow activation of the catalyst affected its performance in the first DACM cycles. However, *in situ* activation of the catalyst made it possible to achieve very high conversion of desorbed CO₂ to CH₄ (>98 %).

Overall, the DACM process should be considered as a promising candidate for renewable energy storage/utilization, which can become another brick in the wall of carbon-neutral economy. That being said, the further technological developments are still necessary including optimisation of ruthenium catalyst activation conditions, as well as minimization of energy consumption and enhancement of H₂ utilization effectiveness.

Acknowledgements

Authors thank Dr. Gerasimov E.Yu. for performing TEM analysis. Characterization of the methanation catalyst was conducted within the framework of budget project No. 0303-2016-0010 for Borekov Institute of Catalysis. Atmospheric CO₂ methanation study was supported by RFBR project 16-33-00198 mol_a.

References

- [1] C. W. Jones, "CO₂ Capture from Dilute Gases as a Component of Modern Global Carbon Management," *Annu. Rev. Chem. Biomol. Eng.*, vol. 2, pp. 31-52, July 2011.
- [2] K. S. Lackner, S. Brennan, J. M. Matter, A. H. A. Park, A. Wright, and B. van der Zwaan, "The urgency of the development of CO₂ capture from ambient air," *Proc. Natl. Acad. Sci.*, vol. 109, pp. 13156–13162, June 2012.
- [3] A. Goeppert, M. Czaun, G. K. S. Prakash, and G. A. Olah, "Air as the renewable carbon source of the future: an overview of CO₂ capture from the atmosphere," *Energy Environ. Sci.*, vol. 5, pp. 7833-7853, May 2012.
- [4] E. S. Sanz-Pérez, C. R. Murdock, S. A. Didas, and C. W. Jones, "Direct Capture of CO₂ from Ambient Air," *Chem. Rev.*, vol. 116, pp. 11840-11876, Aug. 2016.
- [5] C. Janke, M. S. Duyar, M. Hoskins, and R. J. Farrauto, "Catalytic and adsorption studies for the hydrogenation of CO₂ to methane," *Appl. Catal. B: Environ.*, vol. 152, pp. 184-191, June 2014.
- [6] S. Schiebahn, T. Grube, M. Robinius, V. Tietze, B. Kumar, and D. Stolten, "Power to gas: Technological overview, systems analysis and economic assessment for a case study in Germany," *Int. J. Hydrogen Energy*, vol. 40, pp. 4285-4294, Apr. 2015.
- [7] M. S. Duyar, S. Wang, M. A. Arellano-Treviño, and R. J. Farrauto, "CO₂ utilization with a novel dual function material (DFM) for capture and catalytic conversion to synthetic natural gas: An update," *J. CO₂ Utilization*, vol. 15, pp. 65-71, Sept. 2016.

- [8] J. V. Veselovskaya, V. S. Derevschikov, T. Yu. Kardash, O. A. Stonkus, T. A. Trubitsina, and A. G. Okunev, "Direct CO₂ Capture from Ambient Air using K₂CO₃/Al₂O₃ Composite Sorbent," *Int. J. Greenhouse Gas Control*, vol. 17, pp. 332-340, Sept. 2013.
- [9] J. V. Veselovskaya, V. S. Derevschikov, T. Yu. Kardash, and A. G. Okunev, "Direct CO₂ Capture from Ambient Air by K₂CO₃/Alumina Composite Sorbent for Synthesis of Renewable Methane," *Renew. Biores.*, vol. 3, pp. 1-8, Jan. 2015.
- [10] S. Bali, M. A. Sakwa-Novak, and C. W. Jones, "Potassium Incorporated Alumina Based CO₂ Capture Sorbents: Comparison with Supported Amine Sorbents under Ultra-dilute Capture Conditions," *Colloid. Surf. A*, vol. 486, pp. 78-85, Dec. 2015.
- [11] O. N. Sivtsova, O. I. Eremenko, V. S. Derevschikov, and J. V. Veselovskaya, "Kinetics of Carbon Dioxide Absorption from Air in a Flow Reactor with a Fixed Bed of K₂CO₃-Based Sorbent," *Russ. J. Phys. Chem.*, vol. 91, pp. 807-813, May 2017.
- [12] J. F. Moulder, W. F. Stickle, P. E. Sobol and K.D. Bomben, *Handbook of X-ray photoelectron spectroscopy*. Perkin-Elmer Corporation, Physical Electronics Division, Eden Prairie Minnesota, 1992.
- [13] J. V. Veselovskaya, P. D. Parunin, and A. G. Okunev, "Catalytic Process for Methane Production from Atmospheric Carbon Dioxide Utilizing Renewable Energy," *Catal. Today*, 2017 (in press), doi: 10.1016/j.cattod.2017.05.044.
- [14] S. Armenise, L. Roldan, Y. Marco, A. Monzon, and E. García-Bordeje, "Elucidation of Catalyst Support Effect for NH₃ Decomposition Using Ru Nanoparticles on Nitrogen-Functionalized Carbon Nanofiber Monoliths", *J. Phys. Chem. C.*, vol. 116, pp. 26385-26395, Nov. 2012.
- [15] T. Hsieh, C. Chuang, W. Chen, J. Huang, W. Chen, and C. Shu. "Hydrous ruthenium dioxide/multi-walled carbon-nanotube/ titanium electrodes for supercapacitors," *Carbon*, Vol. 50, pp. 1740-1747, Apr. 2012.

Sustainable Solar Energy Storage for Rural Africa

R.G. CHARLES, M.L. DAVIES, P. DOUGLAS, S.M. ATIEMO, MARGARET BATES, A. CLEWS, I. MABBETT, B.S. MARTINCIGH, E.T. MOMBESHORA, JOANNA R. MORGAN, V.O. NYAMORI & D.A. WORSLEY

Abstract Photovoltaics, notably silicon PV, are becoming increasingly important in providing localised energy for rural communities in Africa. Although viewed as ‘green’, these technologies have environmental impacts associated with their production, use, and disposal, and full lifecycle optimisation for the circular economy is necessary to make every aspect of these technologies truly sustainable. One of the key questions when considering installation of solar energy systems is what is the best energy storage technology to use. Here we discuss various battery technologies in terms of their suitability for circular economy and functionality for small-scale domestic installation in South Africa.

Keywords: • solar energy, batteries • circular economy • critical materials • recycling •

CORRESPONDENCE ADDRESS: R.G.Charles, Specific, Swansea University, College of Engineering, Bay Campus, Fabian Way, Skewen, Swansea SA1 8EN, UK; e-mail: r.charles@swansea.ac.uk. M.L.Davies, Sêr Solar, Swansea University, College of Engineering, Bay Campus, Fabian Way, Skewen, Swansea SA1 8EN, e-mail: M.L.Davies@swansea.ac.uk. P.Douglas, Swansea University, College of Medicine, Singleton Park, Swansea SA2 8PP, UK, and University of KwaZulu-Natal, School of Chemistry and Physics, Private Bag X01, Scottsville 3209, South Africa, e-mail: P.Douglas@swansea.ac.uk. S.M.Atiemo, Ghana Atomic Energy Commission, National Nuclear Research Institute, P. O. Box LG80, Legon-Accra, Ghan., e-mail: atiosam@gmail.com. Margaret Bates, University of Northampton, School of Science and Technology, Avenue Campus, St. George’s Avenue, Northampton NN2 6JD, UK, e-mail: Margaret.bates@northampton.ac.uk. A.Clews, Hinckley Group, 29/31 Obafemi Awolowo Way, Ikeja, Lagos, Nigeria, e-mail: aclews@hinckley.com.ng. I.Mabbett, Chemistry, Swansea University, College of Science, Singleton Park, Sketty, Swansea SA2 8PP, UK, e-mail: i.mabbett@swansea.ac.uk. B.S.Martincigh, University of KwaZulu-Natal, School of Chemistry and Physics, Private Bag X01, Scottsville 3209, South Africa, e-mail: martinci@ukzn.ac.za. E.T.Mombeshora, University of KwaZulu-Natal, School of Chemistry and Physics, Private Bag X01, Scottsville 3209, South Africa, e-mail: tamoc88@gmail.com. Joanna R.Morgan, Specific, Swansea University, College of Engineering, Bay Campus, Fabian Way, Skewen, Swansea SA1 8EN, UK; e-mail: joanna.r.morgan@swansea.ac.uk. V.O.Nyamori, University of KwaZulu-Natal, School of Chemistry and Physics, Private Bag X01, Scottsville 3209, South Africa, e-mail: nyamori@ukzn.ac.uk. D.A.Worsley, Specific, Swansea University, College of Engineering, Bay Campus, Fabian Way, Skewen, Swansea SA1 8EN, UK, e-mail: d.a.worsley@swansea.ac.uk.

1 Introduction

Earlier this year the authors met in a workshop in Durban, South Africa, to discuss the multidisciplinary research necessary to develop a functioning circular economy for photovoltaic solar energy systems in Africa. Although photovoltaics represent a ‘green’ energy solution, whole lifecycle optimisation for circular economy of photovoltaic systems is necessary before this technology can be considered truly ‘sustainable’.[1] The key question which arose from the workshop – more significant than choice of solar cell technology - was, “What is the most suitable battery technology for sustainable solar energy storage for small scale domestic use in rural Africa.”

In the UK, at the SPECIFIC Innovation and Knowledge Centre (www.specific.eu.com), D.A.Worsley’s team has constructed a building monitored to test and validate solar energy collection and storage. This ~200 m² building demonstrates the ‘buildings as power stations’ principle being developed at SPECIFIC using technologies embedded into the building envelope to generate, store, and release energy.[2] The building has a 17 kWp building integrated photovoltaic roof installation, and transpired solar air collectors integrated into the south elevation for heating, and 60 kWh capacity of aqueous hybrid ion batteries (cradle-to-cradle certified) for clean and safe energy storage.[3]

In Africa, one of us, (MLD) worked with a team from Swansea University on a project to install a small scale off-grid solar energy structure with integrated photovoltaics for an orphanage in Mutende, Lulamba, Zambia.[4] The total installed capacity of the solar cells was 1.4 kWp. Two 12 V, 102 Ah lead-acid batteries were used for electricity storage. They seemed an obvious choice given they were readily available, easily replaced, durable, and provided the required capacity. But was it the best choice technology?

Here we begin to address the question “What is the most suitable battery technology for sustainable solar energy storage for small scale domestic use in rural Africa.” We will concentrate discussion on rural South Africa. In 2016, ~10% of households in South Africa were without electricity [5]; in its simplest analysis this represents something like 5.5 million people from a population of 55 million. Most of these households will be in rural areas.[6]

2 Defining the system

To give a basis for discussion we first need to define the energy needs to be met. In recent years in South Africa, energy suppliers introduced a scheme to provide 50 kWh/month ‘free basic electricity’ to grid-connected households, with a plan to develop off-grid solar powered systems providing 50 kWh/month to rural households.[6] We have used this 50 kWh/month as an initial target to achieve with a simple off-grid system comprising of photovoltaic panels, a battery and a charge controller. 50 kWh/month is ~1.67 kWh/day, significantly lower than the average daily consumption of homes with grid electricity access in RSA (~8 kWh/day), but nonetheless it is sufficient for basic commodities such

as lighting TV, radio, cell phone charging, washing, possibly refrigeration (See table 1 for typical daily energy consumption values).

Table 1. Daily energy consumption for small domestic appliances.

Item	Energy consumption (kWh/day)	Usage
TV (32 inch LCD)	0.35	5 h
Large AC fridge (180 W)	4.32	24 h
Small DC fridge (50 W)	1.2	24 h
Compact fluorescent light (one 14W bulb)	0.07	5 h
Incandescent light (one 60W bulb)	0.3	5 h
Cell phone charger (5 W)	0.01	3 h
Oven (2.4 kW)	2.4	1 h
Washing machine (500 W)	0.50	1 h

If 90% of this energy was required overnight, then ~1.5 kWh energy storage is needed. Allowing for an annual load growth of 2%/year over the 20 year lifetime of the photovoltaic system requires ~2.1 kWh of battery storage. (We note that increase in electricity demand is such that this year the proposed on-grid ‘free electricity’ allocation in Durban is 65 kWh/month). Battery technology is developing rapidly; here we will concentrate on systems which could be put in place immediately.

Operation conditions have a strong influence on battery performances and lifetimes, and South Africa is a difficult environment in terms of ambient temperatures both day-to-day and across the year. To mitigate this, we propose that batteries be buried at a depth of ~1.5 m where we expect the insulation and thermal lag due to soil cover, to limit temperature variations to ~12-25 °C.[7]

To give some idea of what is involved we have modelled the battery and photovoltaic requirements using the Photovoltaic Geographical Information System [8] with Durban as an example location, and estimated the cost of a system capable of generating a minimum of 50 kWh/month. A 600 W_p photovoltaic system (optimised in terms of orientation and angle) coupled with a 12 V, 250 Ah lead-acid battery with a minimum state of charge cut-off limit of 40% and a daily power consumption of 2 kWh would yield an average of 56.5 kWh/month and 678 kWh/year. We have used a value of 1.3928 R/kWh (0.096 €/kWh) as the consumer cost of electricity in Durban giving a yearly value of €65.09 for the 678 kWh. To provide an indicative cost of this system we have used a price of 0.34 €/W for a multi-Si module [9], totalling €205.32 for 600 W_p; €345.15 for a 250 Ah lead-acid battery based on commercially available batteries in RSA; and €65 for a charge controller and cables. This gives a total initial system cost of €615. Over a period

of 20 years, given the typical number of cycles from a lead-acid battery, the battery would need to be replaced roughly once every 4 years, (5 batteries in total) bringing the 20-year cost of the system to €1,996. Fig 1 shows the cost of the system over time with these battery changes and the value of the electricity produced assuming all costs remain constant.

Most of the system cost is the batteries, and the role of circular economy as a means of reducing these estimated costs is discussed below.

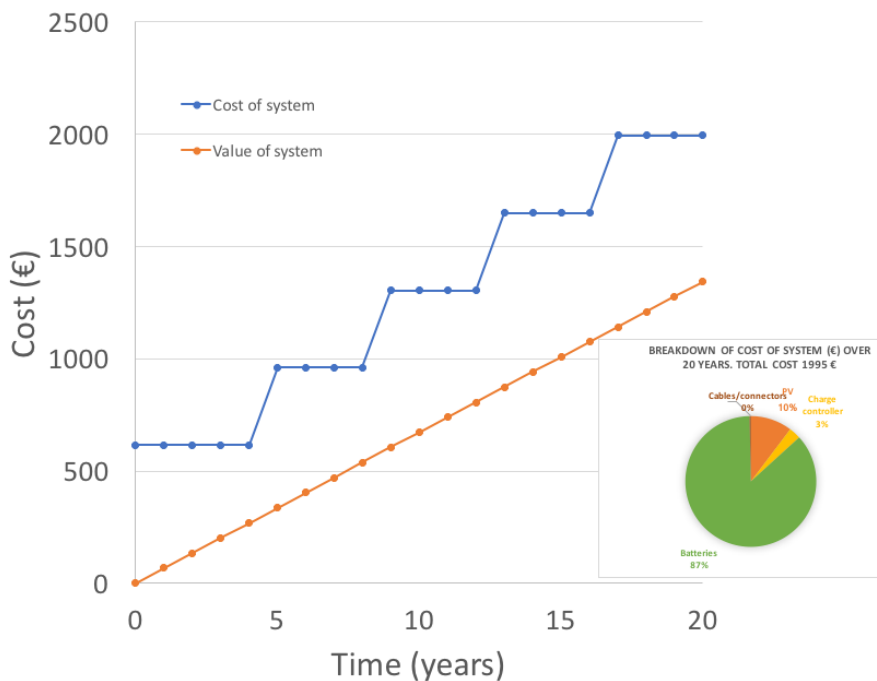


Figure 1. An estimated cost of an off-grid DC, PV system in Durban, South Africa, consisting of 600 Wp silicon module, a 12 V, 250 Ah lead-acid battery and a charge controller and cables. The pie chart shows the breakdown of the estimated costing for the system with batteries being the dominant factor in the overall price.

3 BatTery CHOICES and cost

Four main battery technologies dominate stationary energy storage applications (Table 2).[10] Lithium ion (Li-ion) batteries represent the majority of installed storage capacity and are commonly used in domestic photovoltaic systems. The merits of lead-acid batteries for application in rural Africa have already been highlighted in the discussion

of their use for the Zambia project. Vanadium redox flow batteries (VRFB), require pumps for electrolyte flow and additional energy and storage capacity to support this. This along with the additional mechanical complexity of VRFB systems makes them unsuitable for this small scale application. High temperature NaNiCl batteries are unsuitable because of the hazards associated with molten metal electrodes.

Cost is of paramount importance for this application, and Table 3 compares costs for three candidate technologies for the proposed system i.e. lead-acid, Li-ion batteries and the Aquion saltwater battery (Table 3). Lead-acid batteries are significantly cheaper than LFYP or Aquion batteries (~1/10th and 1/5th the cost respectively). The easy availability and low capital investment costs of lead-acid batteries are very attractive, but lead-acid has comparatively low cycle lives, in comparison to Li-ion and Aquion batteries and a high sensitivity to deep discharge. Significant oversizing of capacity is therefore required. The relatively short lifetimes for lead-acid batteries mean that these must be replaced 4 times over the lifetime of the proposed system, resulting in a total cost of €1,726, which is still only one quarter and one third the price of the longer lifetime LFPs (€7,104) Aquion batteries (€5,040) respectively.

Table 2. Globally installed stationary energy storage capacity by battery type.

Battery Technology	Installed Capacity	
	MW	GWh
Li-ion	~1300	1.27
High temperature NaNiCl	171	1.01
Valve regulated lead-acid (VRLA)	196	0.173
Vanadium Redox-flow batteries (VRFB)	114	412

Table 3. Comparative costs of commercially available batteries over 20 year lifetime of system.

Battery	Cost (€/Ah)	No. replacements	Total cost (€)
VRLA	1.38	4	1,726
LFYP*	14.21	1	7,104
Aquion	6.72	2	5,040

*LFYP - lithium-iron-yttrium-phosphate battery

Of course economies of scale and direct bulk purchase from manufacturers may result in lowering these battery prices. The use of a ‘circular economy’ approach can also give cost savings by: using remanufactured, refurbished or repurposed batteries; purchasing batteries manufactured from recovered materials; and valorising end-of-life batteries to recoup costs by diverting them to refurbishment, remanufacturing and recycling processes. In addition, opportunities which enhance the longevity of batteries should be

explored, to reduce the number of necessary replacements over the system lifetime. Such opportunities for batteries in South Africa are discussed below.

4 Carbon footprint & Lifecycle Impact considerations

A comparison of carbon footprints of lead-acid and different types of Li-ion battery production for the system is given in Fig 2 (we have not found equivalent data for Aquion batteries). When the need for replacement batteries is considered, lead-acid batteries account for a greater contribution to the carbon footprint of the system than Li-ion alternatives, except for lithium titanate batteries (LTO). Lithium-nickel-cobalt-aluminium batteries (NCA) would contribute least to the carbon footprint of the system over its lifetime. It should be noted that utilisation of recovered materials for battery manufacturing would reduce emissions associated with production.

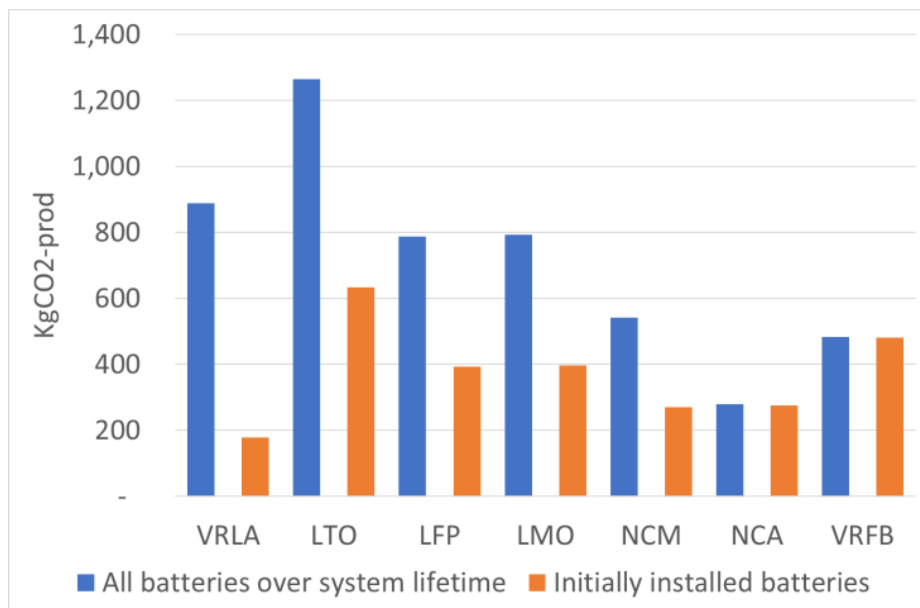


Figure 2. Carbon footprint of batteries for the system including replacements (data used from [10]). VRLA – valve regulated lead-acid; LTO – lithium-iron-phosphate with lithium titanate anode; LFP- lithium-iron-phosphate with carbon anode; LMO- lithium-manganese-oxide; NCM– lithium-nickel-cobalt-manganese; NCA– lithium nickel-cobalt-aluminium-oxide.

Carbon footprint of the production of batteries is useful for a comparison of global warming potential. However, this is a limited picture of the environmental impacts of batteries. Further consideration of emissions during production from primary resources should be made e.g. the production of Li-ion batteries from primary raw materials results

in considerable SO₂ emissions and water contamination. Consideration of the hazardous nature of materials within batteries and their potential impacts if improperly managed during use and end-of-life is also important. Issues relating to end-of-life of Li-ion batteries arise from their metal content e.g. Co present in cathodic materials; fluorine, arsenic or sulfonated compounds present in electrolytes; and the extremely reactive alkali metal – Li. Improper treatment of lead-acid batteries at end of life results in the release of lead and sulfuric acid to the environment. These materials can directly impact human health through contamination of water and soil and accumulate in food chains when batteries are landfilled or recycled improperly.[11]

The discussion indicates that lead-acid batteries are cheapest by a significant margin, however their use results in greater global warming potential over the 20-year lifetime of the system than most Li-ion alternatives.

Optimum battery use requires some knowledge of the technology as does proper handling of waste batteries.[12] Thus, any system installation also requires: i) an additional basic education and training package on the benefits of solar energy, and proper operation, maintenance and replacement of components; and ii) full system performance monitoring and analysis for problem/fault prediction/finding.

5 Resource efficiency and circular economy

5.1 Critical Materials

Table 3. Supply risks of materials in batteries

Element	Relative supply risk index [13]	Relevant battery technology
REEs	9.5	LIBs (LFYP)
V	8.6	VRFB
Co	8.1	LIBs (NMC and NCA)
Li	7.6	All LIBs
Graphite	7.4	LIBs (LFP, LMO, NMC, and NCA), Aquion
Mn	5.7	LIBs (LMO NMC), Aquion
Ni	5.7	LIBs (NMC and NCA)
Pb	5.5	VRLA
Fe	5.2	LIBs
Ti	4.8	LIBs (LTO)
Al	4.8	LIB

Supply risk index runs from 1 (very low risk) to 10 (very high risk); LIBs – Li-ion batteries; LFYP – lithium-iron-yttrium-phosphate; REEs – rare earth elements; highlighted elements included in EU20 critical list.

Critical materials used in batteries are shown in Table 3 with their current supply risk index from the British Geological Survey. The high supply risk associated with vanadium may present future resource security issues for VRFBs, further justifying its elimination as a suitable technology for this application. Li-ion batteries face resource security issues due to Li, Co, graphite and rare earths in the case of lithium-iron-yttrium-phosphate batteries (LFYP), as do Aquion cells which contain graphite. In the interests of global resource security, it is questionable whether technologies containing critical materials should be utilised without further consideration of available infrastructure to support closed-loop recycling, refurbishment and remanufacturing. Lead-acid batteries contain no critical materials.

5.2 End-of-life prospects & compatibility with circular economy

Closed-loop recycling of lead-acid batteries is well established in South Africa. First National Batteries operate a network of collection points across South Africa which divert lead-acid batteries to their smelting facility in Benoni for recycling. Recovered Pb and plastics are used to manufacture new batteries with optimised design for disassembly.[14] This suggests end-of-life costs will be low in comparison to other batteries which cannot be recycled domestically, and that lead-acid batteries are an appropriate choice for circular economy in South Africa, with environmental, economic and social benefits afforded through closed-loop retention of the materials within the South African Economy. Materials cost savings resulting from use of recovered components/materials should rise with volumes of lead-acid-batteries recycled in the future, potentially resulting in cheaper batteries for the proposed photovoltaic system. To maximise this advantage, South African energy companies should engage with First National Battery to optimise circular material flows for lead-acid batteries within South Africa. Several businesses within South Africa operate a lead-acid battery reconditioning service which reverses the sulfation process that limits their working life. This presents opportunities to extend the longevity of lead-acid batteries for the proposed photovoltaic system improving its economic viability through reduction of battery replacement costs over the system lifetime. With this infrastructure in place, opportunities should be explored for utilisation of refurbished automotive lead-acid batteries in a second life, for the proposed system; these are much cheaper than new batteries, and associated environmental, social and economic benefits will result from the initiation of new industry.

No Li-ion battery recycling exists in Africa to the best of the authors' knowledge. In South Africa Li-ion batteries are collected and shipped to Europe for recycling at considerable economic & environmental cost. South Africa also has no Li-ion battery manufacturing through which to valorise recovered materials in closed-loop material flows.[15] This indicates Li-ion end-of-life costs in South Africa will be comparatively

high with significant logistics costs incurred and little of the social and economic value inherent in Li-ion batteries exploited within South Africa. High costs increase the likelihood of improper end-of-life management, and the resulting potential for impacts on health and the environment is high. However, the South African government has funded research seeking to develop domestic Li-ion battery recycling.[15] Were such an industry to emerge, the derivable economic, environmental and social benefits from Li-ion battery recycling within South Africa could be improved significantly. No future prospects for Li-ion refurbishment exist at this time. It may be possible to source used automotive batteries for reuse in the proposed system at reduced costs with associated environmental benefits to the proposed system.[16] As an emerging technology yet to be deployed in Africa, Aquion batteries have few prospects for end-of-life treatment within the continent in the near future.

6 Conclusions

From this preliminary examination of battery technologies for sustainable small-scale (50 kWh/month) domestic installation in rural South Africa it seems that the current best choice is lead-acid batteries despite lower efficiencies and lifetimes than Li-ion and Aquion batteries. This is justified by the ready availability of lead-acid batteries in South Africa through domestic manufacturing; relatively low cost; and existing infrastructure for refurbishment and closed-loop recycling. To maximise the circular economy benefits and achieve economic viability for the proposed PV system, South African energy companies should engage key organisations involved at all stages of lead-acid battery lifecycles, and consider appropriate business models to maximise return of batteries at end-of-life such as ‘lease and takeback’ schemes or deposit schemes for batteries.

Future developments for Li-ion batteries initiated by the South African government may in time enhance the benefits of Li-ions for this application, however high costs, critical materials issues and poor prospects for refurbishment and remanufacturing cast doubt over the suitability of this technology for the proposed system.

Whichever battery technology is used, optimum battery use and management over their lifecycles requires knowledge of the technology. Thus, any system installation also requires an additional basic education and training package on the benefits of solar energy and the proper operation, maintenance and replacement of components; and full system performance monitoring and analysis for problem/fault prediction/finding.

Acknowledgements

We thank Swansea University Internal Global Challenges Research Fund for funding.

References

- [1] R. G. Charles, M. L. Davies, and P. Douglas, "Third generation photovoltaics; Early intervention for circular economy and a sustainable future," in *Electronics Goes Green 2016+ (EGG)*, 2016, pp. 1-8.
- [2] SPECIFIC. (2016, 16/5/17). Active Classroom. Available: http://www.specific.eu.com/assets/downloads/casestudy/Active_Classroom_Web_Case_Study.pdf
- [3] Blue.sky energy gmbh. (2014, 16/5/2017). Clean Energy Requires Clean Batteries, Aquion - the world's safest and cleanest energy storage for your home. Available: http://www.bluesky-energy.eu/aquion-the-saltwater-battery/?gclid=CKmor_O8tMCFe6_7QoduU4CRg
- [4] S. University. (2016, 16/5/17). Zambia Summer Expeditions. Available: <http://www.swansea.ac.uk/engineering/zambia/>
- [5] African News Agency. (2016, 16/5/17). Nearly 90 percent of SA households have electricity, says Eskom. Available: <http://www.enca.com/south-africa/stats-show-that-nearly-90-percent-of-sa-households-have-electricity-says-eskom>
- [6] N. Jamal, "Options for the supply of electricity to rural homes in South Africa," *Journal of Energy in Southern Africa*, vol. 26, pp. 58-65, 2015.
- [7] D. Hillel, Introduction to Soil Physics, 2013.
- [8] European Commission JRC. (2017, 16/5/17). Photovoltaic Geographical Information System - Interactive Maps. Available: <http://re.jrc.ec.europa.eu/pvgis/apps4/pvest.php?map=africa&lang=en>
- [9] EnergyTrend, a Business Division of TrendForce Corp. (2017, 16/5/17). EnergyTrend PV - PV Spot Price. Available: <http://pv.energytrend.com/pricequotes.html>
- [10] M. Baumann, J. F. Peters, M. Weil, and A. Grunwald, "CO₂ Footprint and Life-Cycle Costs of Electrochemical Energy Storage for Stationary Grid Applications," *Energy Technology*, 2017.
- [11] A. Cesaro, A. Marra, V. Belgiorno, and M. Guida, "Effectiveness of WEEE mechanical treatment: Separation yields and recovered material toxicity," *Journal of Cleaner Production*, vol. 142, pp. 2656-2662, 2017.
- [12] A. Manhart, T. Amera, G. Kuepouo, D. Mathai, S. Mng'anya, and T. Schleicher, "The deadly business – Findings from the Lead Recycling Africa Project," Öko-Institut e.V.; 2016.
- [13] British Geological Survey, "Risk List 2015," 2015.
- [14] ESI Africa. (2013, 16/5/17). Recycling of Batteries in South Africa. Available: <https://www.esi-africa.com/news/recycling-of-batteries-in-south-africa/>
- [15] B. J. D. Knights and F. Saloojee, "Lithium Battery Recycling - Keeping the future fully charged," Department of Environmental Affairs, Greenfund and Development Bank of South Africa, 2015.
- [16] L. Ahmadi, S. B. Young, M. Fowler, R. A. Fraser, and M. A. Achachlouei, "A cascaded life cycle: reuse of electric vehicle lithium-ion battery packs in energy storage systems," *International Journal of Life Cycle Assessment*, vol. 22, pp. 111-124, 2017.



 **energetika** *ljubljana*



 **energetika** *ljubljana*



 **energetika** *ljubljana*



 **energetika** *ljubljana*



 **energetika** *ljubljana*



 **energetika** *ljubljana*



 **energetika** *ljubljana*



 **energetika** *ljubljana*



 **energetika** *ljubljana*



 **energetika** *ljubljana*